



published by

Institut für technische Informatik als  
zentrale Einrichtung der Universität Heidelberg  
B6, 26  
68159 Mannheim

designed by

formamentum, Büro für visuelle Kommunikation

## PREFACE

4 | Letter to the Reader

6 | Introduction  
6 | Some Key Numbers  
6 | Research Groups  
7 | Teaching  
7 | B.Sc Applied Computer Science  
8 | M.Sc. Computer Engineering

## INSTITUTE

10 | Chair of Automation Project Overview  
30 | Chair of Circuit Design Project Overview  
48 | Chair of Computer Architecture Project Overview  
58 | Chair of Computer Engineering  
66 | Chair of Computer Science V Project Overview  
70 | Chair of Computer Vision, Graphics and  
Pattern Recognition Project Overview  
94 | Chair of Optoelectronics Project Overview  
118 | Research Groups Project Overview

## RESEARCH

134 | Members and Staff  
138 | Third-party-funded Projects  
140 | Selected Project Partners  
142 | Conferences  
143 | Publications

## DATA

## Dear Reader,

This is the third annual report of the Institute of Computer Engineering (ZITI) since it was transferred from the University of Mannheim to the University of Heidelberg in 2008. The aim of this report is to give you an overview of the research activities carried out at ZITI in 2012.

The chairs of the institute are divided between the Department of Physics and Astronomy and the Department of Mathematics and Computer Science. ZITI collaborates successfully with research initiatives in Heidelberg.

In 2012, Prof. Männer retired, and we set up a search committee for the open position with a new research direction which complements the common research agenda of ZITI. This new direction of research will be “Application-Specific Computing” and should create numerous opportunities for research collaborations with groups in Heidelberg, e.g. the Center for Material Science.

Our new assistant professor, Holger Fröning, has established his chair with a research focus on high-performance computing architectures.

The Master of Computer Engineering was successfully started in winter term 2011/2012 and since then we are now actively educating the new generation of master students in the various courses of Computer Engineering. So far, the students made good progress and we hope to acquire new research associates from this group in the next year. This seems to be very promising, beside that we could take more students. We plan to increase the number of students in the following years.

Besides the chairs, the institute is bundling special research into ten groups, which give young researchers a support system, access to a network of individuals with common interest, an environment for their topics and increases the visibility of their activities. This year, the 10th research group was founded, with the topic “Unmanned Aerial Vehicles”. You will find the description of each research group in our report.

The research areas of the institute can be summarized as:

1. Advanced Computer Architectures
2. High-Performance Computing
3. Process Control and Dependable Systems
4. Next-Generation Networks
5. Advanced Detector Technology

The research topics indicate a focus on high performance in every aspect of computing. The architecture group deals with the utilization of an increasing degree of parallelism and all the challenges involved there. In the network group, optical networks with terabit communication bandwidth and microsecond latency are addressed. The unique mixture of computer engineers and physicists enables these ambitious research programs.

We hope that this report will capture your interest and provide some insight into the structure and the aims of ZITI.

Prof. Dr. Ulrich Brüning  
*Executive Director*



## The Institute of Computer Engineering in 2012: Shifting research focus on Application Specific Computing

Institute of Computer Engineering/Institut für Technische Informatik als zentrale Einrichtung der Universität Heidelberg (ZITI) in 2012: The Institute of Computer Engineering engages in ASC where complex models of behavior are calculated by high performance accelerated computers. This field of research opens a wide variety of innovative and interdisciplinary projects.

### Introduction

The Institute of Computer Engineering (ZITI) is dedicated to the understanding, implementation and optimization of high-performance systems. ZITI's application-oriented research and development complements the University of Heidelberg's focus on fundamental science research.

ZITI applies the latest research from computer engineering to instrumentation, data acquisition and processing in physics, astronomy, biology, medicine and other natural and life sciences. Furthermore ZITI develops integrated hardware and software solutions for high-performance and application-specific computing.

ZITI is recognized for its excellence in specialized research areas like high-performance interconnects, active optical cables, pixel detectors and scalable memory architectures.

From the beginning, ZITI has integrated cutting-edge technologies to enable our graduate students to meet future challenges in industry and research, as evidenced by our spin-off activities.

In 2012 Prof. Maenner retired and with him ZITI lost one of the most innovative and distinguished researchers. Hopefully a new professor can be acquired in the near future to fill this gap.

### Some Key Numbers

Chairs	6
Professors	7
Secretaries	5
Technicians	2
PhD Candidates and Research Assistants	70
Research Groups	7
Projects	25
Funding (spent)	1.996.740 €
Partners	58
Publications	38
Colloquia and Conferences	3

### Research Groups

With the new founding of the institute, ZITI has established a number of research groups, which enable an exchange between different disciplines and provide young scientist with an opportunity to enhance their scientific skills and pursue their own research goals.

In 2012 a new research group was established which covers the area of Unmanned Aerial Vehicles, UAV, which requires expert knowledge for security, robustness and precision of flight controllers.

In June 2010, the following research groups were founded by advanced research assistants:

- Advanced Computer Architecture
- Application Specific Computing
- Accelerated Scientific Computing
- High Speed Short Range Interconnects
- New Detectors for Scientific and Medical Applications
- Next Generation Network Interfaces
- Process Control
- Dependable Robotics
- Virtual Patient Analysis

Research groups act independently under the umbrella of ZITI. They can work interdisciplinarily and foster cooperation between chairs. The research groups are led by group speakers. They have a sharing in ZITI resources.

### Teaching

Apart from various lectures held in the Department of Physics and Astronomy as well as the Department of Mathematics and Computer Science, ZITI mainly provides lectures in 3 programs: Applied Computer Science (B.Sc.), Computer Engineering (Diploma), and Computer Engineering (M.Sc.).

In summer 2012 the lecture Entrepreneurship was given for the first time and was attended by all computer engineering students and some more interested ones from other MSc courses e.g. Physics. With the expert advice of Dr. Ulrich Krackhardt (EXTOLL spin-off), groups of 2 to 3 students created a business idea and a nearly complete business plan and presented their plans in a business pitch colloquium at the end of the course. It was a very creative working environment which was enhanced by external experts for the various themes like financing, patents, legal and business construction.

### B.Sc. Applied Computer Science

The B.Sc. Applied Computer Science is hosted by the Department of Mathematics and Computer Science and is mainly organized by the Institute of Computer Science. It combines knowledge from Mathematics, Computer Science, Computer Engineering, Physics, and Electrical Engineering. Students must complete 180 CP, usually within 6 semesters. In the program, students can choose a major in Computer Engineering, which includes

- Practical Course Measurement Techniques
- Physical Basics of Computer Engineering
- Signals and Systems
- Digital Circuitry
- Elective module

It is also possible to visit single courses without majoring in Computer Engineering.

Since 2010, ZITI is responsible for the lecture 'Introduction to Computer Engineering'. Renowned lecturers try to raise students' interest in Computer Engineering and teach the basic knowledge of this field.

**M.Sc. Computer Engineering**

In 2011, ZITI established the new master's program for Computer Engineering (M.Sc. TI) in winter 2011/12. It is hosted by the Department of Physics and Astronomy. The lectures and application-oriented courses have been designed to educate students in areas of high industrial demand. This program provides a pool of qualified students for ZITI's Ph.D. programs. The nominal duration of the Master in Computer Engineering is 4 semesters.

The M.Sc.TI at Heidelberg University addresses graduates from B.Sc. programs in Computer Science or Natural Sciences with a sufficient minor in Computer Science (>24 CP). According to their personal interest, students can focus on one of the following areas

- Hardware Design,
- Application-Specific Computing,
- Photonic and Optical Signal Processing, or
- Intelligent Autonomous Systems.

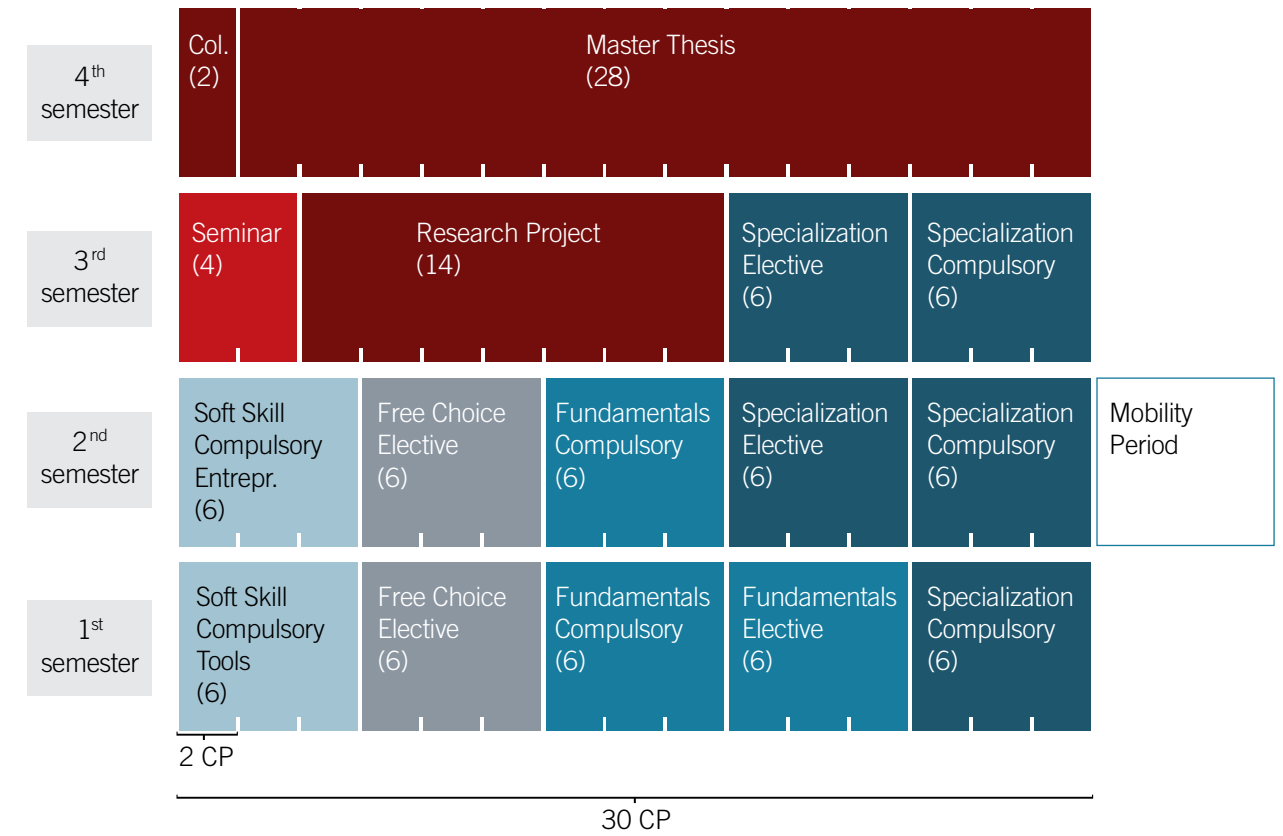
The courses can be classified into four different types, marked in different colors:

- Fundamentals (■, 3 modules),
- Soft skills (■, 2 modules),
- Free courses (■, 2 modules) and
- Specialization (■, ,Major', 5 modules)

In each type, a certain number of modules (or CP) has to be passed. Some modules are compulsory and must be passed, while others are elective modules which can be chosen from various options. Finally, some modules can be chosen freely. Modules in the specialization usually belong to one of four fields of computer engineering (majors). The third semester, also includes

- a seminar ■ (horal presentation of a specialized subject, 4 CP ), and
- a student research project ■ in a research group, which can also be used as a preparation for the master thesis ■ (14 CP).

The master thesis with a final colloquium covers the complete fourth semester.



## CHAIR OF AUTOMATION PROJECT OVERVIEW

• Prof. Dr. sc. techn. Essameddin Badreddin

### 12 | **Cyclobot**

Wagner, A., Nordheimer, E. and Badreddin, E.

### 14 | **Helicopter Plattform**

Koslowski, M. and Badreddin, E.

### 16 | **Hybrid Map-Building and Localization for Unstructured and Moderately Dynamic Environments**

Rady, S. and Badreddin, E.

### 20 | **Photogrammetry based Cascaded Kalman-Particle Filtering for Gyroscope Errors and Robot Attitude Estimation in a Host Target Architecture**

Sadaghzadeh Nokhodberiz, N., Wagner, A., Nordheimer, E., Zouaghi, L. and Badreddin, E.

### 22 | **Robot Navigation Monitoring Using Radio Frequency Identification (RFID) Technology**

Zouaghi, L.

### 24 | **Strategical Decision Making**

Alexopoulos, A. and Badreddin E.

### 26 | **Teaching Bioprocess Control**

Wolf, M.J., Ninov, V., Staudt, R. and Badreddin, E.

# Cyclobot

• Wagner, A., Nordheimer, E. and Badreddin, E.

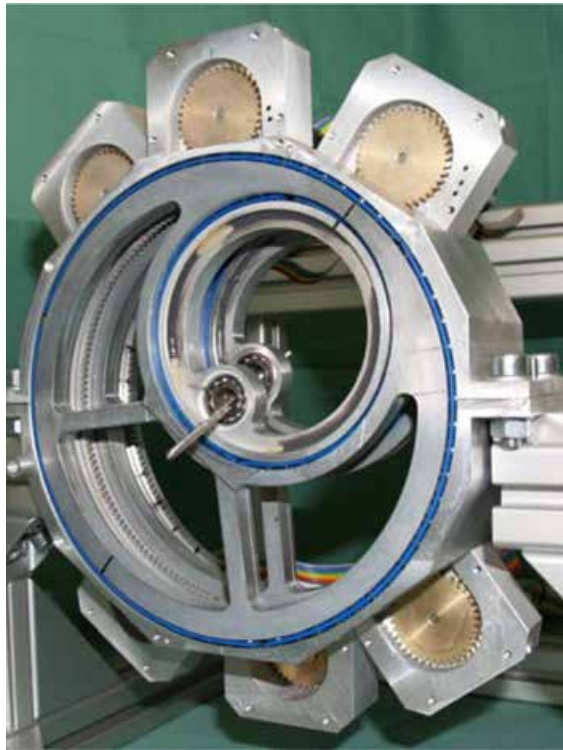


Fig. 1: The novel hybrid kinematics: 1 a) EPIZACTOR - the first functional prototype of the CYCLOBOT

### Introduction

Within the CYCLOBOT project, a novel combination of serial and parallel kinematics, the so-called EPIZACTOR-kinematics has been proposed [1], which promises an advantageous large workspace while providing small dimensions of the robot itself and good mechanical properties such as number of kinematic elements, weight, and dynamic behavior.

This kinematics provides six degrees of freedom (6 DOF) and uses two disc systems (Fig. 1 a). One disc system can be described as a virtual non-redundant serial 2-link planar manipulator with a homokinetic joint as a wrist (Fig. 1 b).

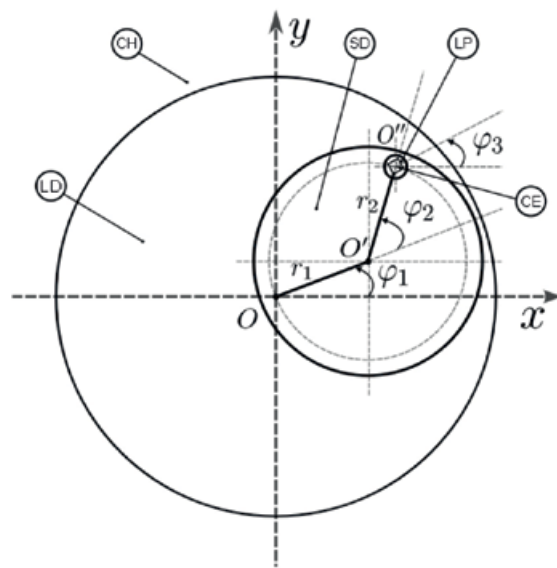


Fig. 1 b) One disc system described as a virtual non-redundant serial 2-link planar manipulator with a homokinetic joint as a wrist.

A connecting element or end-effector is attached to the two disc systems by homokinetic joints. One of these joints has a prismatic inner geometry so that it provides the rotation of the end-effector around its axis while the other joint is provided with a lead screw to move the connecting element in its axis.

### Cascaded constraints feedback control

A cascaded kinematics-based control approach with the Hierarchical Constraint-Based Singularity Avoidance (HCB-SA) has been developed (Fig. 2). In the proposed cascaded control structure, the control behavior is distributed on two control lev-

els, i.e. position control on task level (loop2, upper level) and velocity control on actuator level (loop1, lower level). The HCB-SA-algorithm is based on hierarchical constraint calculation using a metaphor of virtual damping elements and anisotropic clipping in the task space and considering influence of position constraints on velocity control level.

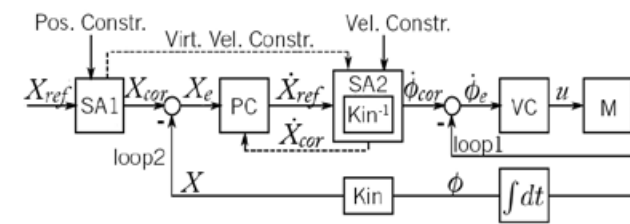


Fig. 2: Cascaded control structure with position control (loop2) and velocity control (loop1), considering the position controlled virtual velocity constraints and anisotropic velocity clipping near singular positions.

### Online-method for singularity avoidance

Singularities in robotic systems occur when the manipulator is a) fully stretched out or b) folded back on itself (Fig. 3). Whereby, latter self-motion singularity is the critical pose inside the workspace.

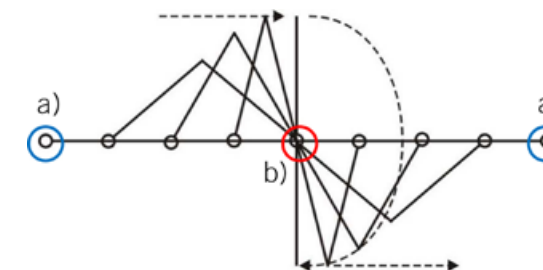


Fig. 3: Singularities in robotic systems: a) The robot arm is fully stretched out, b) The robot arm folded back on itself.

Actuator's angular velocities are approaching infinity in the vicinity of singularities. The developed HCB-SA method contains the following properties: i) consideration of the physical velocity constraints on the actuator level, ii) adaptation of dynamic ve-

locity constraints according to the distance from singular configurations and the desired tool motion in task space, iii) transformation of velocity clipping from actuator to task space and distribution of velocity errors on robot axes and iv) feedback of velocity constraints clipping into the position control level for real-time tool control.

Experimental results for different test trajectories have shown that the robot can reach sufficient static and dynamic position accuracy according to the requirement of complex task in orthopedic surgery [3]. This makes the device especially attractive for the milling cavities with round shape into bone. The control system with Hierarchical Constraint-Based Singularity Avoidance allows also to handle arbitrary trajectories considering kinematics constraints.

The work on project CYCLOBOT is funded by the German Research Society (DFG)

The partners of the project are: Laboratory for Biomechanics and experimental Orthopaedics, OUZ, Heidelberg University, Automation Laboratory, ZITI, Heidelberg University, Institute of CAE, Mannheim University of Applied Science, Laboratory of Coordinate Metrology, Tadeusz Kosciuszko Cracow University of Technology.

### References

[1] Pott PP, Schwarz MLR, Heute S, Weiser P, Wagner A, Badreddin E, "Novel hybrid kinematics with small dimensions and large workspaces make medical robots convenient for orthopaedic surgery". Proc. of the CARS, Berlin, Germany, 2009.  
[2] Wagner A, Nordheimer E, Merscher M, Heute S, Weiser HP, Pott PP, Badreddin E, Schwarz MLR, "Kinematics-Based Position-Control of the 6-DOF Surgical robot EPIZACTOR". In: CAOS 2011, 2011.  
[3] Wagner, A.; Nordheimer, E.; Badreddin, E., "Hierarchical constraint-based singularity avoidance," System Theory, Control and Computing (ICSTCC), 2012 16th International Conference on, 12–14 Oct. 2012 Oct. 2012.

# Helicopter Platform

The Scout B1-100 unmanned helicopter as a research platform  
 • Koslowski, M. and Badreddin, E.

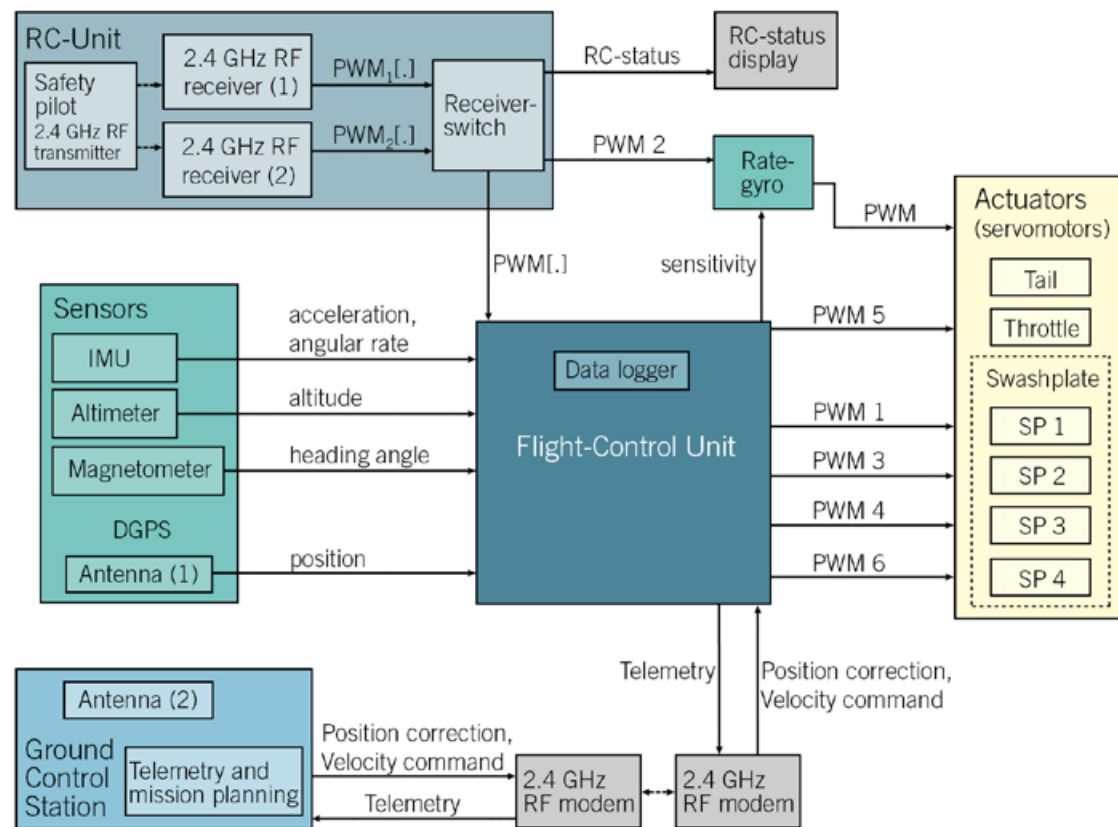


Fig. 1: Integration of sensors, actuators and flight control unit on the autonomous helicopter.

The ZITI Automation Laboratory of Heidelberg University holds an autonomous unmanned helicopter, as a research platform for several research directions such as adaptive flight controller, wind-gusts compensation, Simultaneous Localization and Mapping (SLAM), monitoring, collision-avoidance, navigation and mission planning, just to mention a few. Collaboration with other groups of the Automation Laboratory lead to two publications in international IEEE conferences in 2012. In [1] the unmanned helicopter platform was described, while in [2] a new approach for monitoring was presented.

### Platform Description

The Heidelberg University Scout B1-100 autonomous helicopter is powered by a 100cc two-stroke combustion engine. Its main rotor diameter is about 3.2m and the maximum take-off weight (MTOW) is about 75 kg. The maximum payload is approx. 30 kg with full tanks of fuel (10 Liter), providing a flight time of around 90 minutes. The main rotor consists of two blades and a Bell-Hiller stabilizer bar, which increase the stability of the helicopter. In order to prevent the helicopter from catastrophic failures, such as a crash down, the platform has two redundant subsystems. First-

ly, the flight controller, board sensors and servomotors are powered by two lithium polymer (LiPo) accumulator. Furthermore, the helicopter is equipped with a twin module for the two 2.4 GHz remote control (RC) receivers. In the case of a malfunction, a healthy receiver is switched on within 400 ms.

### Sensors and Actuators

A Crossbow IMU400CD-200 6 DOF Inertial Measurement Unit (IMU), a Honeywell HMR2300 Magnetometer, a Novatel RT-2 Differential Global Positioning System (DGPS) and an altimeter deliver the necessary sensory data for the navigation system. The position accuracy of the DGPS is about 2 cm with an update rate of 20 Hz. The Scout B1-100 has six fully programmable Volz DA 20-12-4112 servomotors as actuators. Four servomotors are used for the triggering of the swashplate. One servomotor controls the throttle of the 2-stroke combustion engine, while another servomotor adjusts the tail rotor blade pitch angle. The servos are shielded against electromagnetic interference (EMI) and radio frequency interference (RFI). A GY401 yaw rate gyro countervails the moment produced by the main rotor to stabilize the helicopter's rotation around its vertical axis. The placement of the sensors and actuators is illustrated in Fig. 1.

### Flight Control System

The integrated flight controller with the position control in hovering flight, the speed control in cruise flight as well as altitude and heading position control ensures a stable flight attitude at all speeds and elevations. The pilot can, also, manually fly the helicopter using the collective, lateral cyclic, longitudinal cyclic and tail collective (directional) servo commands. For this purpose, a commercially 12 channel 2.4 GHz Futaba RC Transmitter is employed. An additional physical switch allows the pilot to switch between (1) the manual mode, (2) the assisted or (3) the mission mode. In the assisted mode the helicopter can be controlled and flown in three different ways. The RC

transmitter, an optional joystick or the keyboard of the ground control station (GCS) computer can be used to give reference velocity commands (i.e. longitudinal, lateral and vertical velocities as well as the heading rates of the helicopter). Missions can be planned offline on the GCS computer and are then uploaded to the helicopter via wireless 2.4 GHz radio frequency (RF) modem.

### Current and Future Research

Improved flight controllers will be developed and implemented using new navigation algorithms and monitoring concepts. Further projects will deal with the mapping and 3D modeling of cultural heritage sites where the helicopter carries a high-resolution digital camera. To avoid collisions with moving and static obstacles frequency modulated continuous wave (FMCW) radar sensors and laser-range finders (LRF) will be installed. Further, a wind-gust compensator is to be designed and implemented.

### References

[1] Koslowski, M., Kandil, A. A. and Badreddin, E.: "Platform Description and System Modelling for Control of an Unmanned Helicopter", IEEE International Conference on Intelligent Systems, Sept. 6-8, 2012, Sofia, Bulgaria.  
 [2] Zouaghi, L., Alexopoulos, A., Koslowski, M., Kandil, A. A. and Badreddin, E.: "An Integrated Distributed Monitoring for Mission-Based Systems", IEEE International Conference on Intelligent Systems, Sept. 6-8, 2012, Sofia, Bulgaria.

# Hybrid Map-Building and Localization for Unstructured and Moderately Dynamic Environments

• Rady, S. and Badreddin, E.

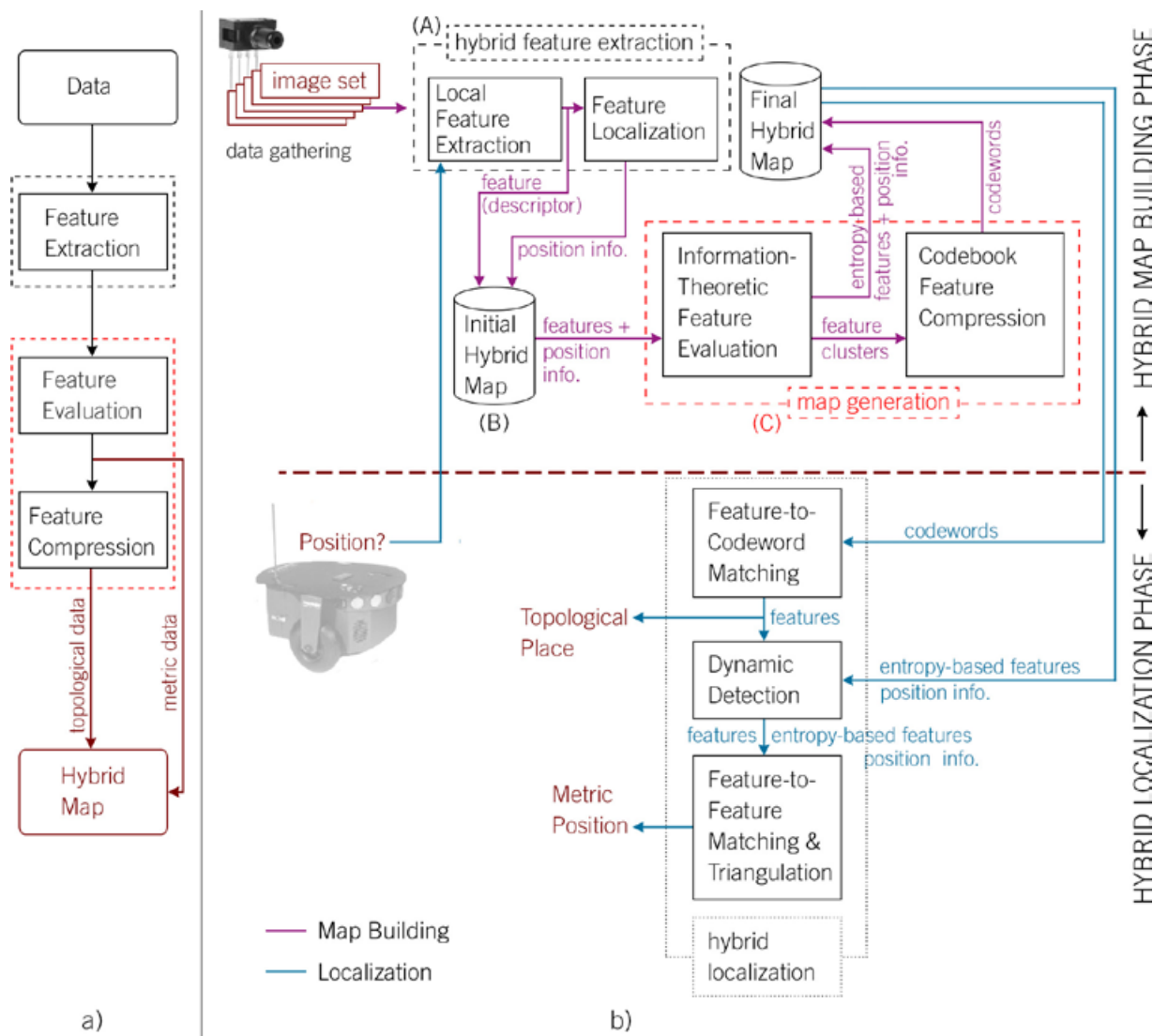


Fig.1 (a) Map-building concept. (b) Solution structure for a hybrid map building and localization.

## Introduction

Map-building and localization are fundamental topics in robotics. Solution approaches are classified into topological and metric in accordance with the type of map employed. Topological maps are

well-suited for autonomous navigation especially indoors, while metric maps conform to specific tasks. Here, a hybrid map-building and localization approach is proposed. The map-building employs local vision-based feature extraction with

additional attention to the combined quality and size of extracted features. For this purpose, an information-theoretic analysis is involved, which evaluates the information content of features. The analytical procedure generates a map consisting of a reduced set that minimizes aliasing and correspondence problems, and hence achieves both localization speed and accuracy. Additionally, hierarchical top-down localization is proposed using a unified hybrid map, where the reduced features are stored in two different resolutions. The first resolution is coarse and is obtained through a dictionary compression component. This feature form comprises non-geometric descriptors and is used in fast topological localization. The second resolution is higher, in which the features are non-compressed and possess additional corresponding geometric descriptors. Based on a previously identified topological solution, the geometric data are used in a triangulation technique and a photogrammetric model to obtain an extended metric position estimate of robot. A criterion for the dynamics detection of environment is proposed. It is applied before the triangulation execution to ensure the robustness and accuracy of the metric solution.

## Map-building and localization approach

Figure 1 introduces the proposed vision-based solution for map-building and localization. The map-building concept is given in fig. 1 (a), with the solution structure in fig. 1 (b). The solution employs local feature extraction to suit densely cluttered environments or those lacking clear structure. Besides the common feature extraction process, the map-building relies on two additional processes: feature evaluation and feature compression (Fig. 1 (a)). The processes generate an information rich and compact map that provides high localization accuracy with fewer features, which consequently induces computational savings in the space memory and processing time of localization. Moreover, the solution structure processes the environment space and features on the topological and metric levels. It makes use of combined topo-

logical and metric data using the same reduced feature set to construct a single hybrid map. The map is viewed in two different resolutions, where it is capable of localizing the robot on the two scales: coarse topological place and precise metric position. Fig.1 (b) outlines a 'hybrid map-building' phase and a 'hybrid robot localization' phase. The map-building phase uses the concept in Fig. 1 (a) by employing a hybrid feature extraction module and map generation module. They are outlined on the figure as modules (A) and (C) respectively. Module (A) consists of a local feature extraction component and a feature localization component. The components represent two distinct feature representations in order to resolve the robot location at the two localizing scales. Such representations are a feature descriptor1 obtained by the local feature extraction component and a corresponding feature's position information obtained by the feature localization component. These data are stored in the temporary storage (B) for further offline processing to obtain an optimized feature-map, which is executed by module (C). Module (C) employs components for feature evaluation and feature compression. The first filters the most relevant set from the extracted features using an information-theoretic method. The second reduces the size of the filtered features further through a Codebook compression. The robot localization phase includes a hybrid localization module (D), which uses the final hybrid map data in addition to extracted features from the current robot view to determine the robot's position. The localizing module affords localizing the robot to a topological place which is done through a feature-to codeword matching component using the codewords. The module also extends the localization hierarchically to a precise metric one, if desired, through the feature-to-feature matching and triangulation component which uses the entropy-based features and their position information. Prior to the metric localization, a dynamics detection component is executed for detecting the environment dynamics and possible topological level mismatches; to ensure the accuracy of metric solution.

## Results

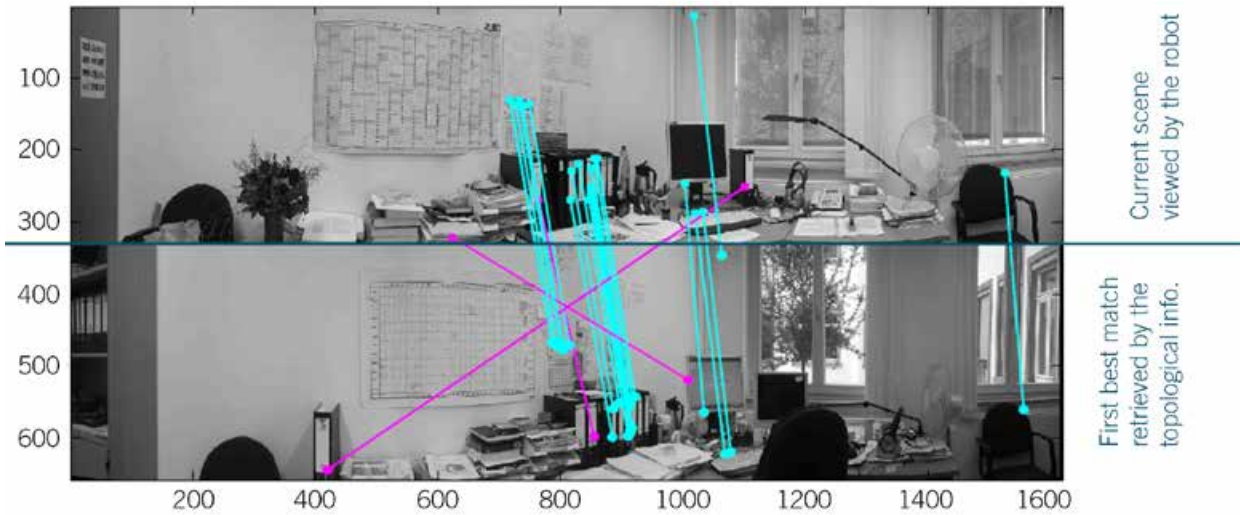


Fig. 2: Dynamics detection component. From matching, features are classified into inliers (shown in cyan) and outliers (shown in magenta). The figure shows two identified dynamic features and a single mismatch. The upper image is the current camera view, and the lower image is the identified topological node.

Figure 2 shows a test example for the dynamics detection component. The two images represent the current camera view as seen by the robot and the best matched place image retrieved by the topological matching component. The detected paired matches by the matching are shown on the images. Using a histogram of three bins to classify the distances, three outliers are detected, from which two are mismatched features, while the third is a feature for a relocated object.

Method	Geometric triangulation method	Iterative Gauss-Newton method
Performance Index		
Average positional x-error (cm)	10.0167	6.1362
Average positional y-error (cm)	34.4958	4.0432
Average rms error (cm)	35.9207	7.3486
Average rotation error (°)	5.0393	2.0789

Table 1: Metric localization performance.

Table 1 summarizes the metric errors of the triangulation component using the Geometric Triangulation and the Iterative Gauss-Newton methods. The Geometric Triangulation applies only three-feature triangulation, while the Iterative Gauss-Newton triangulation uses more than three features. That is why the localization errors in the latter are less than the former. The obtained results indicate an average root mean square position error in the range of 7–36 centimeters and average orientation errors of about 2–5 degrees.

## References

- [1] Rady, S. and E. Badreddin, Hybrid map-building and localization for unstructured and moderately dynamic environments. 6th IEEE International Conference on Intelligent Systems (IS), pp. 380–385, Sofia, Bulgaria, 6–8 Sept. 2012.
- [2] S. Rady and E. Badreddin, “Information-Theoretic Environment Modeling for Efficient Topological Localization,” 10th Int. Conference on Intelligent Systems Design and Applications, pp. 1042–1046, 2010.
- [3] S. Rady, A. Wagner, and E. Badreddin, “Building Efficient Topological Maps for Mobile Robot Localization: An Evaluation Study on COLD Benchmarking Database,” IEEE/RSJ International Conference on Intelligent Robots and Systems, pp. 542–547, 2010.

# Photogrammetry based Cascaded Kalman-Particle Filtering for Gyroscope Errors and Robot Attitude Estimation in a Host Target Architecture

• Sadaghzadeh Nokhodberiz, N., Wagner, A., Nordheimer, E., Zouaghi, L. and Badreddin, E.



Fig.1: The exploited requirements (from left to right): Crista IMU Outside View, Crista IMU Inside View 1, Crista IMU Inside View 2, K600 Krypton Camera

We have designed cascaded observers to estimate robot attitude and gyroscope errors. To this end, we have employed Particle and Kalman filters in a cascaded architecture.

## Background and Goals

Knowing the orientation of robotic vehicles is a prerequisite for control purposes in any robotic application such as territorial, airborne, industrial and surgical robots. With attitude we refer to the robot's orientation relative to a fixed coordinate system. Generally, three-axis gyros are used on board to provide data (angular rate) for attitude estimation. MEMS gyroscopes are employed because these sensors are small, light, inexpensive, and at the same time they consume less power and have short start-up time. In the presence of precisely measured angular rate data, the exact kinematic model can be used in order to estimate the attitude of a moving body. However, gyros' measurements suffer from sensory faults and errors. These faults and errors are mostly in the form of bias, drift and noises which cannot be identified and detected in a standalone use. They are typically used in combination with aiding sensors.

The combination of gyroscope and vision is very suitable for applications in robotics and virtual reality (VR) where more recently Photogrammetry is used to prepare attitude measurement.

## Methods

Based on a cascaded Kalman-Particle Filtering, gyroscope errors and robot attitude estimation method is proposed. Due to noisy and erroneous measurements of MEMS gyroscope, it is combined with Photogrammetry based vision navigation scenario. Quaternions kinematics and robot angular velocity dynamics with augmented drift dynamics of gyroscope are employed as system state space model. Nonlinear attitude kinematics, drift and robot angular movement dynamics each in 3 dimensions create a nonlinear high dimensional system. To reduce the complexity, we propose a decomposition of system to cascaded subsystems and then design separate cascaded observers.

This leads to an easier tuning and more precise debugging from the perspective of programming and such a setting is well suited for a cooperative modular system with noticeably reduced compu-

tation time. Kalman Filtering (KF) is designed for the linear and Gaussian subsystem which consists of angular velocity and drift dynamics together with gyroscope measurement. The estimated angular velocity is utilized as input in the second particle filtering based observer.

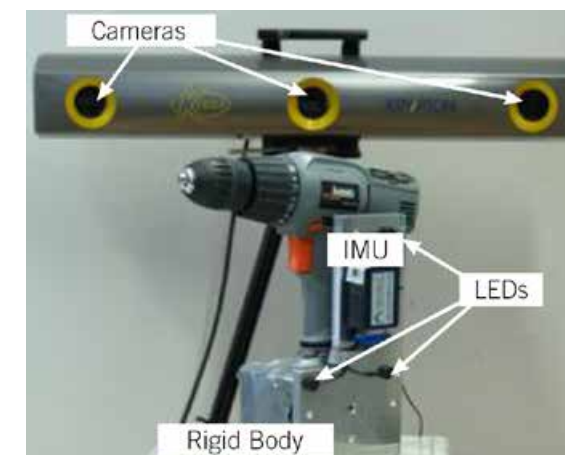


Fig. 2: Camera system, IMU and rigid body

## Experimental Setup and Results

The real data from 3D MEMS IMU and a 3-D camera system are analyzed to investigate the efficiency of the proposed method (Fig. 2). The Crista IMU which is a very small three-axis inertial sensor giving a high resolution angular rate and acceleration measurements, is exploited. The high speed and high accuracy K600 Krypton Camera is used to precisely measure the position of static and dynamic targets in 3-D space. Comprising an optical sensor combined with light sources (LEDs), we employ the camera for close range triangulation-type applications. The real data are gathered from IMU and Camera system interfaced with QNX Neutrino RTOS in a host-target architecture (Fig. 3).

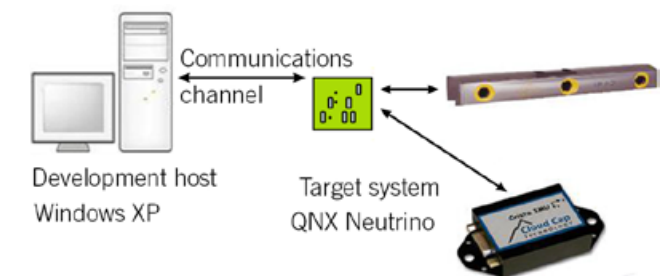


Fig. 3: QNX RTOS in a target-host architecture connected to device

## Outlook and Future Work

We are currently extending our algorithm to estimate attitude as well as position. Since MEMS accelerometers are corrupted with faults and errors, we are estimating faults and filter noises in a modular architecture to reduce the dimensionality and increase computation speed as well.

## References

- [1] J. Hol, Sensor Fusion and Calibration of Inertial Sensors, Vision, Ultra-Wideband and GPS, PhD Dissertation, Department of Electrical Engineering, Division of Automatic Control, Linköping university, 2011.
- [2] F. Bayoud, J. Skaloud, B. Merminod, Photogrammetry Derived Navigation Parameters for INS Kalman Filter Updates, In the Proceeding of XXth International Society for Photogrammetry and Remote Sensing (ISPRS) Congress, Istanbul (Turkey), 2004.
- [3] H. Bolandi, F. Fani Saberi, A. Eslami Mehrjardi, Interacting Multiple Models Adaptive Attitude Estimation for a Stereo Imagery Satellite, International Journal of Innovative Computing Information and Control, Vol. 7, No.7, 2011.
- [4] J. L. Crassidis, F. L. Markley, Unscented Filtering for Spacecraft Attitude Estimation, Journal of Guidance, Control, and Dynamics, Vol. 26, No. 4, pp. 536–542, 2003.

## Robot Navigation Monitoring Using Radio Frequency Identification (RFID) Technology

• Zouaghi, L.



Fig. 1: Integrated RFID-System on the wheelchair  
IdentMX: Compact UHF Reader with Integrated Antenna; UHF Passive Tags, EPC Class1 Gen2

### Introduction

For mobile robot navigation different methods have been proposed over the past few years. These approaches use e.g. dead-reckoning-based, landmark-based, vision-based, and behavior-based techniques. The Automation Laboratory of Heidelberg University holds an autonomous wheelchair which uses for the navigation a combination of dead-reckoning-based and behavior-based approaches. This navigation method is based on continuous encoder readings that provide the po-

sition, orientation, and linear and angular velocities of the robot. These sensor readings are used in the behaviour-based control structure of the wheelchair on different abstraction levels such as path planning, position control, velocity control, etc. However, small sensor precision errors and drifts on the wheels lead to increasing cumulative errors. To overcome this problem we used artificial landmarks, such as Ultra-High-Frequency (UHF) „RFID-Tags“ based on the Radio Frequency Identification (RFID) technology. The RFID tags are

placed in particular locations in the environment. The wheelchair, which is equipped with an RFID reader (IdentMX), communicates with the tags for the self-localization (absolute localization) (Fig. 1). Knowing the actual position (representing the system state) and the estimated position of the wheelchair, a state-estimation-based monitoring enables the early detection of navigation errors. This relative error detection is then improved by an absolute position information coming from the detection of the uniquely identifiable tags with known positions.

### RFID-based localization and monitoring approach

This RFID system communicates with a Petri-Net-based monitoring system and a Petri-Net simulator to monitor the execution of the mission while passing through the areas (marked by RFID-Tags) lying in the planned path. The detection of the tags indicates when navigating in an area and when going towards the next area. At the same time and during the navigation, the x- and y-positions of the wheelchair are tracked using a particle filter and the observations coming from the encoders. It estimates with respect to the robot position if an area is entered or not.

Fig. 2 shows the general architecture of the integrated RFID-system into the wheelchair. It consists of:

- 1 – An UHF Compact Reader identMX with integrated antenna and Power over Ethernet (PoE), which is mounted on the lower side of the wheelchair and represents a part of the sensor system.
- 2 – the module for performing, logging and processing data. It is implemented on the same real-time computer (RTOS-System: QNX) as the behaviour-based navigation control structure.
- 3 – The software for the communication with the RFID-reader, which is located on the same computer for the Man-machine-interaction (Windows System).

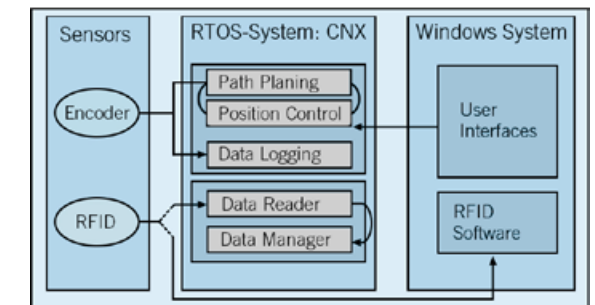


Fig. 2: The general architecture of the integrated RFID-system

The RFID-tags are used for two purposes:

- 1 – to define the desired trajectory of the wheelchair: the RFID-Tags are placed in the environment to build the topological map for the robot and to be used in path planning and navigation.
- 2 – as an external reference for the state-estimation-based monitoring system, which estimates the behavior of the wheelchair using its inputs and outputs signals and a state observer. The estimated behavior and the externally visible behavior are compared to each other in order to detect deviations.

### References

- [1] L. Zouaghi, A. Alexopoulos, A. Wagner, E. Badreddin: „Mission-based online generation of probabilistic monitoring models for mobile robot navigation using Petri nets“. Special issue published in Robotics and Autonomous Systems on 16 August 2012.
- [2] Yamen Mabrouk: „Einsatz von RFID Technologie in der Entwicklung einer Landmarken-basierten Testumgebung für Roboter Navigation“. Bachelorarbeit am Lehrstuhl für Automation unter Betreuung von Dipl. Ing. Leila Zouaghi und Prof. Badreddin.

## Strategical Decision Making

Multi-Agent Pursuit-Evasion Game with Unmanned Aerial Vehicles (UAVs)  
• Alexopoulos, A. and Badreddin, E.

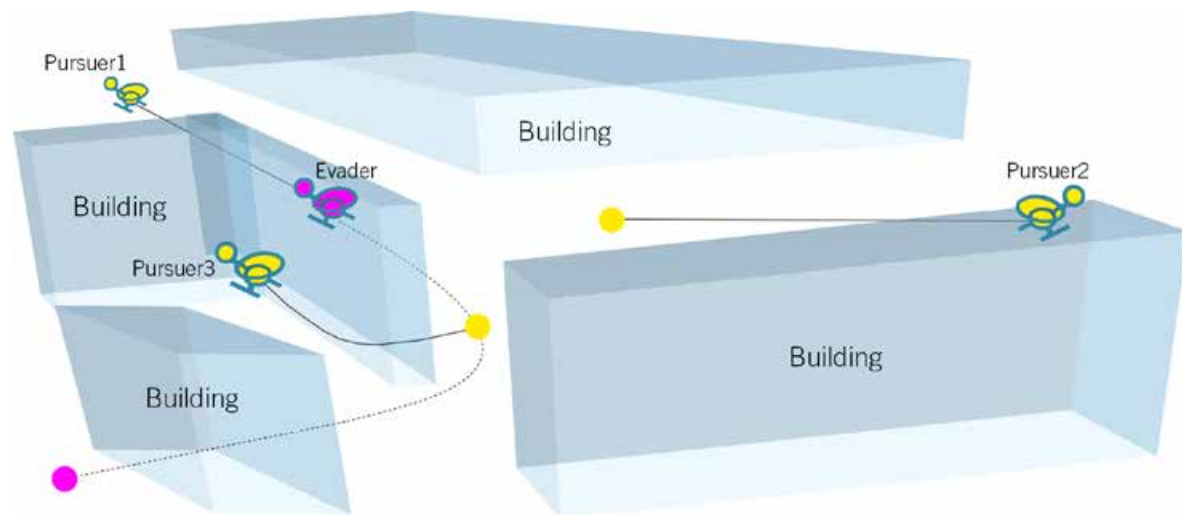


Fig. 1: Pursuit-Evasion Game Situation in Urban Environment

### Introduction

Pursuit-evasion games describe a problem, in which an agent or a team of agents tries to catch an adversarial agent or team of agents, while the meaning of catch is the fulfillment of one or more conditions which depend on the specific problem being considered. A framework for solving such games could be used for a variety of applications like search and rescue missions, surveillance, localization and tracking or even for applications in economics and warfare. A very powerful framework with which this vast number of such problems can be solved is game theory. Game theory is an approach for strategical decision-making, considering that the solution depends on the decision of other agents, while everybody is aware of that. This makes the solution process, especially if the number of players rises, very complex. One can distinguish between non-cooperative and cooperative game theory. Generally, in non-cooperative games or conflict games, all involved parties have differing goals, meaning that every party wants to

maximize its outcome and if possible the loss of the other agents. In cooperative games usually all involved agents have the same overall goal and try to find optimal strategies that maximize the outcome of the team. Definition and solution methods of non-cooperative and cooperative game theory are described in detail in [1] and [2].

### Problem formulation

The problem we want to address is the multi-agent search and pursuit of a faster and more agile evader in an urban environment with UAVs. We assume that the operation area is between buildings and not above them. All agents have also a static 2D-map of the environment given. Therefore, consider the following example situation: An UAV wanted by the police (a team of UAVs) is located in an urban environment and tries to escape. The police UAVs are trying to find and to surround the evader in such a way that an escape is impossible. In this scenario it is assumed that the evader is faster and more maneuverable than the pursu-

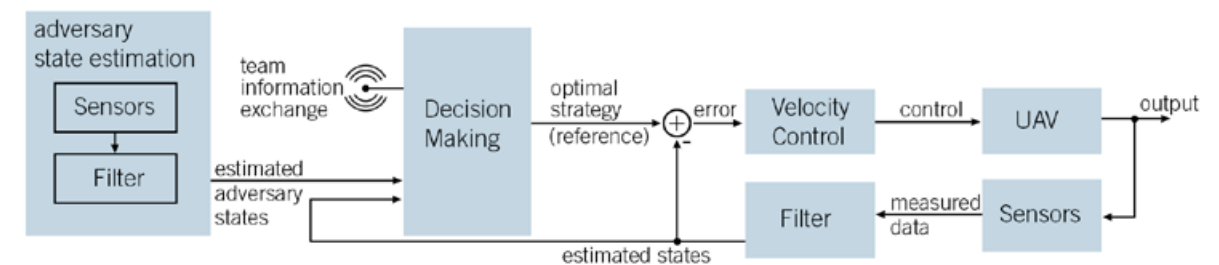


Fig. 2: Decision Making and Velocity Control Loop of each agent

ers. This advantage over the pursuer means that if the evader knows the number and position of all pursuers, a capture is in most cases impossible. Initially it is assumed that the evader doesn't know the number of pursuers. It is also assumed that a detection of an adversarial agent is only possible if there is a line of sight. To have a chance capturing the evader the pursuing team has to cooperate intensively. Figure 1 depicts an example situation of a pursuit-evasion game. Three yellow UAV pursuers are assigned to catch the red UAV evader. Regarding the actual state of the game, the evader has detected two pursuers, chasing him. The pursuers, which are in permanent communication, can transmit gathered adversary information (i.e. position) to all teammates, having no line of sight to the foe. This information advantage can be used now to contain and to catch the evader. An evader is caught when a predefined distance to one of the pursuers was undercut.

### Solution Approach

To conquer this problem one must define an appropriate objective function, optimized by the agents of the to get the desired result. The game theoretic approach takes all agents and their objectives into account, providing an optimal (or equilibrium) solution. Not to play this equilibrium solution would result in a lower and thus a non-optimal outcome for the corresponding agent. Figure 2 depicts the velocity control loop with a preceding decision making block, implemented on every agent. The decision making block provides the optimal strategies (reference velocities) for the UAV

controller. The optimal strategies are determined by computing the Nash-Equilibrium [1] strategy based on the information each agent has about the other agents and himself (states, strategies, objectives, dynamic model). The information has to be gathered with a variety of different sensors to be able to detect other agents and to estimate the relevant states. A secure data link between the pursuers' team is used to exchange information to assure an advantage over the evader.

### Future Work

Due to the high time complexity of computing optimal strategies for a multi-agent game, fast optimization algorithms have to be implemented to be able to operate in real-time. A trade-off between strategy- (control input-) resolution and computation time must also be considered. After handling this issue, the implementation on real systems has to be done, to test the performance of this briefly described approach.

### References

- [1] Basar, T. and Olsder, G. J.: "Dynamic noncooperative game theory", Classics in Applied Mathematics, 1999.
- [2] Peleg, B. and Sudhölter, P.: "Introduction to the theory of cooperative games", Theory and decision library, Kluwer Acad. Publ., 2003, Boston, Mass.

## Teaching Bioprocess Control

Development of a Laboratory Experiment for Teaching Bioprocess Control

• Wolf, M.J., Ninov, V., Staudt, R. and Badreddin, E.

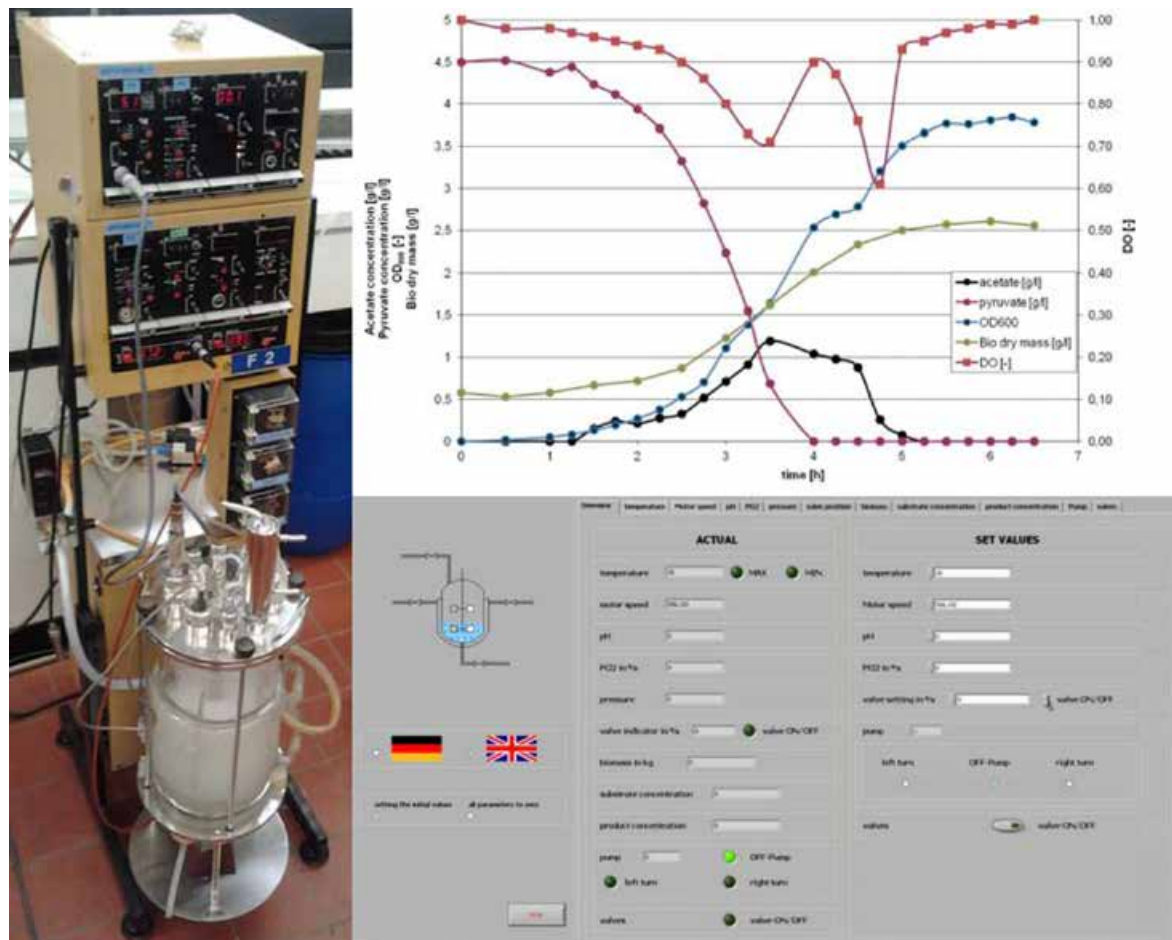


Fig. 1: Bioreactor used (left), metabolic activity and growth of *Vibrio natriegens* in a batch fermentation (upper right), and graphical operator interface of the control system of the bioreactor (lower right).

The overall goal of this project is the development of a laboratory experiment for teaching bioprocess control and automation. The teaching experiment should enable the students to model a fermentation, to determine missing parameters experimentally, to mathematically analyze the model, to simulate different control strategies and to finally verify the simulated results hands-on in the lab; hereby, a deeper understanding of the challenges

and solutions of modern model-based control engineering can be achieved [1]. In bioprocesses, chemical reactions are performed by living microorganisms, which do not only show increased metabolic needs and certain environmental susceptibilities, but also offer huge advantages like highly sophisticated capabilities for synthesizing complex protein products in a reliable, fast, cheap, and safe manner. Therefore

also the plants to be used for bioreactions exhibit, compared to conventional process technology, additional demands e.g. with respect to sterility or aeration. As the dynamics of a bioprocess thus depend on the characteristic metabolic properties of the microorganisms' metabolism as well as on some physical and mechanical properties of the bioreactor used, a bioprocess model also constitutes of two parts: A kinetic model of the microorganisms, and a reactor model. Both model components interact, as e.g. the transport of heat, produced by the microorganisms, out of the reactor and the material transport (e.g. oxygen) into and its dispersion inside the reactor both depend on reactor properties, and influence biological growth.

Within the framework of this project, these two model components as well as additional teaching materials have already been developed. The final teaching concept of the entire experiment, including the experiments' instructions, is still work in progress.

For the reactor model, the four most important characteristics of the bioreactor used have been identified [2] to be power input, homogenization, and gas and heat transfer. Considerations on scale-up of the reactor system were also worked out in greater detail to increase comprehension of the model [3]. The control system used, a portable low-cost host-target real-time computer system, is freely programmable in the Matlab/Simulink development environment; one distinctive feature of this control system is its newly developed graphical user interface [4]. This interface was programmed in Labview and relieves operation of the plant as it does not fall short of commercial ones in any way thus well-prepares students for a latter job.

Elaboration of the process model [5] required identification of requirements of a bioprocess to be suited for a laboratory experiment for students. Finally, the maritime bacterium *Vibrio natriegens* was chosen: The high salinity of its respective medium [6] minimizes the risk of biological con-

tamination. Also does this bacterium not require increased safety treatment, the organisms and the medium are relatively cheap, and its low generation time enables the experiment to be performed in just one whole day. So far, mathematical models for batch, fed-batch and continuous fermentations were developed. Linearization of the nonlinear batch dynamics revealed the system neither to be completely controllable nor to be completely observable – with biological reasons and solutions to this problem already identified. Rules for how to develop a strain of the microorganisms specially adapted to the medium as the basis for a successful fermentation execution were worked out.

With respect to Good Manufacturing Practice (GMP) demands, for the students it is beneficial not only to understand the functional principles, advantages and pitfalls of common measurement methods or upcoming technologies like online spectroscopy, but also to be familiar with sensor signal generation, transmission, sampling, reconstruction and interpretation of measurement data – as one often faces difficulties due to biological variation or impurities of raw materials, final products or even microorganisms that cause interference of measurement signals. Also, data may be distorted in large production sites, thus meaningful data may become mixed with insignificant noise. Disturbing quantities and interfering signals complicate obtaining data adequate for process documentation and automation. Therefore, in some cases it is advisable to process sensor signals before using them for fermentation control or visualization to avoid errors. Addressing these requirements, learning materials covering a broad overview of fundamental concepts of signal processing including the characteristics of different filter types as well as filter design and application in Simulink, are provided to the students. In order to ensure a high degree of accessibility the learning material was developed in a cooperative process with a former student [7], taking into account the perspective of a learner who has attended the course and reached the same level of knowledge about process automation.

In cooperation with the Institute for Technical Microbiology, Mannheim University of Applied Sciences.

---

### References

- [1] Wolf, M.J., Ninov, V., Babel, H., Hütter, K., Staudt, R., Storhas, W., and Badreddin, E.: "A Laboratory Experiment for Teaching Bioprocess Control—Part 1: Hardware Setting", 9th IFAC Symposium on Advances in Control Education 2012, Nizhny Novgorod, Russia, June 19–21, 2012.
- [2] Babel, H.: "Modelling the Dynamics of a Stirred-Tank Bioreactor for a *Vibrio natriegens* Fermentation", Lab Project, Mannheim University of Applied Sciences, 2011.
- [3] Hütter, K.: "Scale-Up: Calculations and Simulink-based Modelling of Thermal Sterilization", Lab Project, Mannheim University of Applied Sciences, 2012.
- [4] Ninov, V.: "Design und Implementierung einer Bedienerchnittstelle in Labview für die Simulink-basierte Echtzeit-Regelung eines Bioreaktors", Bachelor's Thesis, Heidelberg University, 2011.
- [5] Knapp, R.: "Model-Based Development of a Fermentation Process Including Systems Analysis, Used as a Teaching Experiment in Process Automation", Master's Thesis, Mannheim Univ. of Appl. Sciences, 2012.
- [6] Knapp, R.: "Performance Analysis of Selected Defined Media for a *Vibrio natriegens* Fermentation", Lab Project, Mannheim University of Applied Sciences, 2012.
- [7] Kirchgäßner, S.: "Signal conditioning for fermentation processes", Lab Project, Mannheim University of Applied Sciences, 2011.

## CHAIR OF CIRCUIT DESIGN PROJECT OVERVIEW

• Prof. Dr. Peter Fischer

### 32 | A Self Triggered ASIC for Pulse Shape Readout

Krieger, M., Armbruster, T. and Fischer, P.

### 34 | A Spatially Resolving Photon Cluster Detector in CMOS Technology

Fischer, P., Armbruster, T., Ritzert, M. and Sacco, I.

### 36 | Interpolating Silicon Photomultipliers

Fischer, P. and Sacco, I.

### 38 | Chip and Module Development for PET/MRI

Fischer, P., Sacco, I., Ritzert, M. and Blanco, R.

### 40 | Fast Readout System for the DSSC Detector at XFEL

Kirchgessner, M., Soldat, J., Kugel, A. and Fischer, P.

### 42 | The Pixel Readout ASIC for the DSSC Detector at XFEL

Erdinger, F., Kirchgessner, M., Soldat, J. and Fischer, P.

### 44 | The XNAP Fast 2D X-Ray Photon Detector

Thil, C. and Fischer, P.

### 46 | ASICs and Module Design for the Pixel Vertex Detector at Belle II

Knopf, J., Kreidl, C., Peric, I. and Fischer, P.

## A Self Triggered ASIC for Pulse Shape Readout

The CBM experiment (Compressed Baryonic Matter) is being developed at the Facility for Antiproton and Ion Research (FAIR/GSI/Darmstadt) for the quest for the Quark-Gluon-Plasma and for studying phase transitions and the density of state in hot nuclear matter. The collisions between the accelerated beam particles and the target occur at random moments so that the arrival times of hit signals in the various particle detectors are unpredictable. The readout electronics associated with every channel of a detector must therefore be able to react autonomously ('self triggered'). When a hit is detected, its digitized pulse shape is read out. The shape information can be used to reconstruct the hit time for association to other hits. The SPADIC chip is a 32 channel ASIC for such a self triggered readout. It has many additional features to enhance system performance.

• Krieger, M., Armbruster, T. and Fischer, P.

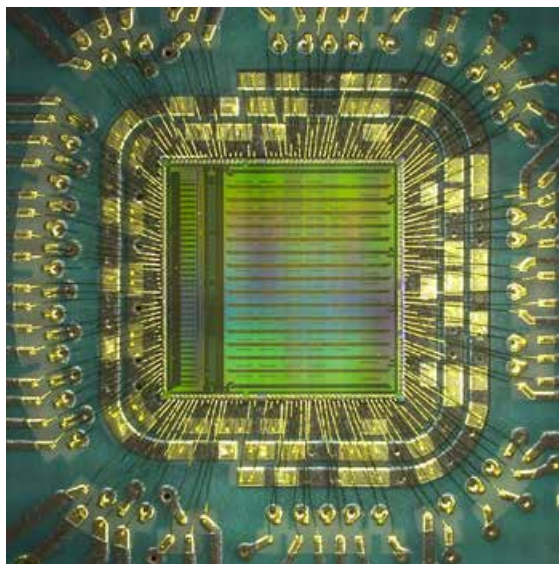


Fig. 1: The SPADIC chip (5x5 mm<sup>2</sup> size) is glued and wire-bonded in-house to a highly optimized carrier PCB.

### The SPADIC Chip

The 'Self Triggered Pulse Amplification and Digitization Integrated Circuit' (SPADIC [1]) has 32 channels, each containing a preamplifier/pulse shaper (CR-RC, 80 ns peaking, 5 mW, ENC < 1000 e@30 pF), an Analog-Digital Converter (9 Bit, 25 MSpS, 5 mW, 0.12 mm<sup>2</sup>), a programmable digital filter (IIR, 4 first order stages), an intelligent hit finder, a circuit to buffer and merge hits from all channels, and a fast serial data

output link (CBMNet, 500 Mbps). The chip has been designed entirely in our group<sup>1</sup> in a 180 nm CMOS technology. Fig.1 shows the chip with a size of 5x5 mm<sup>2</sup> bonded to a printed circuit adapter board.

The 32 channels can be clearly separated in the left part of the chip. Most area is covered by digital circuitry and memory blocks used to process and buffer the digitized data.

### Test Environment

In order to characterize the analogue parts of SPADIC and to verify the digital functionalities, a versatile test environment has been developed. It is based on a custom FPGA board with a fast USB2.0 interface. The chip on its adapter (Fig. 1) is connected through an auxiliary PCB containing additional infrastructure. The setup shown in Fig. 2 can also be connected to prototypes of the transition radiation detector (TRD) of CBM, which will be the first application of SPADIC. The FPGA on the USB board contains a CBMNet implementation and a USB2.0 interface for communication. The multi threaded control and data analysis software on the host Linux PC has been developed in Python. It can be used to operate the setup under test beam conditions.

<sup>1</sup> The HDL code for the CBMNet interface has been developed at the chair for computer architecture



Fig. 2: Test setup used to characterize SPADIC (located under the central copper pad of the upper board).

### Test Status

All features and operation modes of the chip, including special situations like buffer full conditions, overlapping pulses etc. have been characterized in great detail. The chip behaves as expected. Only minor bugs have been identified and understood. As an example, Fig. 3 shows the novel 'pulse-picking' feature: A freely programmable bit pattern (crosses) defines which samples of the digitized pulse (circles) are sent out for readout. This feature will be used to minimize the data volume by acquiring the most relevant information. In the example, the pulse is precisely sampled at the edge but coarsely later to verify correct pulse shape and return to baseline. Next steps will be the absolute calibration of the analogue path and operation on real detectors.

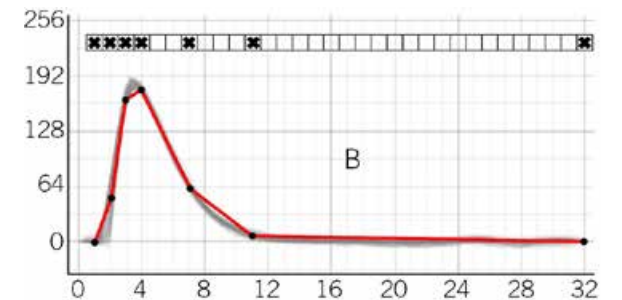


Fig. 3: Example of a measured chip feature: A programmable pattern (crosses) defines which amplitude samples of each detected pulse (dots) are transferred to the readout.

Supported by BMBF under contract 05P12VH-FCF. Cooperation with the CBM Collaboration, mainly with GSI and the universities Frankfurt and Münster

### References

[1] <http://spadic.uni-hd.de>

## A Spatially Resolving Photon Cluster Detector in CMOS Technology

The fast and efficient detection of light flashes with only few photons is a key challenge in many research fields. Important medical applications are PET scanners (Positron Emission Tomography) in which gamma rays stemming from positron annihilations produce such light flashes in crystal scintillators. A present trend in photon detection is the use of silicon based devices with internal signal amplification. Most available structures are fabricated in specialized sensor technologies which only offer signal detection. The use of conventional CMOS processes would allow in addition an immediate intelligent signal processing on the sensor. We have therefore started to develop intelligent photon detectors in CMOS. The first prototype chip focuses on technology evaluation and should deliver the position (centre of gravity) of each photon cluster.

• Fischer, P., Armbruster, T., Ritzert, M. and Sacco, I.

### Principle of Photon Detection

Most modern optical light detectors use silicon crystals to absorb the photons. For very high sensitivity, i.e. the detection of single photons, high electric fields are engineered into the device so that a single photon can trigger an avalanche delivering millions of electrons. Avalanche Photo Diodes (APDs) cover a 'large' area (some mm<sup>2</sup>) with a single structure, so that the sensitivity is very high, but the number and position of photons cannot be resolved. A more recent approach is the segmentation of the active area into many small cells (~50×50 μm<sup>2</sup>) and an analogue summing of signals so that the output is proportional to the number of fired cell. Such Silicon Photomultipliers (SiPMs) or Multi Pixel Photon Counters (MPPCs), as well as APDs, are fabricated in special technologies which deliver good sensitivity and amplification, but do not allow integration of transistors.

An alternative approach is the use of standard CMOS technologies. The available transistors allow the integration of signal processing into the device offering a wide range of new possibilities. Unfortunately, the quality of the Single Photon Avalanche Diodes (SPADs) in such technologies has been poor, so that early attempts delivered structures with unacceptable noise rates. The Philips Company PDPC [1] managed to obtain a suf-

ficient SPAD quality for commercializing devices with integrated time measurement. As the used technology is only available to PDPC, independent developments for particular applications are not possible. Recently, the Fraunhofer Institute for Microelectronic Circuits (IMS) has presented very good SPADs [2] in a 0.35 μm CMOS technology which was made available to our group. We have used this opportunity to design and submit a first two-dimensional array chip.

### The IDP1 Chip

The first prototype chip IDP1 (Interpolating Digital Photodetector) shown in Fig. 1 has 88×88 pixels of ~55×55 μm<sup>2</sup> size in the upper part. The lower part contains mainly digital circuitry to control the array, extract data from the array, and to process the data. Two rows of wired bond pads are used to supply power and to control the chip. The architecture allows a full readout of the two-dimensional hit pattern to study sensor properties or the details of the light distribution in a particular application. An alternative fast readout mode allows summing of the number of hit cells. The cells can be assigned to up to four freely programmable groups, so that for instance a spatial resolution by means of the 'interpolating photo detector' concept [3] can be obtained. Events are fully buffered, de-randomized and serialized on chip. The

arrival time of a photon cluster can be measured with different circuit approaches to evaluate the possibilities of the technology. Testing of the chip has just started.



Fig.1: Photograph of our first CMOS Photon detector array chip. The full chip has a size of 5×6 mm<sup>2</sup>. The SPAD array contains 88×88 cells of ~55×55 μm<sup>2</sup> size.

### The IDP1 Pixel

Each pixel (Fig. 2) contains a SPAD with biasing, power distribution and active circuitry with associated control signals. The SPAD occupies 38% of the pixel area which is a compromise between high sensitivity and intelligence. The pixel circuitry contains a fast hit OR, time gated hit detection, double buffering, serial data readout, masking of bad pixels and some debug and test features.

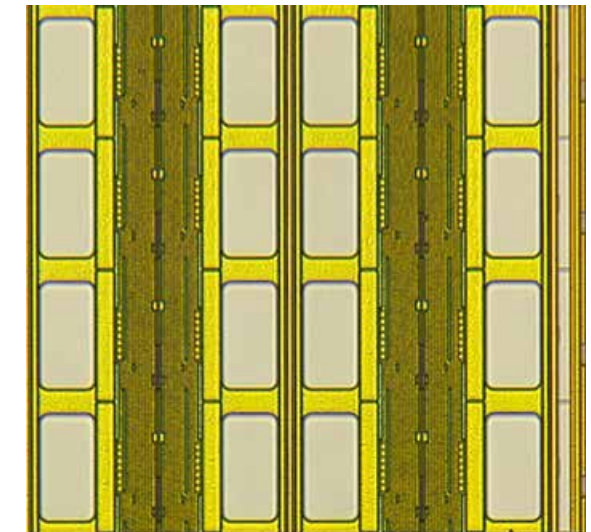


Fig.2: Zoom into the sensitive area showing the active SPADs (white areas) and power and signal distribution. The CMOS circuitry is hidden under the dense wire structure.

Supported by EU within the FP7 project Sublima (contract #241711).

### References

- [1] [www.research.philips.com/initiatives/digital-photon-counting](http://www.research.philips.com/initiatives/digital-photon-counting)
- [2] For instance: F. Villa et al., IEEE photonics journal 4 (2012), Nr.3, S.795-804, DoI:10.1109/JPHOT.2012.2198459.
- [3] Peter Fischer and Claudio Piemonte: Interpolating Silicon Photomultipliers, NIM A718 (2013) 320–322.

## Interpolating Silicon Photomultipliers

Silicon Photomultipliers (SiPMs) are sensors for the detection of very low level light pulses. They consist of an array of Single Photon Avalanche Diodes (SPADs) which, when hit by an optical photon, deliver a pulse of constant amplitude. The signals of all SPADs are normally merged, so that the number of photons can be estimated but no spatial information is available. In the recently proposed Interpolating Silicon Photomultiplier (ISiPM [1]), the SPAD signals are assigned to several output channels such that the centre of gravity of the photon distribution can be reconstructed. Two device versions have been designed, produced and characterized. The measurements confirm that a high spatial resolution of better than 1/10 of the device size can be obtained easily.

• Fischer, P. and Sacco, I.

### ISiPM Devices

The basic idea of the Interpolating SiPM is to assign the cells to one of (usually four) output signals such that the position can be reconstructed. The cell assignment map can be calculated from the chosen reconstruction formula, the easiest embodiment being simply the centre of gravity of four output signals. Maps have been generated for two types of devices with  $120 \times 120$  and  $160 \times 160$  cells, respectively. Using custom 'SKILL' scripts, the maps have been converted to geometrical layout information for technologies with one and two metal layers. Prototype devices have been produced at FBK in Italy. As an example, Fig. 1 shows a corner of a two metal structure.

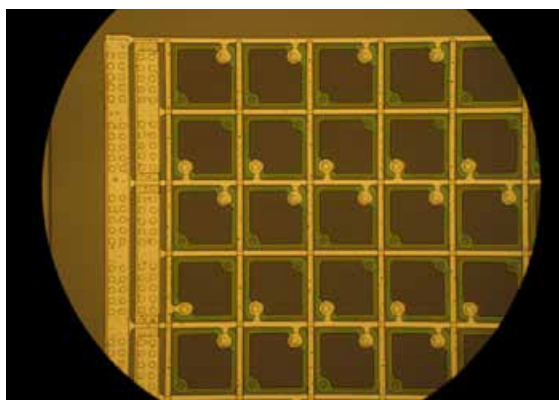


Fig. 1: Micro-Photograph of an ISiPM with  $45 \times 45 \mu\text{m}^2$  cells fabricated in a technology with two metal layers. The two wide metal traces on the left collect two of the four sum signals.



Fig. 2: Test setup showing an ISiPM in a carrier, three scintillation crystals wrapped by diffusely reflecting tape and a radioactive  $^{22}\text{Na}$  source to illuminate the crystals with 511 keV gamma rays. The setup is operated in a dark box.

### Test Setups

The ISiPM devices are glued and wire bonded to ceramic carriers or PCBs for testing. Single crystals (as shown in Fig. 2) or crystal arrays are optically coupled to the active area. In order to protect the surface of the structures from scratches, and to protect the wire bonds, a thin glass plate is glued on the device. The crystals are then irradiated with gamma rays of the typical PET energy of 511 keV from a radioactive source. The four ISiPM signals are amplified by discrete amplifiers (or by our multi channel amplifier chip 'PETA'). Readout has initially been done through a digital oscilloscope. For faster readout with higher amplitude

resolution, a dedicated board with four fast ADCs and USB readout has been developed and commissioned.

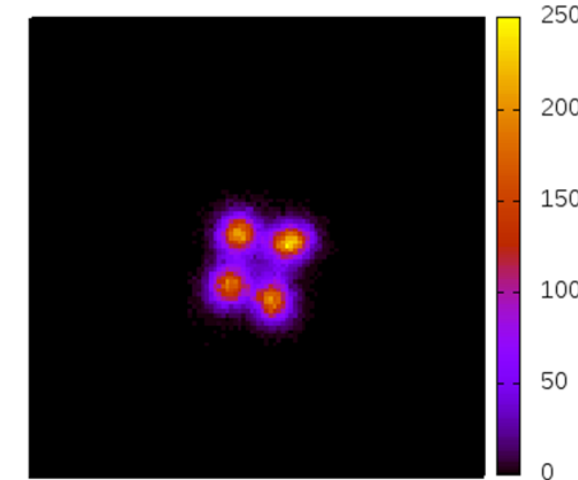


Fig. 3: Measurement showing the reconstructed signal positions when four crystals of  $0.8 \times 0.8 \text{ mm}^2$  size are standing on the ISiPM. The crystals can be clearly resolved.

### Results

The working principle could be immediately confirmed. The achievable spatial resolution depends strongly on the optical properties of the crystal arrays. When the optical separation is bad, i.e. light from one crystal can penetrate to neighbours, the images are strongly compressed (to the centre of the structure) and separation of the individual crystals becomes difficult. When crystals are well isolated optically, very high spatial resolutions can be obtained. As an example, the measurement in Fig. 3 shows that our smallest available crystals of 0.8 mm side length can be clearly resolved. The reconstruction works for arbitrary positions of the arrays on the sensor which is demonstrated by the intentional rotation of the array in Fig. 3.

### Outlook

Characterization will continue using smaller crystal arrays. A new production of devices will be used on a full Sublima module to demonstrate the feasibility of ISiPM in real applications.

Supported by EU within the FP7 project Sublima (contract #241711). Collaboration with FBK, Italy.

### References

[1] Peter Fischer and Claudio Piemonte: Interpolating Silicon Photomultipliers, NIM A718 (2013) 320–322.

## Chip and Module Development for PET/MRI

The next generation of PET Scanners (Positron Emission Tomography) should offer superior performance in terms of spatial resolution and sensitivity. In addition, there is increasing interest in combining functional PET imaging with high resolution and time resolving MRI (Magnetic Resonance Imaging). The new MR tolerant PET scanners must be very compact (to fit into the MR 'tube') and offer high resolution, which is, among other methods, achieved by increasing the number of readout channels. As a consequence, highly integrated solutions for signal amplification and processing and for the mechanical arrangement of the components are required. In the framework of the Sublima EU project, we are developing a fully integrated readout chip for time and amplitude measurement in PET and construct compact MR compatible modules with novel mechanical and thermal concepts.

• Fischer, P., Sacco, I., Ritzert, M. and Blanco, R.

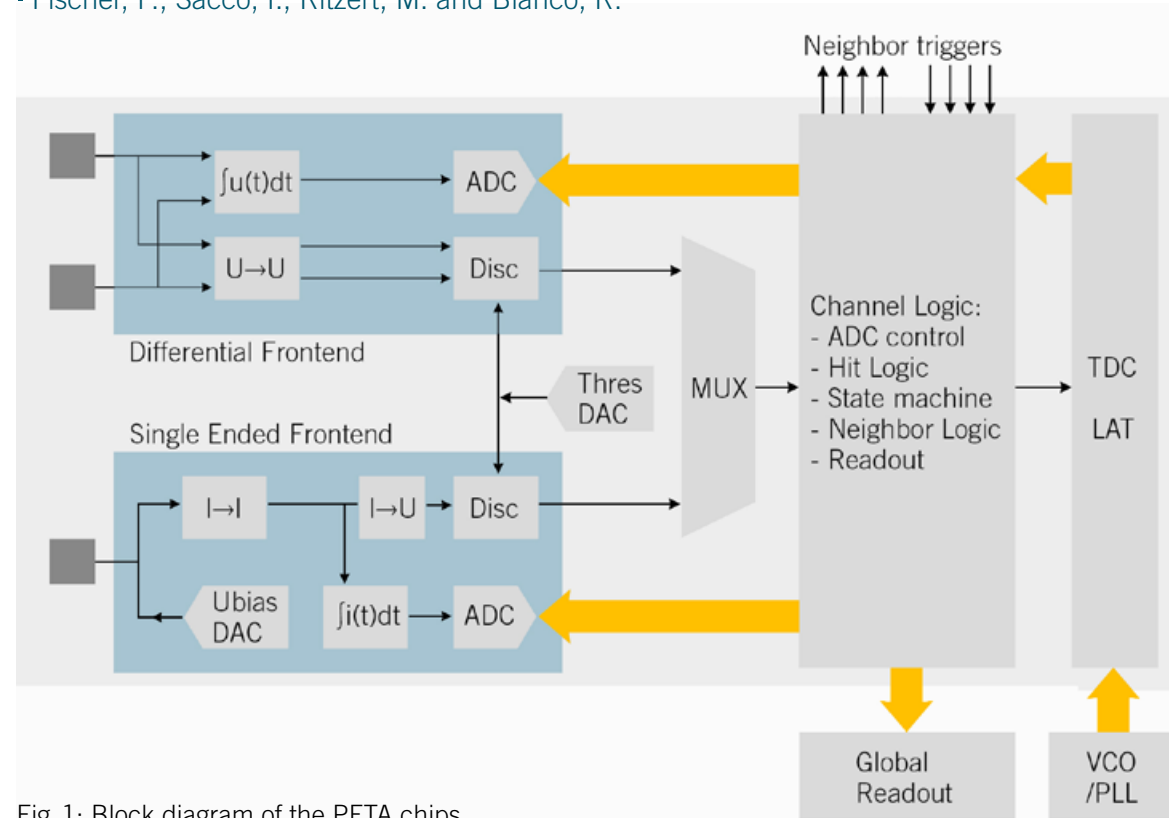


Fig. 1: Block diagram of the PETA chips

### PET/MRI Imaging

The goals of the EU project Sublima [1] are performance improvements of the basic PET components (crystals, sensors, electronics...), the construction and operation of MRI compatible systems and the development of novel methods for data processing and fusion. The operation of a PET detector ring inside a running MR scanner is

a technological challenge, because the high static magnetic field, the fast switching magnetic gradients and the intense RF fields of the MR disturb PET operation on one hand, while the presence of the PET material and its electrical activity must not degrade MR quality on the other hand. The expected benefits are a precise localization of the PET images in the body and the compensation of

patient motion (breathing, heart beat) to avoid motion blurring. Due to the space constraints in the MR bore (and because of an increasing number of heavy patients), the PET ring must be thin. This calls for integrated solutions for sensor readout and for compact modules.

### The PETA Readout Chips

The PETA chip developed entirely at the chair is a fully integrated readout system for 36 channels on a chip area of  $5 \times 5 \text{mm}^2$ . Every channel contains (see Fig. 1) a single ended (more compact) and a differential (possibly more MR tolerant) frontend with a low noise hit discriminator, a charge integrator and an ADC. A detected hit is time-stamped with a precision of 50 ps in a Time-Digital-Converter (TDC). An important feature is a neighbour logic which can trigger channels below threshold for better position reconstruction. The hit information (time, amplitude and channel) is autonomously collected and read out serially. Fig. 2 shows a photograph of the chip which uses solder balls for electrical interconnection for compact module design.

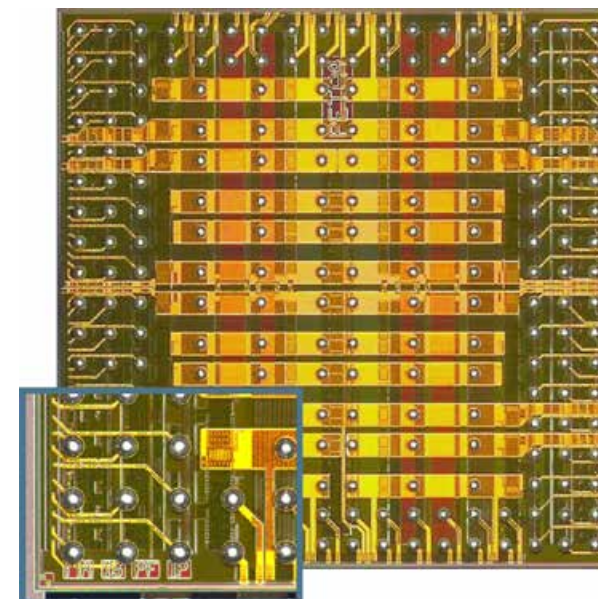


Fig. 2: Photograph of the  $5 \times 5 \text{mm}^2$  PETA4 chip. The connection to the chip is done through solder balls, which are clearly visible in the detail of the corner.

### Compact Module Design

The first generation modules used a stack of three printed circuit boards (PCBs) for a) photo detectors and coupling components, b) the wire-bonded readout ASICs and c) voltage regulators and components for chip control and readout. Cooling of the power dissipated in sensors, ASICs and regulators was achieved by a cooling tube between the PCBs. The next generation design uses ceramic carriers with the photo detectors on one side and flip-chip mounted ASICs on the other side (Fig. 3). Most other components could be eliminated by using a single ended frontend or by adding functionality to the chip. Very efficient cooling is achieved by channels running inside of the ceramic. Suited connection methods for the cooling liquid still need to be developed.

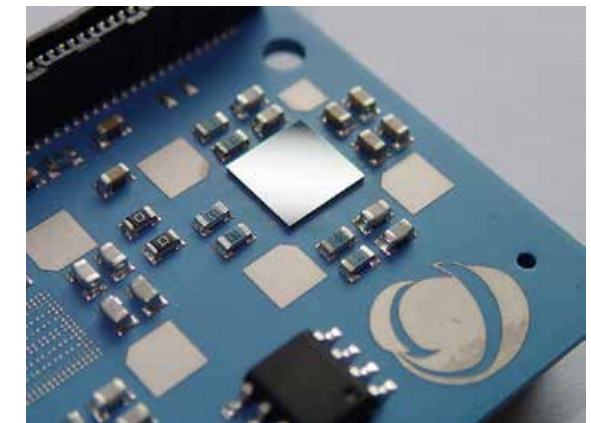


Fig. 3: Ceramic carrier board a one flip chip mounted PETA chip. A second chip can be mounted at the bottom left.

Supported by the EU within the FP7 project Sublima (contract #241711). Collaboration with Philips research, FBK, MSE, Technolution, PDPC, King's College, EPFL and the Universities of Delft, Ghent and Klinikum Aachen.

### References

[1] [www.sublima-pet-mr.eu](http://www.sublima-pet-mr.eu)

## Fast Readout System for the DSSC Detector at XFEL

The X-Ray Free Electron Laser (XFEL) at DESY will produce very intense bursts of photons in the energy range of a few keV. This low energy and the particular time structure (10 bursts per second, each burst containing 2880 photon bunches spaced by 221 ns) require novel detector systems. The DSSC (DEPFET Sensor with Signal Compression) will be 1 MPixel camera which can take up to ~800 pictures per burst, i.e. operate at a frame rate of 4.5 MHz. The data from one burst must be transferred within 100 ms from the pixel chips to the XFEL data acquisition. This is achieved with two specialized boards developed by our group.

• Kirchgessner, M., Soldat, J., Kugel, A. and Fischer, P.

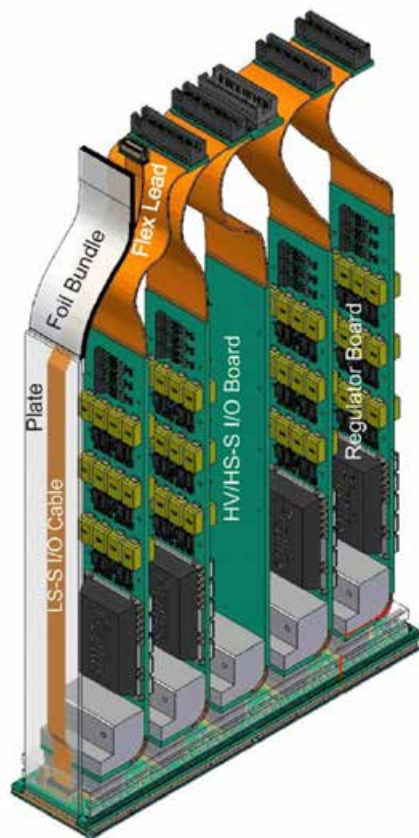


Fig. 1: One module of the DSSC camera. Sensors and ASICs are at the bottom side (not visible). Power is supplied from the top through four Regulator Boards. The module is controlled by the central 'IOB' card.

### The DSSC Detector

The DSSC Camera [1] will be a two dimensional photon detector with 1 million hexagonal pixels of ~206×236 μm<sup>2</sup> size. Signals from DEPFET (De-

pleted Field Effect Transistors) sensors are amplified and immediately digitized with 9Bit resolution in ASICs (see this report) with 4096 pixels each. The events occur at rates of up to 4.5 MHz, so that data is generated in each ASIC with ~166 GBit/second. This rate cannot be transferred with reasonable means, so that the hit data is stored locally in RAMs with space for up to 800 events. The accumulated ~30 MBit are then transferred off-chip during the 100 ms long burst gaps. This requires a rate of only ~300 MBit/second, which is feasible using a single LVDS link per ASIC.

The basic building blocks of the DSSC camera are modules with 16 ASIC (Fig. 1). In order to cover a large area with minimal gaps, all connections to the ASIC (at the bottom of Fig. 1) are coming from the top. Four boards ('Regulator Boards') are used to supply power during the burst. The central board in Fig. 1 is the 'Input Output Board', IOB, which controls the module and collects data.

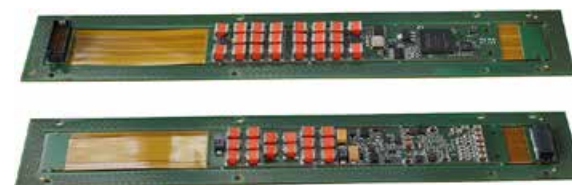


Fig. 2: This 1<sup>st</sup> level data aggregation board 'IOB' will be mounted close to the readout ASICs on the detector. It bundles data and transfers it to the PPT (Fig. 3).



Fig. 3: The 2<sup>nd</sup> level of data aggregation is performed by this Patch Panel Transceiver (PPT). It sends out data through four 10 Gbit optical links.

### The IOB

The IOB collects the data from the 16 LVDS links (one per ASICs), bundles events and sends them away through three serial links running at 3.125 Gbps using the AURORA protocol. It also passes timing information to the module, controls the Regulator Boards on the module (e.g. turns on power just before a burst starts) and provides two additional switched voltages. All functions are performed in an FPGA. During run time, it can be controlled via an embedded PC. The data flow control and the embedded PC require significant firmware and software development. Fig. 2 shows both sides of the production version IOB. A flex-

rigid PCB is used for stress relief of the connectors. A small piggy-back board with additional capacitors will be connected to the top side.

### The PPT

Data from four modules, i.e. IOBs (which corresponds to ¼ of the full camera) is sent to a 2<sup>nd</sup> level data combiner board, the Patch Panel Transceiver (PPT) located at the end flange of the Camera outside of the vacuum volume containing the modules. The PPT (Fig. 3) buffers data from several bursts in a fast DDR3 memory to allow event reordering. The output to the XFEL data acquisition uses four optical links running at 10 GBit/second. Several additional tasks in the PPT, like the control of the camera timing and configuration and monitoring of the IOBs are performed with an embedded PC. The full data chain using prototype ASICs, Regulator- and IOBoards and a PPT has been successfully operated at full speed.

Supported by the EU-XFEL GmbH. Collaboration in this Work Package mainly with DESY.

### References

- [1] M. Porro et al.: Development of the DEPFET Sensor with Signal Compression: a Large Format X-ray Imager with Mega-Frame Readout Capability for the European XFEL, IEEE Transactions on Nuclear Science, Volume 59, Issue 6, Part 2, 2012, Pages: 3339–3351, DOI: 10.1109/TNS.2012.2217755

## The Pixel Readout ASIC for the DSSC Detector at XFEL

Synchrotron X-Ray sources are popular and valuable facilities for material studies and fundamental research. A next big step in intensity and brilliance will be made by the X-Ray Free Electron Laser (XFEL) which is being constructed at DESY in Hamburg. In order to exploit the unprecedented possibilities of the machine, the EU-XFEL GmbH is funding the development of novel 2D detector arrays which can image photons with energies of only a few keV at frame rates of up to 4.5 MHz. The heart of the DSSC 'camera' will be a monolithic 2D-array of DEPFET sensors which convert the X-Ray photons into small current signals. The readout of these signals is done with specialized ASICs which are mounted on top of the DEPFET sensors with many parallel electrical (bump bond) connections. The development of the pixel readout ASIC is lead by our group.

• Erdinger, F., Kirchgessner, M., Soldat, J. and Fischer, P.

### The DSSC Detector

The DSSC Camera [1] will be a two dimensional photon detector with 1 million hexagonal pixels of  $206 \times 236 \mu\text{m}^2$  size. X-Ray photons with energies of as low as 0.5 keV are absorbed in a silicon crystal containing an array of Depleted Field Effect Transistors. These 'DEPFETs' convert the small electric charges generated by the X-Ray absorption into currents ( $\sim 0.5 \text{ nA}$  per electron). The readout of 4096 DEPFET currents is done in parallel by a pixel ASIC mounted on top of the sensor and connected to every pixel with a solder connection.

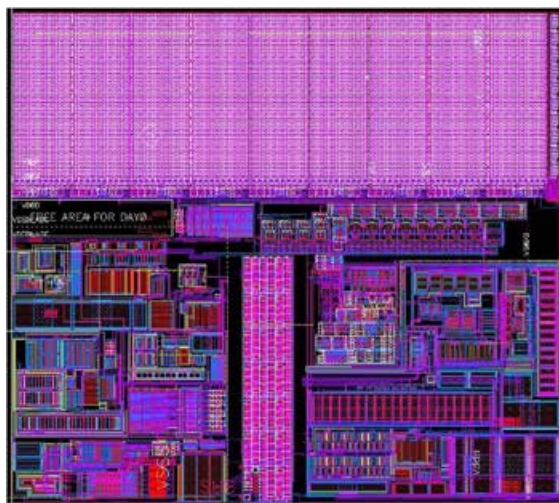


Fig. 1: Layout of one pixel of the pixel ASIC. It has a size of  $206 \times 236 \mu\text{m}^2$  and contains an analogue preamplifier/filter (left), a test injection (bottom

left), an ADC with current and voltage reference (right), a digital control part (bottom middle), time stamp and control signal receivers (right middle) and a large digital memory (top).

### The Pixel Electronics

Each pixel of the ASIC (Fig. 1) contains an amplifier and a switched capacitor filter for noise reduction. The filter output voltage is transferred to a capacitor which is then discharged with a very constant current. The time required to bring the capacitor voltage back to its initial value being proportional to the amplitude is measured in every pixel by storing the status of an 8 Bit 'time stamp' value when the capacitor is discharged. The time stamps are clocked with  $\sim 800 \text{ MHz}$  to achieve one conversion in  $\sim 220 \text{ ns}$ . They are generated in the periphery of the chip (Fig. 2), are distributed along the long columns and received in the pixels with low power differential receivers (see Fig. 1). The digitized values are stored in a dense digital Memory in every pixel for later 'slow' readout so that the camera can take pictures with a frame rate of up to 4.5 MHz until the  $\sim 800$  words per pixel are filled up. Further building blocks in each pixel are a digital control section, a test pulse injector, and switchable decoupling capacitors.

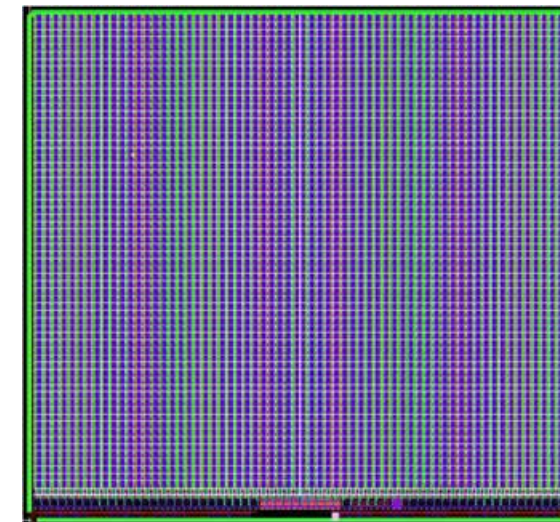


Fig. 2: The final pixel ASIC will have a size of  $15 \times 14 \text{ mm}^2$  with  $64 \times 64$  pixels. All inputs and outputs are at the bottom edge so that two rows of chips can be arranged without dead areas.

### The Pixel ASIC

Most area of the ASIC (Fig. 2) is covered by pixel circuitry. The peripheral part at the bottom contains infrastructure to operate the chip with a minimum of (3 slow + 3 fast) control signals: A programmable sequencer generates all signals required for data talking under various operating conditions, for the management of the RAM addresses (individual events can be discarded during operation to free memory space) and for the readout. Bias DACs are used for current setting and test injection. Fast Gray Counters and buffers with timing adjustments create the global time stamps. The full ASIC has a size of  $15 \times 14 \text{ mm}^2$  and will be produced in a 130 nm CMOS technology.

### Non Linear Frontend

In order to accommodate a very high dynamic range of 1–10000 X-Ray photons with only 8 Bit of ADC resolution, several photons are assigned to higher ADC bins. This does not lead to information loss because the primary photon number is fluctuating anyway due to Poisson statistics.

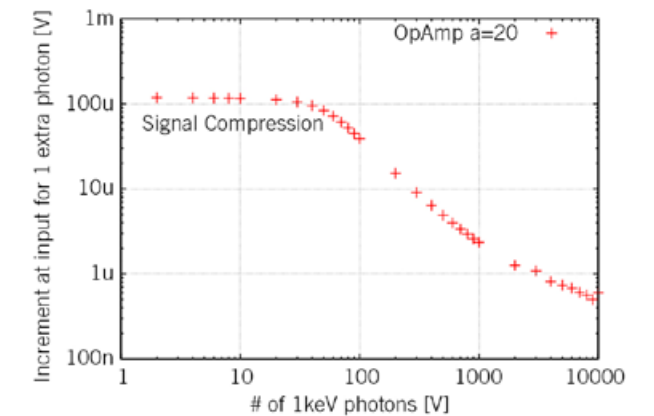


Fig. 3: Simulated gain compression of our novel input stage: The signal per X-Ray photon is constant for a low number of input photons. It drops by over two orders of magnitude for large photon numbers so that the dynamic range is significantly extended.

The signal compression is achieved by a special type of DEPFET device. In order to exploit the feasibility of standard silicon sensors (PiN diodes or silicon drift detectors with lower input capacitance), we have proposed a novel non-linear frontend with a high compression for large signals, as shown in Fig. 3.

Supported by the EU-XFEL GmbH. Collaboration in this Work Package mainly with DESY, Politecnico di Milano and University of Bergamo/Pavia.

### References

- [1] M. Porro et al.: Development of the DEPFET Sensor with Signal Compression: a Large Format X-ray Imager with Mega-Frame Readout Capability for the European XFEL, IEEE Transactions on Nuclear Science, Volume 59, Issue 6, Part 2, 2012, Pages: 3339–3351, DOI: 10.1109/TNS.2012.2217755

## The XNAP Fast 2D X-Ray Photon Detector

Synchrotron light sources like the European Synchrotron Radiation Facility ESRF in Grenoble use their intense, focussed X-ray photon beams to generate diffraction patterns from crystallized samples or to study the atomic composition by fluorescence techniques. In order to image the diffracted X-Rays with high time resolution (Nanoseconds), a novel two dimensional camera based on depleted Avalanche Photo Detectors (APDs) is being developed within the XNAP project. After successful tests with small sensors and ASICs, an array of 1024 pixels using four ASICs is being built.

• Thil, C. and Fischer, P.

The XNAP project (Xray Nanosecond Array of Pixels) has been initiated by detector groups at Synchrotron Photon Sources (ESRF/Grenoble, PETRA/DESY/Hamburg, SPring-8/Riken/Japan) with the aim to develop the next generation of instrumentation for fast, time resolved photon imaging. While present detectors use single or few time resolved photon detector cells, XNAP aims at building a 'large' array with 1024 pixels of  $280 \times 280 \mu\text{m}^2$  size. Fig. 1 shows the basic arrangement consisting of the monolithic array of avalanche photon detector (APD) cells, an interposer for mechanical stability and radiation shielding, and the ASICs for signal processing.

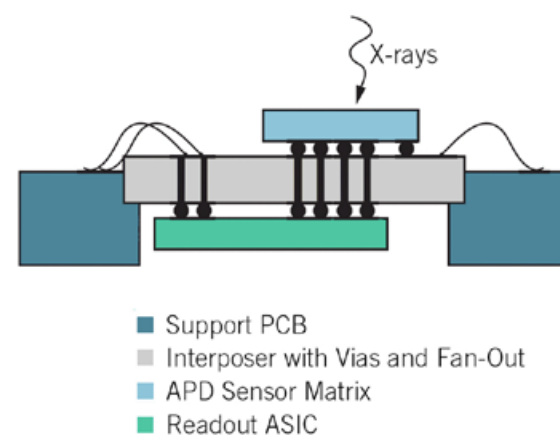


Fig. 1: Cross section of the XNAP assembly: Synchrotron X-Rays impinging from the top are absorbed and amplified in a silicon Avalanche Photo Diode. The sensor is flipped to a passive interposer which passes the signals from all pixels to the readout ASICs mounted to the bottom side.

### The XNAP ASIC

The ASIC (Fig. 2) contains  $16 \times 16$  pixels on an area of  $5 \times 5 \text{ mm}^2$ . Each pixel has a fast amplifier / discriminator with programmable threshold to detect the photon hits. In one operation mode, hits are counted in every pixel with up to 100 million counts/second. By means of a second counter and ping-pong readout, dead time free operation is achieved. In timing mode, individual hits are passed to chip pins with very low time skew so that they can be timed externally with better than 1 nanosecond resolution (the limit being set by drift time variations in the sensor). After associating the hit time to the firing pixel address, the pixel is released. One hit cycle will take  $< 50 \text{ ns}$ .

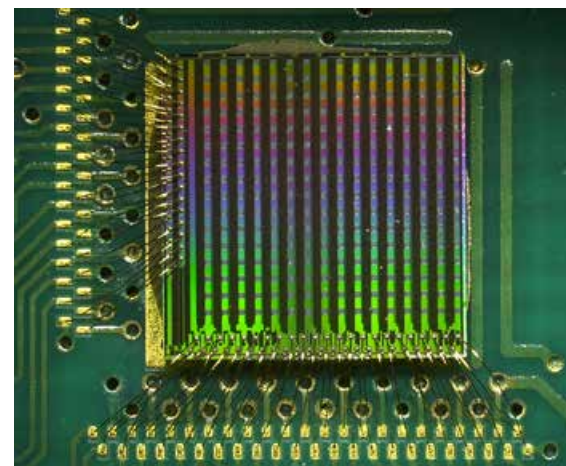


Fig. 2: XNAP pixel ASIC with  $16 \times 16$  pixels on a chip area of  $5 \times 5 \text{ mm}^2$ .

### Module Assemblies

Due to the small pitch of only  $280 \mu\text{m}$ , the production of a suited interposer (see Fig. 1) turned out to be a technological challenge. Several technologies had to be evaluated and prototypes had to be built. Two competing technologies seem to be suitable: A very high density organic printed circuit board has been designed by our partner Excellitas, while we have developed and produced a Low Temperature Cofired Ceramic (LTCC) design. The next challenge is the simultaneous mounting of the sensitive sensors and ASICs on the two sides of the interposer. Fig. 3 shows a PCB interposer with ASICs flip chip mounted by C. Kreidl from our group.

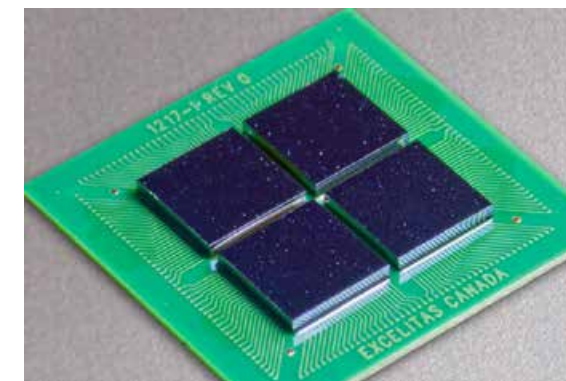


Fig. 3: Four ASICs mounted to an interposer PCB. Ceramic interposers have been produced as well.



Fig. 4: USB based test system used for characterization. The interposers with ASICs and sensors are located under the protective cover at the right.

### Test System

Initial characterization is done with a USB based test system and suited adapter PCBs as shown in Fig. 4. The beam line setup will house most components in a cooled aluminium box and use a dedicated readout card.

Supported by the ESRF and DESY. Collaboration with ESRF (P. Fajardo), DESY (H. Graafsma) and Excellitas (Canada)

### References

[1] Ch. Thil et al.: Pixel readout ASIC for an APD based 2D X-ray hybrid pixel detector with sub-nanosecond resolution, NIMA, Vol. 628, Issue 1, 1 February 2011, Pages 461–464.

## ASICs and Module Design for the Pixel Vertex Detector at Belle II

The Belle Experiment at the KeK accelerator centre in Japan has made significant contributions to B-Meson physics, in particular to parity violation. The topic being still very relevant for understanding the fundamental forces of nature, the KeK machine is being upgraded to a much higher luminosity ( $\sim \times 10$ ), in order to produce significantly more collisions for more detailed studies with better statistics. In order to cope with the resulting enormous event and data rates, and to provide state of the art measurements of the collision products, the existing Belle detector will be upgraded within the next years. The Belle-II detector will also contain a novel pixel detector (PXD) in the very central part of the experiment to improve the measurement precision of the particle decay position. The PXD uses a  $\sim 450 \mu\text{m}$  thin silicon crystal as an active substrate with several flip-chip mounted ASICs for sensor control, readout and digital processing yielding a very low mass tracker. Our group is developing 2 of the 3 chip types, provides the layout of the silicon module, and helps in flip chip mounting and prototype construction.

• Knopf, J., Kreidl, C., Peric, I. and Fischer, P.

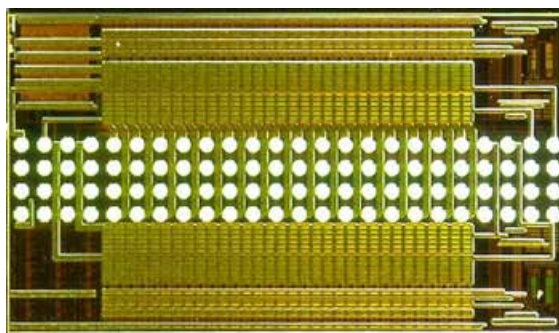


Fig. 1: Photograph of the SWITCHER chip which controls the readout of the DEPFET Matrix. The Bumps are all connected in a peculiar pattern in the centre to simplify routing on the small edge of the module (Fig. 3).

### The BelleII Pixel Vertex Detector

The Pixel Vertex Detector (PXD) of BelleII is located at a few centimetre distance of the collision point and is the first element to track the flight path of the generated collision particles. As any material traversed by the particles deflects their flight path, a very thin ('low radiation length') tracker is required. The PXD addresses this by using the active silicon substrate as a mechanical support for the readout ASICs. The sensing ele-

ments are pixels with an integrated Depleted Field Effect Transistor (DEPFET). They are read out in a 'rolling shutter' mode, i.e. by enabling one row after the other. This requires fast voltage transients of  $\sim 20\text{V}$ , provided by special SWITCHER chips (Fig. 1) developed by our group. The DEPFETs send signal currents to the end of the active area where Drain Current Digitizers (DCD) chips (also developed by us) digitize the signals and pass them to Data Handling Processor chips (DHP, by Bonn University and Spanish groups) for digital processing and serial readout.

### The PXD Module

Fig. 2 shows a PXD Module prototype which contains all routing for the 14 ASICs on only 3 metal layers. Additional SMD components are required for decoupling, energy storage and line termination. The prototype module shown has test structures instead of real DEPFETs in the large active region. When populated with chips (as shown in the lower part of Fig. 2) and connected with a capton cable, all functionalities can be tested.

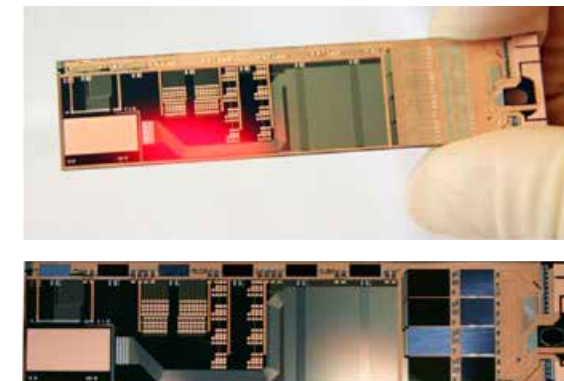


Fig. 2: This silicon substrate shows the (small) size of one PXD module (top), compared to a finger. The lower picture shows the same module after assembly of six SWITCHER chips (top row), four DCD chips and four DHP chips (right). A flexible capton cable will be glued and wire bonded to the right side.

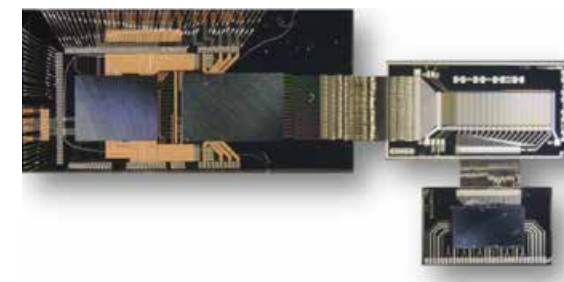
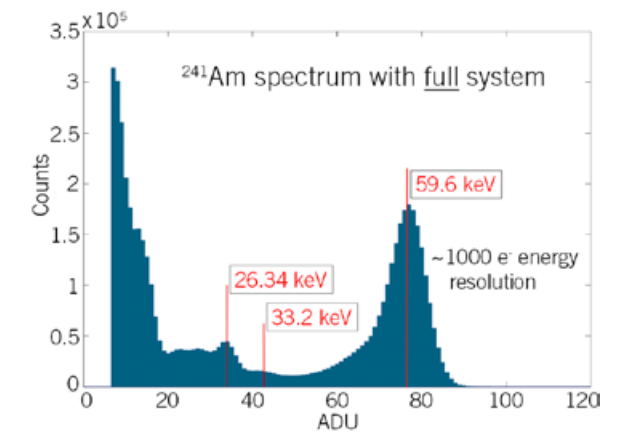


Fig. 3: Test arrangement with most relevant components: A small DEPFET sensor matrix is located in the upper right. It is controlled by a SWITCHER chip (as shown in Fig. 1) which is flipped on an auxiliary substrate and wire-bonded to the sensor (bottom right). The readout is achieved by a DCD chip and an additional driver chip flipped to a second substrate (left).

### Detector and Chip Tests

In order to test all critical components during the development, smaller test setups like the one shown in Fig. 3 have been assembled (see text in caption). The large number of different parts and interconnection technologies make this a mechanically very challenging task. As an example of a successful measurement using realistic Belle-II speed, Fig. 4 shows a  $^{241}\text{Am}$  spectrum taken with a setup similar to Fig. 3.



Supported by BMBF under contact number 05H09VH8. Main partners are MPI Munich, Universities of Bonn, Aachen, Siegen, Valencia, Barcelona, Krakau...

### References

[1] J. Knopf, P. Fischer, C. Kreidl and I. Peric: 256 Channel 8-Bit Current Digitizer ASIC for the Belle II PXD, JISNT 6 (2011) C01085 (Volume 6, January 2011), doi:10.1088/1748-0221/6/01/C01085

## CHAIR OF COMPUTER ARCHITECTURE PROJECT OVERVIEW

• Prof. Dr. Ulrich Brüning

### **50 | Chair of Computer Architecture – An Introduction**

Brüning, U. and team

### **54 | Customized Hardware and Interconnection Network Development for the CBM Project at Fair**

Lemke, F., Schatral, S. and Brüning, U.

### **56 | The DEEP Project**

Nüssle, M. and Brüning, U.

## Chair of Computer Architecture – An Introduction

• Brüning, U. and team

The ZITI chair for Computer Architecture at the University of Heidelberg has the expertise to design complex hardware/software systems. As system architects, we not only cover the theory of operation, we also have the technology and the software to build real working prototypes. The Computer Architecture Group (CAG) has profound expertise in the areas of design space analysis, hardware design of processors and devices, interconnection networks, and software driver development, especially for the construction of large computing clusters based on PC technology.

All levels of system design are covered, starting at the application programming interface, e.g. the message passing interface library (MPI), through the efficient design of device drivers, and finishing with custom-built hardware devices based on standard-cell ASIC and FPGAs.

The goals of the applied research activities are to cover a broad range of methodologies for the design of complete high performance systems with the possibility to optimize every level and educate students on the various real world topics.

The group mainly focuses on the design of parallel architectures, which achieve their high performance by improving communication between computational devices/units. Scaling such systems is a great challenge to the architecture of interconnection networks (IN) and network interface controllers (NIC). The EXTOLL project is an examples where a holistic optimization approach leads to a very low latency and high performance network interface controller (NIC).

In 2012 the spin-off company EXTOLL GmbH was able to acquire the necessary capital in order to manufacture a high performance ASIC based on EXTOLL technology. The cooperation between CAG and EXTOLL was increased to build the ASIC backend team. Most of the components for an

ASIC had been prepared, e.g., the standard cells, the IO cells and the SRAM generators. Also the very important function of a serializer-deserializer (SerDes) for the PCIe interface and the communication links had been evaluated before to make sure this part could be purchased from an Intellectual Property (IP)-provider in a silicon-proven design. SerDes functions are getting more and more important in the design of high performance chips, because they provide a significant higher bandwidth per IO-pin than standard IO-cells and thus try to overcome the pin limitation constraint.

The design team established a tool flow in cooperation with Cadence, an EDA-company and a long-term partner in research and education for analog and digital hardware designs.

Extensive regression tests have been executed for the digital parts to make sure that we could verify all functional modules and try to be first time right with our ASIC.

The backend work went well until the day in September 2012, when we needed the SerDes IP for integration, and EXTOLL wanted to sign the contract for the IP. Just at this point in time the IP-company was sold and got out of the SerDes business. This was a stroke of fate which shifted our chip submission to an unknown time in the future. All efforts were made to find a new IP-Provider, but no other silicon-proven SerDes for our selected process technology could be found. Thus we had to negotiate a deal with an IP-company which proposed to design a SerDes concerning our specification in a time frame of 3 months, which delayed the project into next years reporting time of 2013. While we are busy working on the very exciting ASIC project with the code name Tourmalet we were also carrying out further development projects for industry partners and also research for the BMBF-funded project CBM and for the EU-funded project DEEP.

DEEP must be viewed as closely related to the EXTOLL ASIC Tourmalet. The architecture design of the DEEP project is unique because of its separation of weak scaling and strong scaling parts of applications into specific computing parts called cluster and booster. For the booster part, EXTOLL was selected as interconnect because of its very low latency and its high message rate. The booster computing engine is the Intel Xeon Phi chip (KNC) which contains 60 CPUs, a high bandwidth memory interface and a PCIe interface. The EXTOLL ASIC matches this x16 PCIe interface perfectly and could drive the Xeon Phi without any other logic. While the ASIC was under development, we adapted the FPGA version of EXTOLL to a prototype board from one of the project partners, EuroTech, equipped with an Altera Stratix 5 in order to make a Proto-Booster system available for the software development in the DEEP project. In addition, EuroTech sponsored the porting of EXTOLL to their Stratix 4 FPGA on node board based on Westmere /SandyBridge Intel CPUs with 30k Euros. This task was completed successfully for the Westmere Intel CPU board, but the new CPU type SandyBridge board showed some strange behavior in the power supply of the FPGA so that the second port could not be completed.



Fig. 1: EXTOLL ASIC Tourmalet

Another industrial partner for the application of EXTOLL is a company working in the area of vision processing for wafer inspection. They continued

their support with a grant of 30k USD for the completion of a prototype test using Xilinx V7 FPGAs. This project showed many problems due to the use of initial engineering sample FPGA chips from Xilinx. The expected data rate of 10Gb/s could not be achieved due to missing software support in the design environment, and the PCIe core was not capable to operate at the gen3 data rate. Therefore, only parts of the design could reach the projected bandwidth. There will be further development work required to achieve the 10GB/s bandwidth.

In the reporting periode 2012 EXTOLL/CAG has jointly presented the results of our research at many events mainly at ISC 12 in Hamburg and at SC12 in Salt Lake City, USA. In cooperation with the JP Holger Froening from ZITI, we could demonstrate a direct method of communication between NVIDIA GPUs without host intervention at the SC12. This feature was of great interest to NVIDIA, and some closer collaboration was agreed upon for the near future.

An invited talk at the EUROMPI in Vienna was also given and provided the MPI programming community with the latest news of the EXTOLL project.

In October, a workshop at the A\*STAR computing center in Singapore was arranged by Dr. Marek Michalewicz, a senior director at A\*STAR. We attended it and found many common interests in research for parallel computing. Therefore it was agreed to intensify the collaboration between CAG and A\*STAR. In addition, connections to a group in China have been established.

The industrial cooperation with the high-frequency trading company IMC has continued. Two of our excellently educated Ph.D. students have been hired by the company. In 2012, the continuation phase of the project was funded with about 116 k Euro. Specific functional units for the support of trading have been added to the design.

For the CBM project, a new 3 year project proposal was prepared and submitted to the BMBF in 2011. The project was funded in 2012, but with significant reduction in personal budget, and there was significantly less money assigned for the development of an ASIC for the read-out chain in the CBM detector system. This ASIC has been found to be necessary due to space limitations in the inner detector design and CAG has agreed to develop this chip. Due to the budget cuts, this plan was reduced to first prototypes and test chips.

In order to design and develop complex hardware components, CAG runs some internal developments in the area of EDA tools for closing specific design gaps. This is mainly done for productivity reasons and for raising the level of abstraction in the design phase.

For the design of finite state machines, our FSM-Designer has been improved for the next release. The development of the tool has been continued as an open source project on Source Forge.

The CAG of the University of Heidelberg is member of the Cadence Academic Network and plays a major role in this network, as we are the "Lead University for Functional Verification". The Cadence Academic Network is a university/industry collaboration to support and improve Universities' activities in the design of analog and digital semiconductors and to educate students with the latest tool generation. This project continues, and the network idea established many new connections among the member universities. In the area of chip design, CAG is working with Prof. Stefan Heinen from RWTH Aachen, and first results have been successfully used by both groups.

The collaboration with ST Microelectronics, which started in 2011, did not show any results due to high communication latencies. Information exchanges have been completed, but no results were achieved so far. It seems to require significantly more personnel effort and a much longer time frame.

## Customized Hardware and Interconnection Network Development for the CBM Project at Fair

• Lemke, F., Schatral, S. and Brüning, U.

The Computer Architecture Group's (CAG) activities within the Compressed Baryonic Matter Collaboration at the Facility for Antiproton and Ion Research (FAIR) at GSI Darmstadt focus on the design and implementation of the DAQ system. For the CBM read-out chain from the FEE detector ASICs to the cluster, a hierarchical network structure was developed [1], which is optimized for the CBM experiment. In addition to providing a built-in network communication block, the idea was to create a set of modules with well-defined interfaces and functions, which can be used in different CBM network devices. Thus, they can benefit by reusing well-tested hardware. This approach saves design time and uses reliable components. The goal is to provide this set of generic modules not only for FPGAs, but also for the FEE ASICs. The generic modules include the CBMnet implementation, some special PHY implementations, and deliver features generally required in CBM network devices. These features include: an automatically generated register file (RF) supporting user-specific parts for analog designers, an I2C interface for debug and test purposes, special blocks for analog register chain access or sub-RFs, and serializers/deserializers (SERDES) implementations for different technologies to provide required communication bandwidth to all CBM network parts. Various FPGA implementations use this concept and it is used within a first FEE ASIC for its digital communication block, the SPADIC [2]. The test readout chain for SPADIC testing is shown in figure 1. After the first successful tests configuring the SPADIC and reading out its configuration, tests verified that data, control, and synchronization messages work reliably. These results gave the confidence to integrate these modules also into other ASICs. Thus, they were

integrated into the STSXYTER, which was submitted in Q3 of 2012. All setups are prepared and its testing is planned for Q1 2013.



Fig. 1: Beam time readout and laboratory setup

Delivering the readout density required for CBM is a challenging task. Therefore a specific intermediate ASIC for early data aggregation and FEE control is planned. This device, the HUB ASIC [3],[4], is planned to provide at least 32 front-end links each with 500Mb/s and up to 4 back-end links with at least 5 Gb/s. There are various difficult tasks to handle within this device including deadlock avoidance for all traffic types. A block diagram of the inner HUB ASIC structure is presented in figure 2. It depicts the handling of the three virtual traffic classes and shows its general structure. First prototyping for design parts has been done using Xilinx Spartan 6 evaluation boards. The new Spartan based ROC, currently developed in the collaboration, will provide a platform for further prototyping. The target technology for the HUB ASIC is 65nm and a miniASIC submission will be prepared in 2013.

Supported by: BMBF (06HD9117I, 06HD7137), Cooperation with GSI

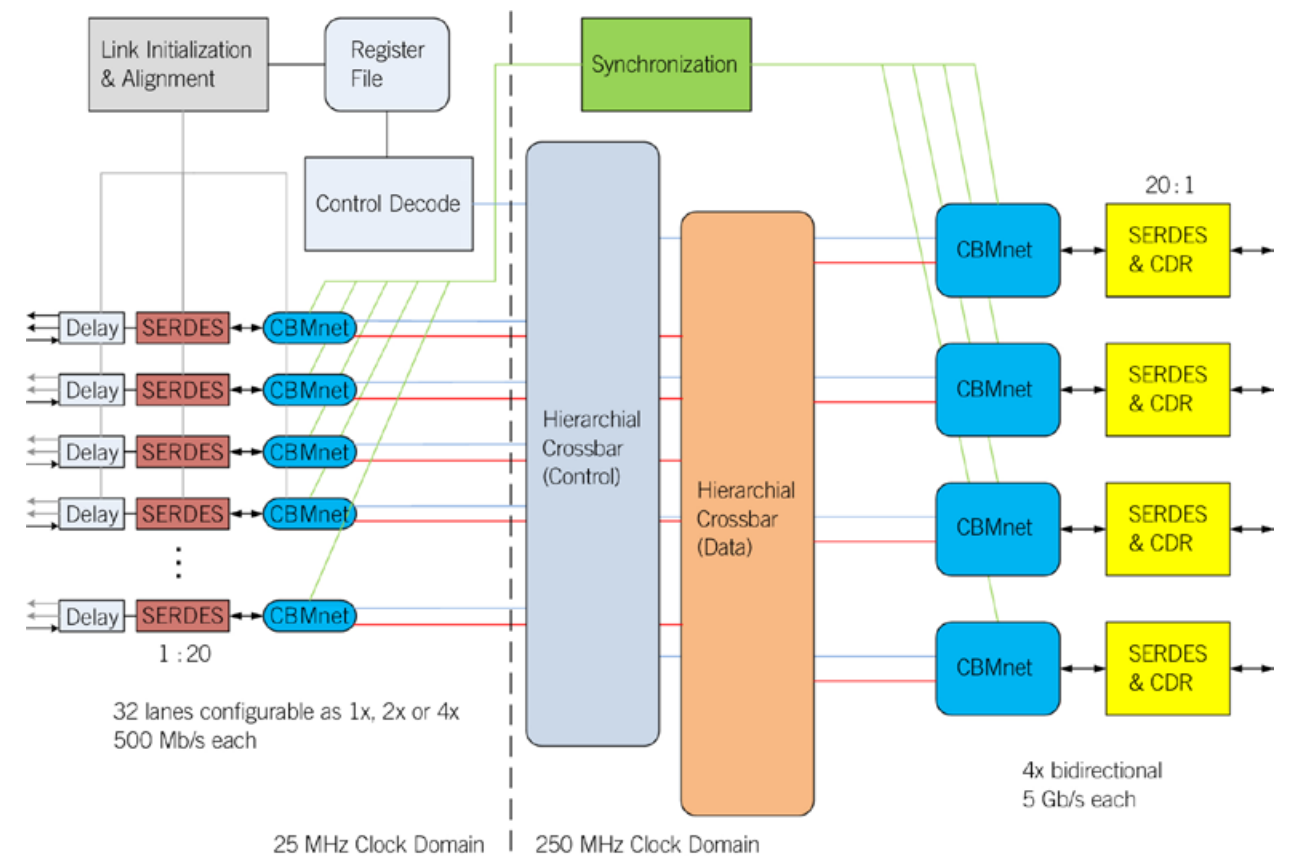


Fig. 2: Block diagram of HUB ASIC data path.

### References

- [1] Lemke F., Schenk S., Bruening U., "The Hierarchical CBM Network Structure and the CBMnet V2.0 Protocol", Deutsche Physikalische Gesellschaft EV (DPG12), Frühjahrstagung, Mainz, Germany, March 19-23, 2012.  
[2] Armbruster T., Fischer P., Krieger M. and Peric I., "Multi-Channel Charge Pulse Amplification, Digitization and Processing ASIC for Detector Applications", 2012 NSS Conference Record (IEEE), Anaheim, USA, October 2012.

- [3] Lemke F., Bruening U., "Design Concepts for a Hierarchical Synchronized Data Acquisition Network for CBM", IEEE 18th Real-Time Conference 2012 (RT12), Berkeley, CA, USA, June 11-15, 2012.  
[4] Frank Lemke, "Unified Synchronized Data Acquisition Networks", Ph.D. thesis, University of Mannheim, Mannheim, Germany, Nov. 2012.

## The DEEP Project

• Nüssle, M. and Brüning, U.

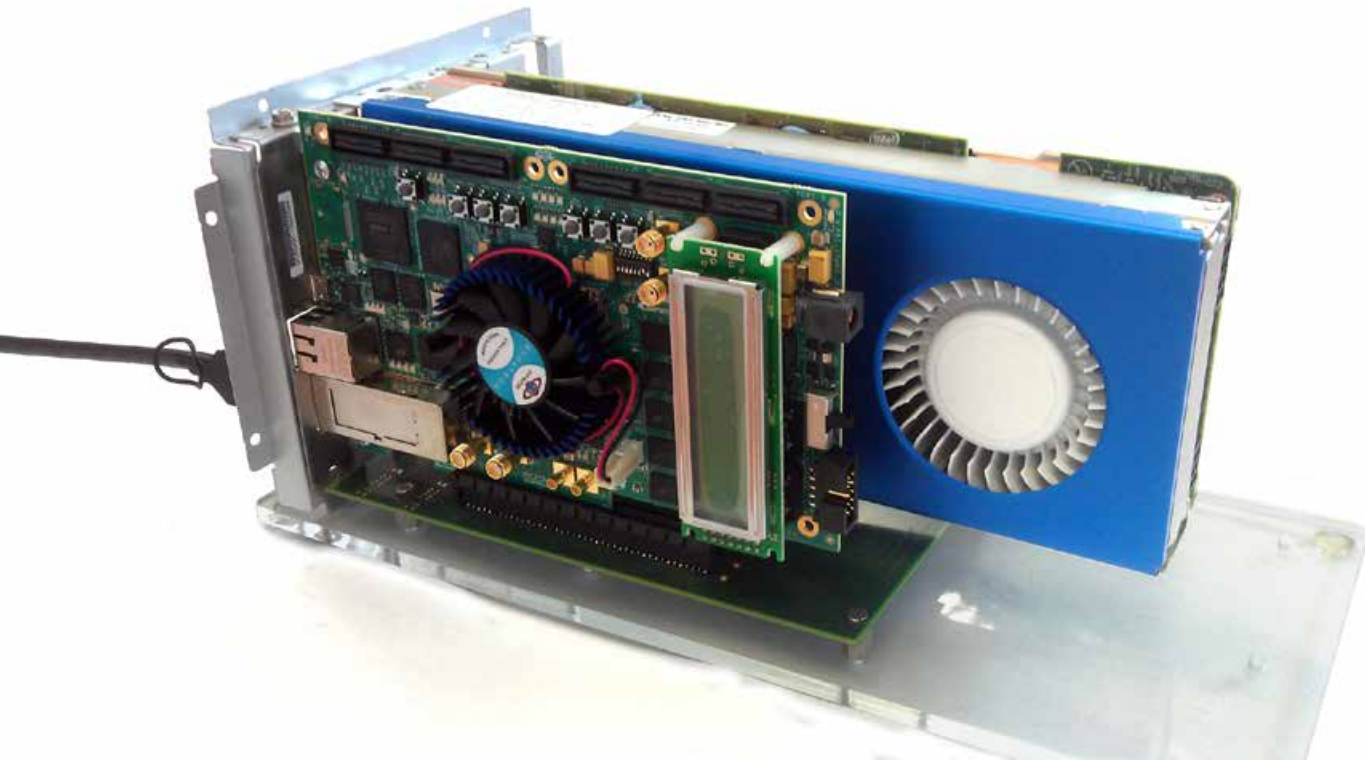


Fig.1: Prototype Backplane with Galibier and KNC

The EU-funded DEEP project was started in December 2011 and worked on the architecture definition and the first prototype implementations throughout 2012. The main objectives of the project are defined as follows:

“The Dynamical Exascale Entry Platform project (DEEP) proposes to develop a prototype hardware and software supercomputing system with the potential to reach a peak performance of 100 PFlop/s in 2014, paving the way towards Exascale end of the decade. DEEP will optimise a set of grand-challenge applications with high societal impact and generic algorithmic structure for this platform. The key innovation of the DEEP project is its holistic Exascale-enabling concept integrating the architectural, system software and appli-

cation level. The strategic goals of DEEP are (i) to contribute to an independent provision of general purpose Exascale performance supercomputers for the European HPC research infrastructure PRACE, (ii) to advance the growth of ICT and HPC hardware and software technology developed and produced in Europe, and (iii) to expand worldwide leadership and competitiveness of Europe’s computational scientists and engineers” [1].

The main architectural goals of the DEEP project are summarized in the following three paragraphs. An innovative prototype hardware platform will be developed consisting of a Cluster element based on multi-core-chips (supporting the weak scaling part of applications with high single thread perfor-

mance) and a Booster element based on many-core technology (supporting the highly parallel portion of applications with strong scaling). The elements are connected by appropriate interconnects, following the commercial-off-the-shelf philosophy. [2]

Innovative and modern technologies are combined for the Booster element: the Intel many-core processors (Intel Xeon Phi, codename Knights Corner KNC) and the high-speed interconnect EXTOLL. Improvement of current cluster energy efficiency by an order of magnitude will result in a power usage effectiveness approaching a value of 1. This can be achieved by exploiting novel many-core chip technologies and advanced software-aided cooling technologies using hot water cooling.

The project is organized in 9 workpackages (WP) and the Computer Architecture Group (CAG) is participating in WP3, WP4 and WP9.

- WP3 System Hardware
- WP4 System Software
- WP9 Exascale Projections

The architecture design of the DEEP project is unique due to the separation of weak scaling and strong scaling parts of applications into specific computing parts called Cluster and Booster. For the booster part, EXTOLL was selected as the interconnect because of its very low latency and its high message rate. The Booster computing engine is the Intel Xeon Phi chip (KNC) which contains 60 CPUs, a high bandwidth memory interface and a PCIe interface. The EXTOLL ASIC codename “Tourmalet” would perfectly fit to this x16 PCIe interface and could drive the Xeon Phi without any other logic.

To demonstrate the feasibility of this “hostless” setup, CAG developed, designed, and brought up a PCIe backplane which can connect two x16 boards directly. We used the PCIe FPGA board “Galibier” to connect to the KNC and implemented the required software for the transparent map-

ping of external control messages to the KNC. Initial peer to peer device communication tests with the EXTOLL network were conducted by CAG.

While the ASIC was under development, we adapted the FPGA version of EXTOLL to a prototype board from a project partner, EuroTech, equipped with an Altera Stratix 5 in order to make a Proto-Booster system available for software development within the DEEP project. This task was much more difficult than expected and could not be completed in 2012.

In the 2012 reporting period, EXTOLL/CAG jointly presented DEEP research results at ISC 12 in Hamburg and at SC12 in Salt Lake City, USA. AT SC12, we participated in the joint European Exascale booth to explain the conference attendees the advantages of the DEEP concepts [3].

### References

- [1] FP7-ICT-2011-7 Integrated project proposal: DEEP, Large scale integrating project (IP), Exascale computing, software and simulation, Prof. Dr. Dr. Thomas Lippert.
- [2] Alvarez Mallon, D.; Eicker, N.; Innocenti, M.E.; Lapenta, G.; Lippert, T.; Suarez, E.; On the scalability of the clusters-booster concept: a critical assessment of the DEEP architecture, FutureHPC ‘12, in: Proceedings of the Future HPC Systems: the Challenges of Power-Constrained Performance, ACM New York, NY, USA, 2012, 978-1-4503-1453-4, Article No. 3.
- [3] DEEP-Project web page: [http://www.deep-project.eu/deep-project/EN/Home/home\\_node.html](http://www.deep-project.eu/deep-project/EN/Home/home_node.html).

## CHAIR OF COMPUTER ENGINEERING PROJECT OVERVIEW

• Juniorprof. Dr. Holger Fröning

**60 | The Computer Engineering Group – An Introduction**

Fröning, H.

**62 | Efficient Communication Schemes**

Fröning, H.

**64 | The Onchilla Runtime for Accelerated Clusters**

Fröning, H., Young, J., and Yalamanchili, S.

## The Computer Engineering Group – An Introduction

### Application-specific Computing of Compute- and Data-intensive Problems

• Fröning, H.

#### Overview

The Computer Engineering Group (<http://ce.uni-hd.de>) was established in November 2011, and is responsible for the specialization “Application-specific Computing” within the Master of Science in Computer Engineering at the Ruprecht-Karls University of Heidelberg. The current research is exploring parallel architectures for High Performance Computing and Big Data, for instance the efficiency of parallel computing in terms of performance and productivity, energy-aware computing, high performance computing architectures, and the use of specialized devices for compute-intensive and data-intensive tasks. In particular, GPU Computing in combination with data-intensive problems has moved into the research focus. During 2012, the group expanded to 10 people total, including associated PhD students and research assistants.

The group strongly collaborates with the group led by Jose Duato at the Technical University of Valencia (Spain), the group led by Sudhakar Yalamanchili at the Georgia Institute of Technology (Georgia, US), and the group led by Fransisco Quiles at the University of Castilla-La Mancha (Spain). Furthermore, a local collaboration with the group led by Ulrich Brüning exists.

Besides regular dissemination in form of publications, the group is periodically presenting latest research results at the exhibitions of the Supercomputing Conference (US), and the International Supercomputer Conference (ISC) in Germany. Also, the PI of the group is co-organizer of the annual international workshop on “Heterogeneous Unconventional Cluster Architectures and Applications” (HUCAA), held in conjunction with the “International Conference on Parallel Processing” (ICPP) [1].

The group is also responsible for the CUDA Research and Teaching Center at the Ruprecht-Karls University, providing teaching related to GPU Computing to students, consulting to PhD candidates and of course exploring research questions within this context.

#### Research Projects

The current research focus of the group is to employ specialized architectures for HPC workloads to improve the efficiency of parallel computing, both in terms of energy and time. In addition, we try to use insights from the HPC area to other areas, in particular for workloads related to Big Data. The most important examples of such workloads are information retrieval, data-mining and data-warehousing. In the following, we present a short excerpt of current research efforts:

· GGAS: Modern GPUs are powerful high-core-count processors. They are no longer used solely for graphics applications, but are also employed to accelerate computationally intensive general-purpose tasks. For peak performance, GPUs are distributed throughout the cluster to accelerate parallel portions of the workload. Current solutions typically combine the bulk-synchronous task model of GPUs with message passing semantics, which significantly increases complexity and requires the CPUs to communicate among distributed GPUs. Global GPU Address Spaces (GGAS) span over the device memories of GPUs at the cluster level for sharing and aggregation purposes. GGAS allow low overhead synchronization and efficient data movement between GPUs and confine control flow to the GPU domain for all computation and communication tasks. Both aspects contribute to time and energy savings. In addition, GGAS maintain the GPUs bulk-synchronous programming model by relying on a thread-collective com-

munication model, which reduces the complexity of parallel programming on distributed GPUs significantly. Furthermore, GGAS is a zero-copy communication mechanism and avoids the complexity associated with hybrid programming paradigms like MPI+CUDA or similar.

· ONCILLA: Oncilla is a new project lead by Sudhakar Yalamanchili from Georgia Tech that aims to provide a commodity-based non-coherent global address space (GAS) to support efficient data movement between host memory (DRAM) and accelerators (GPUs) using tightly integrated “converged fabrics”. By using a custom NIC, low-latency, non-coherent put/get operations are available to access remote memory and to build a large, non-coherent GAS system [2].

· MEMSCALE: A new memory architecture for clusters and datacenters, with the objective to overcome memory capacity constraints and to minimize over-provisioning of scarce resources. Key are global address spaces (GAS) across physically distributed resources. The scalability problem of coherence is addressed by reverting to highly relaxed model consistency models. Goal of this work is to overcome the current static resource partitioning in clusters, and thereby to facilitate a highly dynamic aggregation and disaggregation of resources. This approach can help to dramatically reduce resource over-provisioning and to maximize utilization, thus improving the energy-efficiency of clusters and datacenters. First results include the acceleration of in-memory databases, the acceleration of data-intensive applications and combining the scalability of message passing with the ease of programming of shared memory for future multi-/many-core architectures. This is a collaboration with the Parallel Architectures Group led by Jose Duato at the Technical University of Valencia, Spain.

· EXTOLL: A new ultra-low latency cluster interconnect designed from scratch for the use in HPC systems. Key properties are high message rates, high scalability and inherent support for multi-core processors by virtualizing the network interface. Current FPGA implementations of this de-

sign are able to outperform state-of-the-art silicon for selected applications and benchmarks. This is a collaboration with the Computer Architecture Group led by Ulrich Brüning at the same institute and the EXTOLL company [3].

For a more detailed description of the GGAS and ONCILLA project, we refer to dedicated articles in this report.

#### Additional Dissemination of Results

In addition to the previously stated dissemination efforts, in 2012 two invited talks were given. The first talk was at the Systems Seminar at Georgia Tech (US) [4], and included a review of the research issues addressed within the MEMSCALE project and possible future work. The second talk was at the Annual Computer Science Day at the Ruprecht-Karls University of Heidelberg [5], and investigated how cloud computing can benefit from dynamic resource aggregation techniques like MEMSCALE.

We gratefully acknowledge the generous support of our research efforts by NVidia Corporation, and Xilinx, Inc.

#### References

- [1] Workshop on Heterogeneous Unconventional Cluster Architectures and Applications (HUCAA), <http://www.hucaa-workshop.org>
- [2] The Oncilla Project, <http://gpuocelot.gatech.edu/projects/compiler-projects/oncilla-gas-infrastructure>
- [3] The EXTOLL company, <http://www.extoll.de>
- [4] Fröning, H.: “MEMSCALE: A New Memory Architecture For Clusters”, CERCS Systems Seminar, sponsored by Sudhakar Yalamanchili, Georgia Tech, April 11, 2012, Atlanta, GA, US.
- [5] Fröning, H.: “(Weather) Forecast: Mostly Cloudy”, Annual Computer Science Day at Ruprecht-Karls University of Heidelberg, June 22, 2012, Heidelberg, Germany.

# Efficient Communication Schemes for Data-Parallel Processors

A new technique allowing GPUs to autonomously source and sink network traffic  
• Fröning, H. and Oden, L.

## Overview

Modern GPUs are powerful high-core-count processors, which are no longer used only for graphics applications, but are also employed to accelerate computationally intensive general-purpose tasks. For the utmost performance, GPUs are distributed throughout the cluster to assist the CPUs in processing parallel programs. While GPUs can help minimizing execution time for a variety of applications, in particular for distributed systems several severe limitations are present: first, the communication between GPUs requires CPU assistance and often intermediate copies, both with huge impacts on energy and time. Also, the common communication approach for clusters, message passing, is conflictive with the GPU thread-collective task model, thus the user has to employ multiple programming paradigms. Last, all heterogeneity and concurrency is exposed to the user instead of using suitable abstractions to maintain the beauty and simplicity of the GPU's task model.

Here we present a new innovative approach that allows for the first time to maintain the GPU's thread-collective execution model for communication purposes. Using this approach, the beauty and simplicity of GPU Computing can be maintained and the overhead associated with hybrid communication mechanism can completely be avoided.

## Global GPU Address Spaces

We recently introduced Global GPU Address Spaces (GGAS) as communication model that is completely in-line with the GPU task model and facilitates a direct communication between distributed GPUs. The following list shows the contributions of GGAS compared to previous work:

1. GGAS maintains the GPUs bulk-synchronous,

massively parallel programming model by relying on thread-collective communication.

2. Opposed to communication layers based on message passing, GGAS minimizes branch divergence, as communication can be performed by all threads in a block collaboratively.

3. GGAS allows confining the control flow to the GPU domain, bypassing the CPUs for all computation and communication tasks and avoiding context switches that are costly in terms of energy and time.

4. GGAS is a direct, zero-copy communication model that moves data without intermediate copies between distributed GPU memories, again contributing to the minimization of time and energy.

Figure 1 shows the system and the user view of a GGAS cluster. The system view is composed of distributed nodes, each equipped with a GPU for acceleration purposes and connected to a network. Without GGAS, each GPU in the system has only access to local resources, and communication requires huge effort and imposes large overhead.

However, using GGAS this system view is translated into a simplified user view, which aggregates the distributed GPU's special memory and maintains the Bulk-Synchronous Parallel (BSP) model of the processing cores. Now, each GPU respectively each GPU core can access any memory location in the system. Although this is location-independent, it is certainly beneficial to expose locality to the user to allow appropriate optimizations.

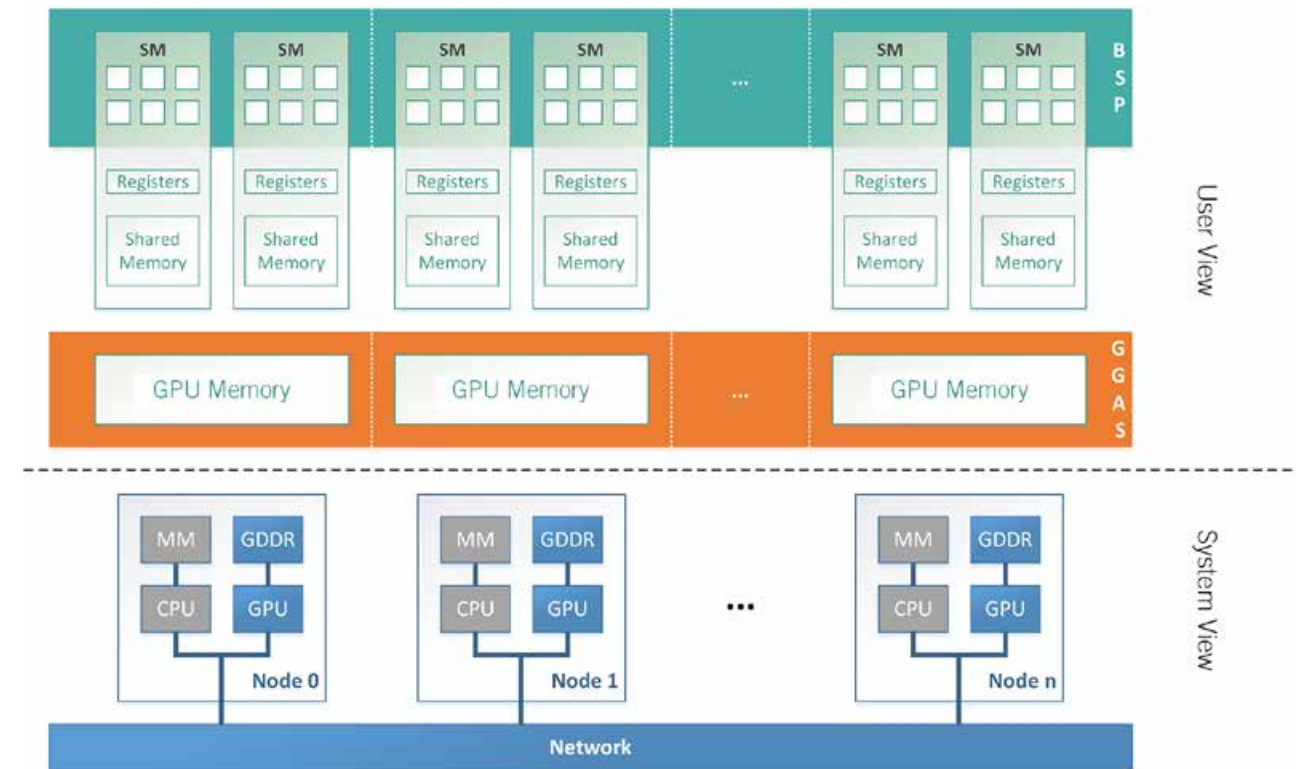


Fig. 1: System and User View of a Heterogeneous Compute Cluster using GGAS

## First Results

The communication principle of GGAS is based on remote loads and stores, although remote stores are preferred as such a dissemination approach allows for better locality optimizations.

In addition, polling for completion can dramatically benefit from locality, minimizing associated network traffic and resource utilization in general. Using remote stores, communication between distributed GPUs is as easy as obtaining a pointer to the remote memory location (using a call to our custom GGAS library), and then to use this pointer as target for a store instruction.

More complex communication methods like sends, receives, etc., can be based on these semantics. Compared to message passing as state-of-the-art, we are seeing in our preliminary experiments a speed-up of up to 2x for basic communication patterns like Ping-Pong, or barriers, and up to 1.7x for more complex workloads like stencil computations. In particular, we'd like to highlight that in this experiment a frequency-limited FPGA implementation was compared against a fully-flavored ASIC-based Infiniband network.

We'd also like to emphasize that this development is perfectly matching the recently introduced Dynamic Parallelism feature by NVidia, which allows GPU to autonomously start new kernels. Combining both techniques, the complete execution can be confined to the GPU domain, leaving the CPU idle for reduced energy consumption or improved overlap between host CPU and accelerator.

## Future plans

Future work will be manifold: first, we plan to scale our test system with regard to number of GPUs in order to validate the strong scaling our analyses are reporting. Second, various workloads will have to be tested on this disruptive approach. Last, in order to fully maintain the simplicity of GPU Computing we need to address programmability in a way that we offer an easy migration path from single-GPU CUDA programs to scale-out systems.

We gratefully acknowledge the generous support of this research effort by NVidia Corporation and Xilinx, Inc.

# The Onchilla Runtime for Accelerated Clusters

Supporting data-warehousing workloads by efficient data movements and resource allocations in heterogeneous clusters

• Fröning, H., Young, J. and Yalamanchili, S.

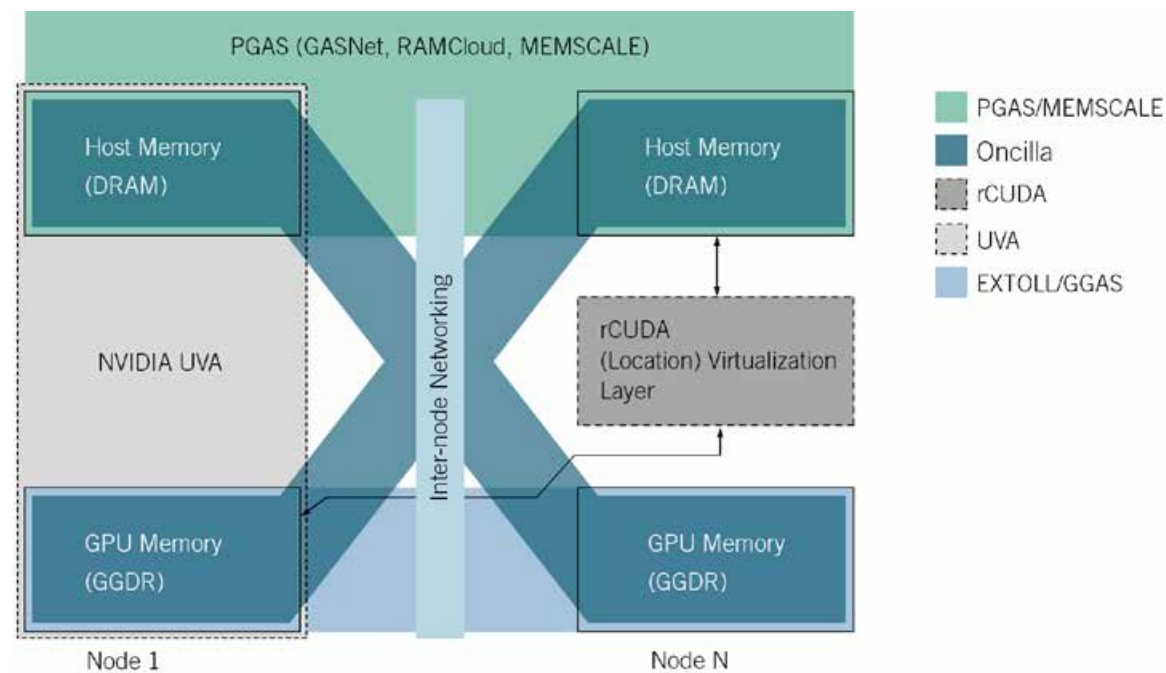


Fig.1: Address space models for accelerator clusters

## Overview

Big Data significantly pushes the demand for high performance storage, and DRAM memory is still several orders of magnitude faster than any other technology. While it is already difficult to provide Big Data applications sufficient main memory, accelerated and in-core implementations are even more challenging as the amount of on-board memory of such accelerators is significantly limited in its capacity. While for host memory several TBs are possible, typical accelerators come with 4-8GB, resulting in a 500-fold gap. Thus, efficient data transfers are mandatory to reduce the performance overheads of moving data to and from off-chip accelerators. Here we present Oncilla as a new system architecture and runtime for resource

allocation and efficient data movements in accelerated clusters. First experiments with Oncilla focus on data-warehousing workloads based on the Red Fox GPU compiler infrastructure; such workloads are a prominent representative of Big Data.

## The Oncilla Runtime

The main idea behind Oncilla is to combine host and accelerator memory into a large logical partition, providing either opacity or transparency from a user's point of view. Access to this logical partition is enabled by efficient Put/Get operations from user-level, independent of the memory type. Also, application performance might see differences between the two distinct types of memory in the logical partition, but application scaling is

not restricted by the memory location. Fig.1 shows the different address space models available for heterogeneous clusters today. As can be seen, the Oncilla data path is the first approach that connects all memory resources by direct data paths.

Additionally, Oncilla includes support for unconstrained resource allocations in a way that a user can request memory resources without specifying its type. The runtime will determine if host or accelerator memory is more appropriate and will later take care of the corresponding data movements. Also, such allocation calls can be combined with resource aggregation, allowing the user to request more memory than a single host or accelerator can serve. Such transparency is certainly helpful for productivity or applications with varying characteristics, but for locality reasons these calls support parameters that instruct the runtime to use only certain memory types or certain aggregation policies.

## Integrating EXTOLL in Oncilla

EXTOLL tightly integrates accelerators and networks bypassing the standard host-based stacks, making EXTOLL a basis for aggregation of resources (memory and accelerators) which is critical for Big Data. In this regard, one benefit of using the Oncilla runtime is that it separates the network layer from the resource allocation layer by the use of a common API, so that EXTOLL, Infiniband, Ethernet, or another protocol could be used according to each network layer's cost and performance benefits.

## Preliminary Results

The first experiments with Oncilla focus on an assessment of overhead associated with data movements between heterogeneous resources. Put/Get operations are used for all these movements, and special attention is put on the registration scheme required for such semantics. First results show that EXTOLL and IB perform better for different sizes of data movement and allocation. Using the well-known TPC-H data-warehousing work-

load, this runtime enables a reduction in runtime of about 80% in average, compared to standard disk-based storage techniques.

## Future plans

As Oncilla is a complex runtime that addresses several critical aspects of current architectures and workloads, multiple aspects will be addressed in the future. First, more data movement paths have to be integrated and analyzed accordingly to improve allocation and movement decisions. In addition to this, we plan for a simplified allocation scheme that is agnostic of memory types and capacity constraints. The user optionally can specify constraints about memory type (accelerator or host) and if and how resource aggregation should be employed. In the simplest case this task is done by the runtime, offering additional optimization opportunities during the execution. Such a feature is in particular beneficial for workloads with a highly dynamic resource utilization and varying locality.

We gratefully acknowledge the generous support of this research effort by NVidia Corporation and Xilinx, Inc.

## CHAIR OF COMPUTER SCIENCE V PROJECT OVERVIEW

• Prof. Dr. Reinhard Männer

### Overview | Chair of Computer Science V

Due to the retirement of Prof. Männer in August 2012 the projects at the department went through a substantial reorganization process since the beginning of 2012. The activities related to ATLAS and XFEL were taken over entirely by the „research group application specific computing“. The 2012 results are documented in the corresponding section of this report. Two projects - „Neurosim“ and „Online processing of cell images“ - were successfully completed with the PhD thesis' of Dr. Beier [1] and Dr. Gipp [2]. Responsibility for the „Microsim“ project was transferred to the collaboration partner VRMagic and is being continued at that location. The educational project „embedded systems“ was continued at the department.

### References

[1] Beier, F. : Entwicklung eines neurochirurgischen Trainingssimulators für intrakranielle Eingriffe , <http://www.ub.uni-heidelberg.de/archiv/13418>

[2] Gipp, M.: Online- und Offline-Prozessierung von biologischen Zellbildern auf FPGAs und GPUs, <http://www.ub.uni-heidelberg.de/archiv/13349>

### 68 | Hardware-/Softwareproject: Embedded Systems

Wurz, A.

# HARDWARE-/SOFTWAREPROJECT: EMBEDDED SYSTEMS

• Wurz, A.

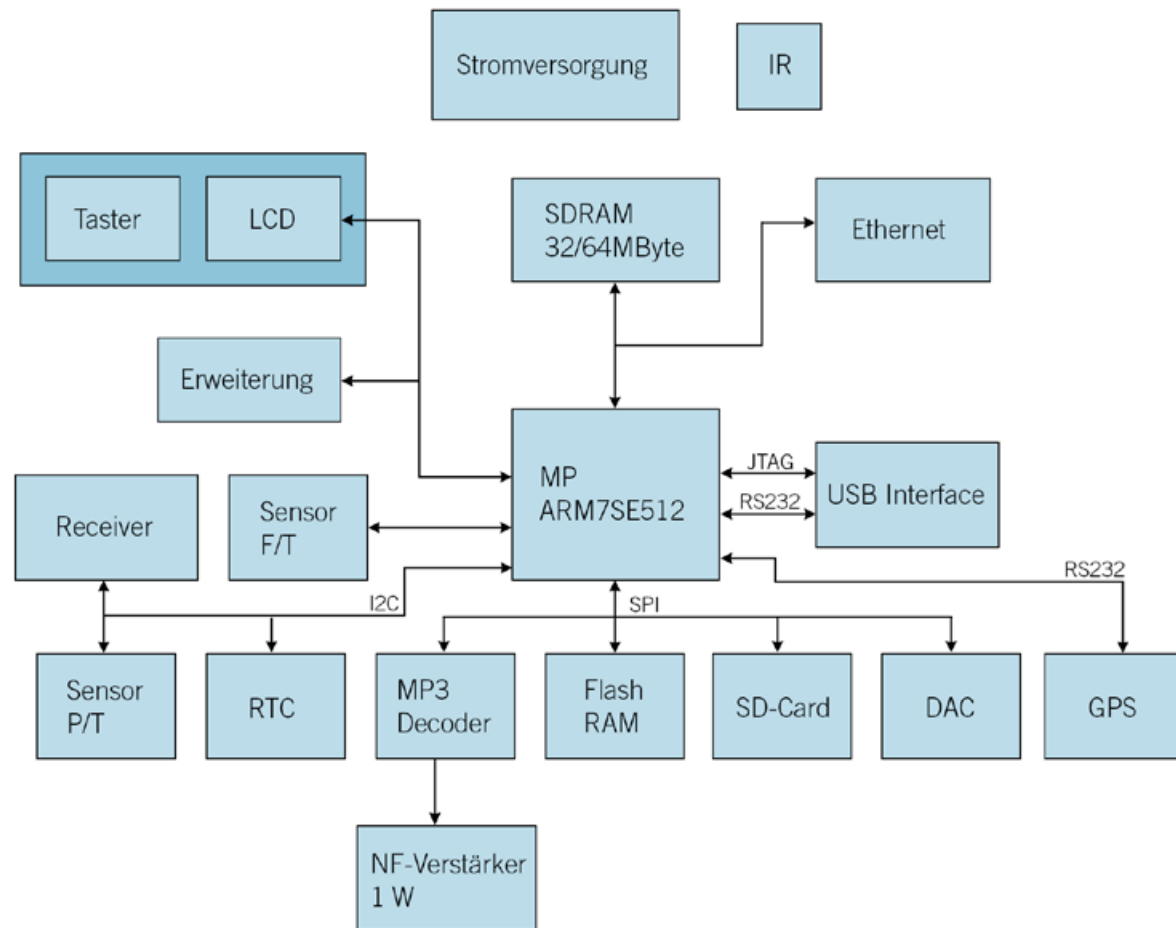


Fig. 1: Block circuit

The project encloses the realization of a microcontroller circuit for implementing of an Internet/UKW radio and a MP3 player with a graphical user interface. The realization is based on an ARM7 processor with external SDRAM (32 MB) and FLASH RAM (4 MB). The implementation consists of three boards, assembled one above the other: Power supply + battery charger board, microprocessor board with interfaces and the graphic display board with touch screen. The board of the graphic display also contains several buttons for menu selection and a rotary encoder.

The microprocessor board includes the following hardware components: Ethernet-Interface (10/100 Mbps), WLAN, interface for SD/SD-HC cards, MP3 decoder, real-time clock (RTC), ADCs + DACs, sensors for temperature, pressure and humidity, GPS module, interface for LCD colour graphics display, a radio chip and USB-Interface.

As development environment the Eclipse C/C++ Development Toolkit is used. The programming of the processor occurs with OPENOCD using USB and FTDI JTAG-Interface.

The following software functions were implemented:

- File system FAT32 for SD-Card, FLASH-RAM and RAM-Disk
- USB Mass Storage Device of SD-Card, FLASH-RAM and RAM-Disk
- Synchronisation of the RTC with time Server
- GPS position
- Sensor readout for pressure and temperature
- RDS radio for UKW + LW/MW/KW
- Internet Radio
- User interface for graphic display with touch screen, keyboard and rotary encoder query
- WLAN interface [1]

All functions were tested in 2012 successfully.



Fig. 2: Board with microcontroller



Fig. 3: Power supply, battery charger and accumulators

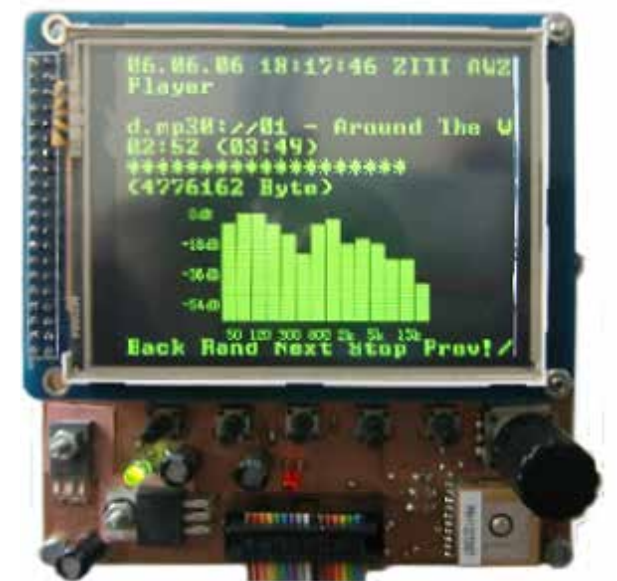


Fig. 4: LCD-Grafikdisplay (320\*240)

## References

- [1] N. P., Pfeiffer V.: Bachelorarbeit: Implementierung einer WLAN-Schnittstelle für ARM Prozessoren; SS2012.

## CHAIR OF COMPUTER VISION, GRAPHICS & PATTERN RECOGNITION PROJECT OVERVIEW

• Prof. Dr. Christoph Schnörr

**72 | Convex Models and Global Optimization for Image Segmentation and Labeling**

Lellmann, J., Breitenreicher, D., Kappes, J.H., Becker, F. and Schnörr, C.

**75 | Discrete Tomography for Particle Image Velocimetry**

Petra, S., Becker, F. and Schnörr, C.

**78 | Generative Modeling of Appearance and Shape for Medical Image Analysis**

Rathke, F., Schmidt, S. and Schnörr, C.

**80 | Globally Optimal Image Segmentation by Multicuts**

Kappes, J. H., Speth, M., Andres, B., Hamprecht, F. and Schnörr, C.

**83 | Image Denoising with Adaptive Total Variation**

Lenzen, F. and Becker, F.

**86 | Inference in Markov Random Fields based on Primal-Dual Convex Optimization**

Savchynskyy, B., Schmidt, S. and Kappes, J. H.

**88 | Pedestrian Path Prediction using Learned Motion Models**

Keller, C. and Schnörr, C.

**90 | Variational Methods for Image Segmentation with Shape Priors**

Schmitzer, B. and Schnörr, C.

**92 | Variational Recursive Joint Estimation of Scene Structure and Egomotion  
from Monocular Image Sequences**

Becker, F., Lenzen, F. and Schnörr, C.

## Convex Models and Global Optimization for Image Segmentation and Labeling

In this project, we study approaches to construct convex formulations of variational problems in image processing. We focus on problems that can be approximated by convex partitioning problems on continuous image domains. Using specially developed algorithms, these problems can be globally optimized even for very general data terms, which allows to clearly separate modeling and optimization effects.

• Lellmann, J., Breitenreicher, D., Kappes, J. H., Becker, F. and Schnörr, C.



Fig. 1: Application of the proposed approach for finding optimal partitions.

Left: Original image. Center: Selection of seed regions by the user. Right: Histogram-based multiclass segmentation. The originally combinatorial problem is relaxed to a convex problem and solved globally optimal using specialized algorithms. The spatially continuous framework avoids discretization-based artifacts and allows to obtain solutions with sub-pixel accuracy.

### Background and Goals

One of the key problems in image analysis is the partitioning problem. Here one seeks to decompose a given image domain  $\Omega \subset \mathbb{R}^d$  into several regions according to some data consistency and spatial coherency constraints.

Classical applications include image- or 3D volume segmentation and 3D reconstruction. In many cases the resulting problems can be formulated as convex optimization problems, which allows to solve them to global optimality. Any undesired or unexpected results can thus be attributed to the model, which is a clear advantage for model development.

Moreover, using a lifting technique [1], many originally non-convex variational problems such as image registration and optical flow can be reduced to higher-dimensional convex partitioning problems.

In this project, we focus on deriving convex relaxations for partitioning problems and developing efficient numerical solvers.

In contrast to grid- or graph cut-based methods, we consider the problem in the functional-analytic framework and from a spatially continuous perspective, i.e. we regard the image domain as a connected set rather than a finite set of individual points. In contrast to “discretize first” approaches, this “analyze first” approach allows to get a deeper insight into the underlying problem, obtain sub-pixel accurate solutions, and abstract from inaccuracies caused by the discretization.

### Methods and Results

The task of segmenting the image domain  $\Omega \subset \mathbb{R}^d$  into several regions  $P_1, \dots, P_l$  can be posed as

finding a labeling function  $u : \Omega \rightarrow \{1, \dots, l\}$  minimizing

$$\inf_{u: \Omega \rightarrow \{1, \dots, l\}} \int_{\Omega} \langle u(x), s(x) \rangle dx + J(u) \quad (1)$$

where  $s : \Omega \rightarrow \mathbb{R}^l$  constitutes the local data fidelity term, and the regularizer  $J(u)$  ensures a certain smoothness of the boundaries.

A way to solve this originally combinatorial problem is to allow intermediate solutions, i.e. to relax the constraint set to  $u : \Omega \rightarrow \Delta_l$ , where  $\Delta_l$  is the  $l$ -dimensional unit simplex. By a suitable extension of the regularizer  $J$  to this enlarged feasible set, one obtains a relaxed problem. From the solution of the relaxed problem, an approximate – and, in the case of two labels, exact – solution of the original problem can then be recovered.

This is particularly appealing in cases where  $J$  can be extended in a convex way, since then the overall problem can be solved to global optimality without potentially getting stuck in local minima. It is therefore of central importance to characterize regularizers for which such extensions exist, and to provide ways to construct such extensions. We focus on a class of regularizers where jumps between labels are penalized differently according to an interaction potential  $d$ , i.e. boundary length weighted by some scalar  $d(i, j)$  depending on the labels  $i$  and  $j$  of the adjoining regions (Fig. 2). In [4] we considered the special class of Euclidean distances, which are naturally handled by the above model.

Non-Euclidean distances can still be approximated by offline solving an auxiliary convex problem. Under several reasonable assumptions on the regularizer, we showed that any interaction potential must be a metric [4]. In addition, we extended an existing result [1] to show how a regularizer can be constructed for any such interaction potential. This completely characterizes the class of interaction potentials.

Regarding optimization, the model (1) can be posed as a (convex-concave) saddle-point problem. We studied several methods to solve such problems, with a special focus on primal-dual

methods that allow to solve the problems to a prescribed accuracy and provide optimality certificates [4]. Compared to existing methods, the proposed Douglas-Rachford method is robust and works on many synthetic and real-world problems without further parameter tuning. When combined with an improved rounding technique, the approach allows to recover very good solutions of the original combinatorial problem with sub-pixel accuracy, and without the staircasing artifact commonly encountered with graph-based methods.

The quality of the segmentation can be further improved by employing tighter relaxations of the regularizer. These pose a problem for existing methods, as they require to iteratively solve inner problems at each step. In [2] we demonstrate how this can be avoided, increasing numerical robustness and speed at the same time. The proposed technique also works for a large class of general image processing problems that can be formulated in saddle-point form (Fig. 2, see page 74). Finally, we established a priori suboptimality bounds of combinatorial image labelings computed by our convex variational framework [3, 5].

### Outlook and Future Work

Image labeling provides a key subroutine for a range of increasingly sophisticated image analysis tasks.

Two major directions of research concern the combination of image labeling with (i) shape prior information and (ii) with prior information in terms of empirical measures of either raw image data or coefficients of dictionaries, in order to cover increasingly larger image classes without compromising mathematical rigor or provable performance of corresponding algorithms.



Fig. 2: Left: Effect of choosing nonstandard interaction potentials. The original image (left) is segmented into 12 regions corresponding to prototypical colors vectors. By modifying the interaction potential, the regularization strength is selectively adjusted to suppress foreground structures while allowing for fine details in the background. Such non-standard regularizers require special techniques in order to formulate them in a convex way. Right: Mumford-Shah denoising of a grayscale image (left) using a nonconvex regularizer to remove fine structures while preserving hard edges (right). Using a lifting technique, many similar variational problems can be formulated and solved in the considered framework.

#### References

- [1] Chambolle, A., Cremers, D., and Pock, T. “A convex approach for computing minimal partitions”. Tech. Rep. 649, Ecole Polytechnique CMAP, 2008.
- [2] Lellmann, J., Breitenreicher, D., and Schnörr, C. “Fast and exact primal-dual iterations for variational problems in computer vision”. In Daniilidis, K., Maragos, P., and Paragios, N., editors, European Conference on Computer Vision (ECCV), volume 6312 of LNCS, pp 494–505. Springer Berlin / Heidelberg, 2010.
- [3] Lellmann, J., Lenzen, F., and Schnörr, C. “Optimality bounds for a variational relaxation of the image partitioning problem”, Dec 2011.
- [4] Lellmann, J. and Schnörr, C. “Continuous Multiclass Labeling Approaches and Algorithms”. *SIAM J. Imag. Sci.*, 4(4):1049–1096, 2011.
- [5] Lellmann, J. and Schnörr, C. “Continuous multiclass labeling approaches and algorithms”. *CoRR*, abs / 1102.5448, 2011.

## Discrete Tomography for Particle Image Velocimetry

We study the discrete tomography problem in Experimental Fluid Dynamics – Tomographic Particle Image Velocimetry (TomoPIV) – and focus on conditions for unique volume reconstruction in representative ill-posed scenarios. Ill-posedness is due to undersampling but also intimately connected to the particle density. Higher densities ease subsequent flow estimation but also aggravate ill-posedness of the reconstruction problem. A theoretical investigation of this trade-off is studied in the present work.

• Petra, S., Becker, F. and Schnörr, C.

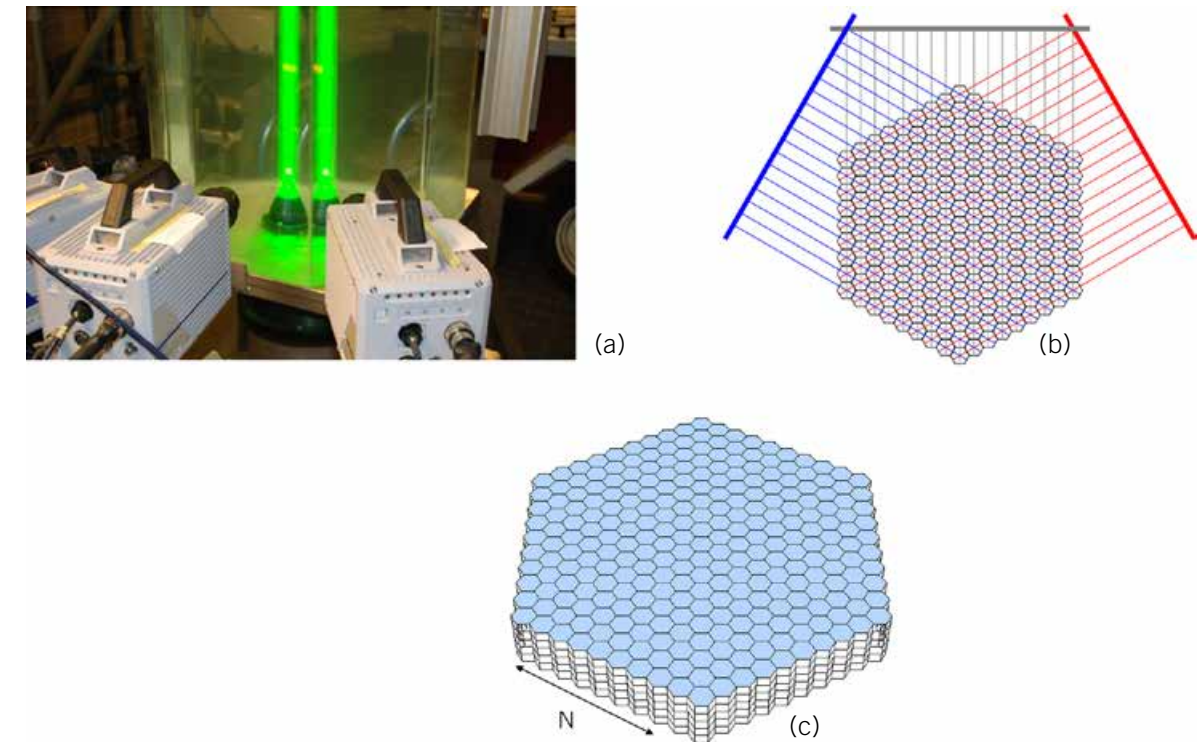
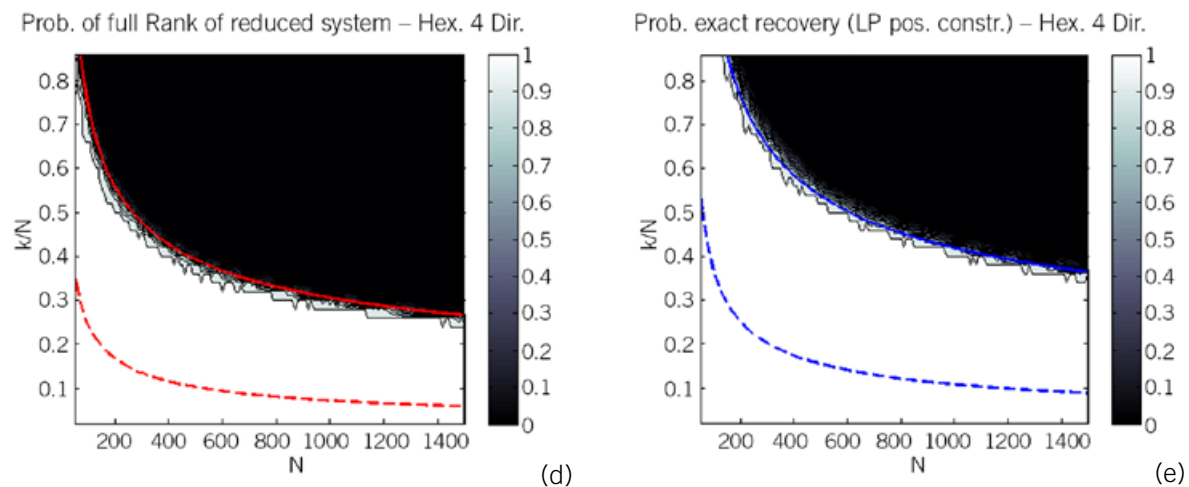


Fig. 1: (a) TomoPIV is based on a multiple camera-system, three-dimensional volume illumination and subsequent 3D reconstruction, and employs only few projections due to cost and complexity of the necessary measurement apparatus. The particle displacement (hence velocity) within the interrogation volume is then obtained by the 3D cross-correlation of the reconstructed particle distribution at the two exposures. In [1] a variational adaptive correlation method is developed.

(b) Sketch of a 3-camera setup in 2D. The corresponding 0/1 sensing matrix  $A^{3(2N+1) \times (3N^2+3N+1)}$  is underdetermined and marks in each row corresponding to a projection ray all incident discretization cells by the entry 1.

(c) This geometry can be easily extended to 3D by enhancing both cameras and volume by one dimension, thus representing scenarios of practical relevance as in (a), where a free jet inside an illuminated cylinder was imaged by cameras aligned on a line.



Recovery via (d) standard TomoPIV measurement system versus recovery via (e) the improved measurement system. (d) shows success and failure empirical phase transition for a 4-camera binary measurement system along with the analytical phase transition (dashed), see (1), for the binary 3-camera system from (b).

(e) shows success and failure empirical phase transition for an improved 4-camera measurement system along with the analytical phase transition  $k(N)/N \approx 6N^{0.342-1+0.011 \log(N)}$  (dashed) for the improved 3-camera system corresponding to the geometry from (b). The results indicate that at least a 150% times better reconstruction performance may be obtained in practice within the considered range of image resolution.

### Background and Goals

We analyze representative ill-posed scenarios of tomographic PIV with a focus on conditions for unique volume reconstruction. Based on sparse random seedings of a region of interest with small particles, the corresponding systems of linear projection equations are probabilistically analyzed in order to determine

(i) the ability of unique reconstruction in terms of the imaging geometry and a single critical sparsity parameter, and

(ii) sharpness of the transition to non-unique reconstruction with ghost particles when choosing the sparsity parameter improperly.

The sparsity parameter directly relates to the seeding density used for PIV in experimental fluids dynamics that is chosen empirically to date. Our results provide a basic mathematical characterization of the PIV volume reconstruction problem that is an essential prerequisite for any algorithm used to actually compute the reconstruction.

Accordingly, we also investigate the role of various reconstruction algorithms currently used in PIV from the optimization point of view, see [2]. Finally, we outline connections to major developments in other disciplines (compressed sensing) and indicate how the imaging set-up may be further improved.

### Methods and Results

The reconstruction of particle volume functions from few projections can be modeled as finding the sparsest solution of an underdetermined linear system of equations, since the original particle distribution can be well approximated with only a very small number of active basis functions relative to the number of possible particle positions in a 3D domain. In general the search for the sparsest solution is intractable (NP-hard), however. In [3] it was shown that if the solution of  $A$  is known to be sufficiently sparse and positive it is also the unique positive solution. If  $A$  has only nonnegative

entries, zero or negligible measurements can be eliminated along with the corresponding incident basis functions. This leads to an "equivalent" feasible set of reduced dimensionality.

It can be shown that a binary matrix recovers *all*  $k$ -sparse binary vectors if and only if all these reduced systems are overdetermined full-rank systems. The maximal such  $k$  is related to the minimal number of negative (or positive) entries in the sparsest nullspace of  $A$  and for the considered geometry, see Fig. 1 (c), equals 2. We estimated the critical  $k$  such that for most arbitrary  $k$ -sparse vectors the reduced systems are indeed overdetermined and obtained the relation

$$k(N) \approx 4N^{0.342+0.011 \log(N)} \quad (1)$$

depending on the problem size  $N$ . Additionally, we proved a tail bound entailing that for increasing large problem sizes  $N \rightarrow \infty$ , the critical  $k$  acts like a threshold that sharply discriminates successful reconstruction from failure. Our average case analysis of correct reconstruction revealed that by adding a fourth camera the critical  $k$  increases to

$$k(N) \approx 7.3N^{0.43+0.016 \log(N)}.$$

Fig. 1 illustrates this fact as well as results for sensing matrices that have been improved in a specific way.

### Outlook and Future Work

We currently study the tomographic problem of reconstructing particle volume functions from the general viewpoint of compressed sensing. In a nutshell, we show that the TomoPIV problem is quite degenerate from the viewpoint of compressed sensing, thus leading to poor performance guarantees. On the other hand, the probabilistic analysis of [4] yields average performance bounds that back up current rules of thumb of engineers for choosing particle densities in practice. Moreover, simulations demonstrate that slight random perturbations of the TomoPIV measurement matrix considerably boost both worst-case and expected

reconstruction performance. This finding is interesting for CS theory and for the design of TomoPIV measurement systems in practice. Our work aims at pointing out connections between the fields of compressed sensing and discrete tomography in order to stimulate further research.

In cooperation with: B. Wienecke (LaVision, Göttingen), S. Gesemann, A. Schröder (DLR, Göttingen)

Funding: DFG, grant SCHN457 / 11

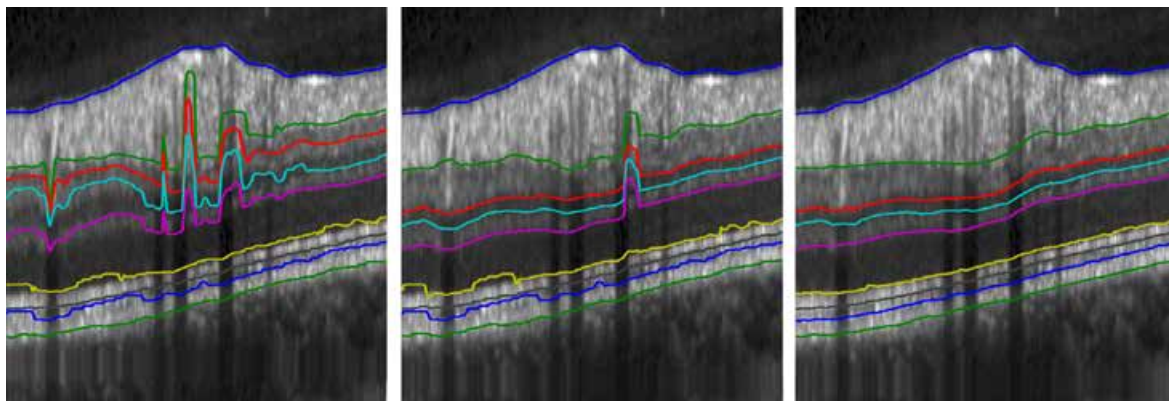
### References

- [1] Becker, F., Wienecke, B., Petra, S., Schröder, A., and Schnörr, C. "Variational Adaptive Correlation Method for Flow Estimation". IEEE Transactions on Image Processing, 2011. accepted.
- [2] Nicola, A., Petra, S., Popa, C., and Schnörr, C. "A general extending and constraining procedure for linear iterative methods". Int. J. Comp. Math., 2011. in press.
- [3] Petra, S. and Schnörr, C. "TomoPIV meets compressed sensing". Pure Math. Appl., 20 (1-2):49-76, 2009.
- [4] Petra, S., Schnörr, C., and Schröder, A. "Reconstruction properties of sensing matrices in tomographic particle imaging velocimetry". In Volume Reconstruction Techniques Applied to 3D Fluid and Solid Mechanics, Proc. of FVR 2011, 2011.

## Generative Modeling of Appearance and Shape for Medical Image Analysis

The project focuses on classes of image data given by partitions with randomly varying geometry and fixed topology, and with class-specific appearance of each component of the partition. The application scenario concerns 2D OCT scans of retinal tissue. A probabilistic approach is presented, which combines discrete exact inference and a global shape prior, that produces accurate segmentations which preserve the physiological order of intra-retinal layers.

• Rathke, F., Schmidt, S. and Schnörr, C.



a) Uniform Prior

b) Shape Prior

c) SP + Post Processing

Fig. 1: Close-up view of segmentation results for three models of increasing complexity.

Left: The model utilizes texture information only. Furthermore inference is performed for each column separately. For distinctive partition transitions this leads to accurate segmentation results, but fails for less well-defined ones.

Center: Shape information is added to the model column-wise. Although still lacking communication across columns, the predicted segmentation improves in many image columns. For columns with strong texture artifacts, such as shadowing caused by blood vessels, the segmentation may still fail.

Right: The final model with added communication across image columns, governed by the global shape prior. This leads to improved segmentations for difficult image regions as well.

### Background and Goals

Over the last years Optical Coherence Tomography (OCT) has become a key technique for non-invasive diagnostic retina imaging. Quantitative measurement of the intra-retinal layers plays a central role for the early diagnosis of diseases like glaucoma or age-related macular degeneration. Since manual segmentation is tedious and time-consuming, there is a high demand for automated algorithms.

### Methods and Results

Our framework combines local appearance models with a global shape prior, all modeled probabilistically via Gaussian distributions and learned offline on a set of labeled training images.

To obtain segmentations, we rely on the following iterative procedure: a) Exact inference is performed column-wise fusing appearance and shape information for the respective column.

b) In a regularization step, smoothness across image columns is enforced utilizing the global shape prior, by altering the appearance terms. Both steps are iterated until convergence of the predicted segmentation.

For further details please refer to [1].

### Outlook and Future Work

Variational methods will be studied, that infer not segmentations but distributions over segmentations. This enables local assessment of predictions, i.e. locate potential weak spots in the segmentation. In an abnormality detection setting, these may correspond to pathological variations in the retina.

Funding: DFG RTG 1653

### References

[1] Rathke, F., Schmidt, S., and Schnörr, C. "Order preserving and shape prior constrained intra-retinal layer segmentation in optical coherence tomography." In Fichtinger, G., Martel, A. L., and Peters, T. M., editors, MICCAI, volume 6893 of Lecture Notes in Computer Science, pp 370–377. Springer, 2011.

## Globally Optimal Image Segmentation by Multicuts

Segmentation of images into a given number of classes is an important problem for many computer vision applications. If the number of classes is unknown the problem renders much harder. We develop a branch-and-cut framework that solves these problems to global optimality. While the asymptotic run-time is in general exponential, we observe run-times on real world problems comparable or better than state-of-the-art methods. Furthermore the framework can be extended by using super-pixel for speed-up and to make it applicable to large-scale problem

• Kappes, J. H., Speth, M., Andres, B., Hamprecht, F. and Schnörr, C.

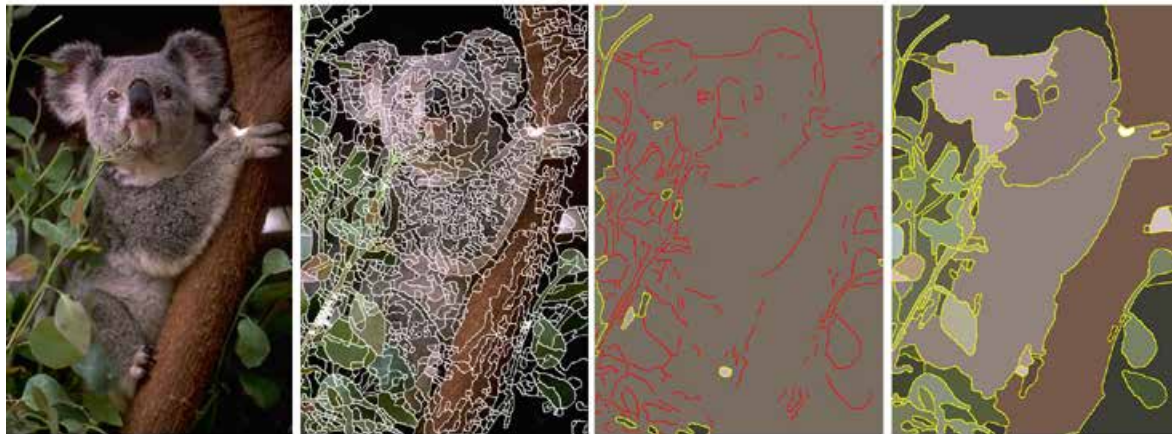


Fig.1: Example for segmenting an image in a priori unknown number of classes. The images above are taken from [1] and show from left to right: (1) the original image, (2) the over-segmentation that defines super-pixels, (3) a segmentation only based on decision-tree-classifiers trained on boundaries and (4) a segmentation using closeness constraints that enforce the edge-labeling to be in the multicut-polytope. Without this additional constraint, many edges (red) are inside a connected component and therefore ambiguous. Ignoring this ambiguity leads often to undesirable under-segmentation.

### Background and Goals

The overall goal of this project is to segment images into (i) a given number of predefined class (P1) or (ii) a unknown number of unknown classes (P2). Both problems can be formulated in terms of a Markov Random Field (MRF). Finding the most likely segmentation reduce to minimizing an objective function given by a sum of unary terms  $f_a(x_a)$ , which depend on local measurements on (super-)pixel  $a$ , and higher-order-terms  $f_c(x_c)$ , which depend on two or more (super-)pixels summarized by the sets  $C \in \mathcal{C}$ . In the simplest case

$\mathcal{C}$  includes all pairs of neighbored (super-)pixels. For the case when a predefined number of classes is given, the problem reads

$$\min_{x \in X} \sum_{v \in V} f_v(x_v) + \sum_{C \in \mathcal{C}} f_C(x_C). \quad (\text{P1})$$

For the case a unknown number of classes, we assume w.l.o.g. that the number of classes is equal to the number of (super-)pixels, but includes no unary terms:

$$\min_{x \in X} \sum_{C \in \mathcal{C}} f_C(x_C), \quad \forall C \in \mathcal{C} : |C| \geq 2. \quad (\text{P2})$$

A notable characteristic of the later problem is, that its objective function is invariant to a permutation of the state-space, i.e. the configurations  $x = (0, 1, 0, 2, 3, 1)$  have the same energy as  $x = (6, 0, 6, 1, 4, 0)$ , which renders the problems challenging for state-of-the-art methods, which try to assign a labeling to each variable/pixel.

### Methods and Results

We restrict the non-unary-terms of our objective function to be invariant to permutations of the state-space. While this is no restriction for (P2), for (P1) it is quite natural. Many common terms fall into this family, e.g. potts-functions. Let us number the set of valid partitions of a set with  $n$  elements<sup>1</sup> and let  $\alpha : \Omega^{\mathcal{C}} \rightarrow \mathbb{N}$  be a mapping from a labeling to its partition number. Than any real valued function that is invariant to permutations of the state-space can be written as:

$$f_C(x_C) = \beta_{C,\alpha(x_C)}, \quad \beta_{C,\alpha} \in \mathbb{R} \quad (1)$$

With this slightly restriction at hand we optimize no longer over the set of all node labelings. Instead we optimize over the set of all separating boundaries related to valid partitions, which is known as the multicut problem. While this does change nothing on the NP-hardness of our problem it has two major advantages: (i) it overcomes the ambiguity of optimal solutions in (P2), (ii) it provides a less memory consuming representation of both problems in form of an (integer) linear program.

We refer the reader to [2] to a general description for the second order case, i.e.  $\forall C \in \mathcal{C} : |C| \leq 2$ . In [1] we describe an application using also higher order terms. A description of the method for arbitrary order is in progress, we will give here a rough overview.

Problems (P1) and (P2) can be transformed into a linear program of moderate size together with a system of affine inequalities, defining the so called multicut polytope. While the number of inequali-

<sup>1</sup> The number of possible partitions is given by the bell number

ties is exponential we start with a polynomial subset of this system, apply separation procedures to find efficiently violated constraints out of this set and add those iteratively to our problem. If no more violated constraints can be found we apply branching techniques and proceed with detecting violated constraints as long as the optimal solution has been founded.

While for problems (P2) our methods outperform any method we compare with, for problems (P1) alternative state-of-the-art methods often provides comparable but approximative results much faster. However, if one is interested in optimal solutions, our method seems to be currently the fastest one. For the case of unknown classes Fig.1, we pre-segment the image-domain in the first step. This results in sets of pixels, also known as super-pixels. Working on super-pixels instead of the pixel level has two mayor advantages: (i) it drastically reduces the problem size and (ii) during the pre-segmentation it often makes inconsiderable decisions which hardly determinable in the overall problem. Local classifiers give a prediction if a single boundary element between two super-pixels should belong to the overall boundary. A segmentation based only on this information leads to under-segmentation and active edges inside connected components (plotted in red). If we additionally enforce closeness constraints, i.e. solution have to be inside the multicut-polytope, we obtain accurate segmentations. Details how these models are learned and how the level of segmentation can be selected are reported in [1].

For the problem (P2), in which the set of classes is unknown, we compare our method with TRW-S, one of the state-of-the-art methods. Fig.2 shows the result for a four-class problem, without using super-pixels. While visually the results of our multicut method (bottom-left) and TRW-S (bottom-right) are comparable, a detailed look at the difference of labelings (top-right) shows that they differ on the object boundaries. Furthermore, TRW-S does not converge on this instance. We stop TRW-S after the same time, in which our method has found the global optimum.

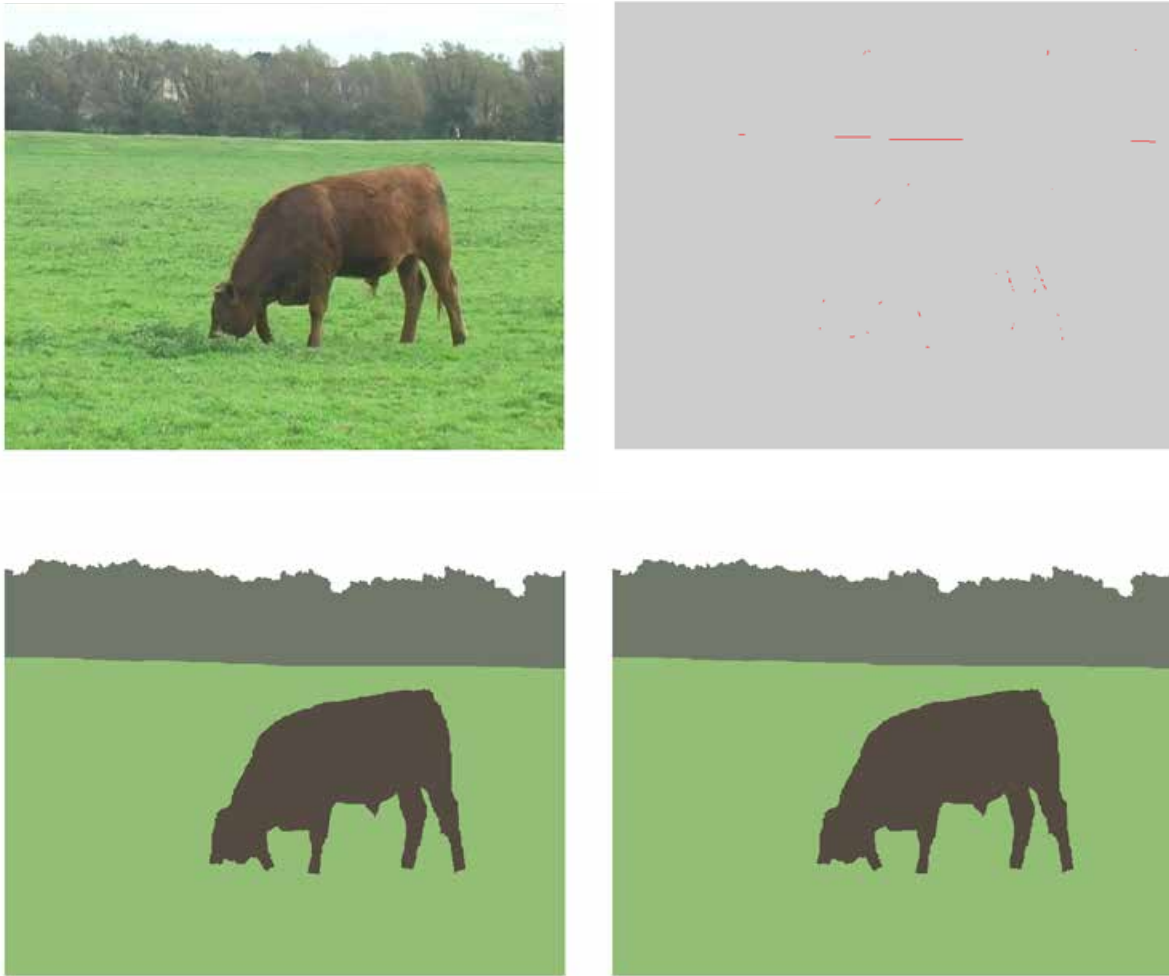


Fig. 2: The original image (top-left) is segmented in 4 predefined classes. The resulting segmentation is shown for our multicut method (bottom-left) and TRW-S (bottom-right). While our method guarantee for optimality, TRW-S found a suboptimal solution. The difference between these two segmentations (top-right) are located at object-boundaries.

### Outlook and Future Work

We already extended our method to deal with higher order terms. For some types of functions we can deal up to orders of a few hundred. While for complex models we can not expect to find optimal solutions in reasonable time, we are looking for alternative cut defining procedures and better rounding schemes to obtain good solutions and bounds for earlier iterations.

### References

- [1] Andres, B., Kappes, J. H., Beier, T., Köthe, U., and Hamprecht, F. "Probabilistic image segmentation with closedness constraints". In Proceedings of ICCV, 2011. to appear.
- [2] Kappes, J. H., Speth, M., Andres, B., Reinelt, G., and Schnörr, C. "Globally optimal image partitioning by multicuts". In EMMCVPR. Springer, 2011.

## Image Denoising with Adaptive Total Variation

Adaptive total variation (TV) is a state-of-the-art approach to regularize inverse problems. We propose a generalization of this approach, where the adaptivity does not depend on the noisy input data, but on the unknown solution. The benefits of this generalization are demonstrated by means of image denoising. Compared to the classical approach of adaptivity, our method is able to much better preserve edge structures. In general our approach is applicable for arbitrary inverse problems.

• Lenzen, F. and Becker, F.



Fig. 1: Comparison of data-dependent (middle) and solution-dependent (right) adaptive TV regularization for denoising a test image (left). We use a strong anisotropy to preserve as much edges as possible. For the data-dependent approach this leads to a significant preservation of noise structure in the image. The proposed solution-dependent approach does not show these artifacts. Decreasing the anisotropy to avoid artifacts for the data-dependent approach will, however, lead to an inferior preservation of true edge structures.

### Background and Goals

Many image restoration methods are based on the idea of decomposing a given image into two or even more additive components, and, by this, dividing the original image content into a cartoon-like part, a texture part and a noisy part.

A prominent example is the method proposed by Rudin, Osher and Fatemi (ROF) [6], which utilizes Total Variation (TV) regularization. The ROF method deals with two image components, one for the noise-free cartoon content and one for both texture and noise. Fig. 2 shows a examples of decomposing a noisy test image into such parts. Interpreting both image parts as functions, they can be characterized as follows:

- The cartoon-like part, commonly denoted by  $u$ , is given as function of bounded total variation.
- Due to the work of Meyer [4], the texture + noise part denoted by  $v$  can be described by introducing the so-called G-space, a space of functions, which are given as the divergence of some function  $p$ .
- The sum of  $u$  and  $v$  gives the input data  $f$ .

For the ROF approach, it turns out that function  $p$  has to lie in a certain convex set  $\mathcal{D}$ . Therefore, we can find a smoothed version of noisy data  $f$  by projecting them onto the convex set  $\mathcal{C}$  given as  $\mathcal{C} = \text{div } \mathcal{D}$ , i.e. we have to find  $v$ , such that  $v = \text{div } p$  and  $p$  lies in the given set  $\mathcal{D}$ .



Fig. 2: Decomposition of a noisy image  $f$  into a geometric component  $u$  and a noise component  $v$ . Here we used the ROF model [6]. The noise component contains unwanted structures from the original noise-free data.

### Methods

The above geometrical formulation of TV regularization based on constraint set allows for an intuitive generalization. For the standard ROF model, the constraint set  $\mathcal{D}$  can be locally characterized as circles of fixed radius. An adaptive generalization then is to consider circles of locally varying size, or in view of anisotropic variants, to move from circles to other convex sets like rectangles, parallelograms or ellipses. In each case adaptivity has to be steered by additional information obtained from the image structure, e.g. edge location and direction. In order to obtain the required information, two concurrent strategies exist in literature. The first evaluates the noisy input data in a preprocessing step. Gaussian presmoothing is used to reduce the influence of noise. The second strategy is to estimate the required data parallel to the primary optimization problem.

In our work [2, 3] we propose a new strategy, where the adaptivity is defined directly depending on the unknown noise-free image. We refer to this approach as solution-dependent adaptivity. By this approach structural information is not influenced by the noise of the input data. As a result, adaptivity can be tuned in more effectively, see Sect. below.

Due to the proposed generalization we move from a convex optimization problem to a non-convex one and thus theory of convex optimization can

no longer be applied. In our theoretical work, we therefore reformulate the optimization problem as a quasi-variational inequality (QVI), which allows us to adapt existing theory from this field as well as suitable algorithms (cf. [1, 5]).

### Results

We compare our approach of solution-dependent adaptivity for TV regularization to two TV approaches from literature: the standard ROF model and an adaptive TV approach, where the adaptivity is determined by examining the noisy input image (we refer to this as data-dependent adaptivity). Fig. 1 and Fig. 2 show the different results for denoising a test image (left image). Smoothing with the standard ROF model (Fig. 2 middle) removes the noise but also some of the image structures, which become part of the noise component  $v$  (cf. Fig. 2 right). For both TV variants with data- and solution-dependent adaptivity, we use the same parameters providing a weak presmoothing and a relatively strong anisotropy, which in both cases results in a good preservation of image structures. With the data-dependent adaptivity (Fig. 1 middle), however, a part of the noise is regarded as image structures and thus is also preserved. This is due to the fact that the adaptivity is defined based on the noisy input data. In contrast, the result of the solution-dependent approach (Fig. 1 right) shows a good denoising capability while preserving most

of the edges and without producing artifacts from noise. Increasing the presmoothing parameters or decreasing the anisotropy would prevent noise artifacts in the data-adaptive approach but also the preservation of weak image structures and thus lead to a inferior quality of the denoised image.

To sum up, solution-dependent adaptivity allows us to refrain from a strong presmoothing and to use a strong anisotropy to preserve and regularize image edges.

We successfully applied our approach to various applications within the HCI research projects, e.g. for regularizing depth maps or optical flow.

Funding: HCI

### References

- [1] Chan, D. and Pang, T. "The generalized quasi-variational inequality problem". *Math. Operat. Res.*, 7(2):211–222, 1982.
- [2] Lenzen, F., Becker, F., Lellmann, J., Petra, S., and Schnörr, C. "A class of quasi-variational inequalities for adaptive image denoising and decomposition". *Computational Optimization and Applications*, 2012.
- [3] Lenzen, F., Becker, F., Lellmann, J., Petra, S., and Schnörr, C. "Variational image denoising with adaptive constraint sets". In *Proceedings of the 3rd International Conference on Scale Space and Variational Methods in Computer Vision 2011*. Springer, 2012.
- [4] Meyer, Y. *Oscillating Patterns in Image Processing and Nonlinear Evolution Equations*, volume 22 of *Univ. Lect. Series. Amer. Math. Soc.*, 2001.
- [5] Nesterov, Y. and Scriali, L. "Solving strongly monotone variational and quasi-variational inequalities". *Core Discussion Paper 2006 / 107* [http://www.core.ucl.ac.be/services/psfiles/dp06/dp2006\\_107.pdf](http://www.core.ucl.ac.be/services/psfiles/dp06/dp2006_107.pdf), Nov 2006.
- [6] Rudin, L. I., Osher, S., and Fatemi, E. "Non-linear total variation based noise removal algorithms". *Physica D*, 60(1-4):259–268, 1992.

# Inference in Markov Random Fields based on Primal-Dual Convex Optimization

We investigate a novel primal-dual optimization algorithm for maximum a posteriori inference for graphical models. Such models became an important tool for image analysis nowadays. In its turn the inference problem is the central for in many applications.

• Savchynskyy, B., Schmidt, S. and Kappes, J. H.

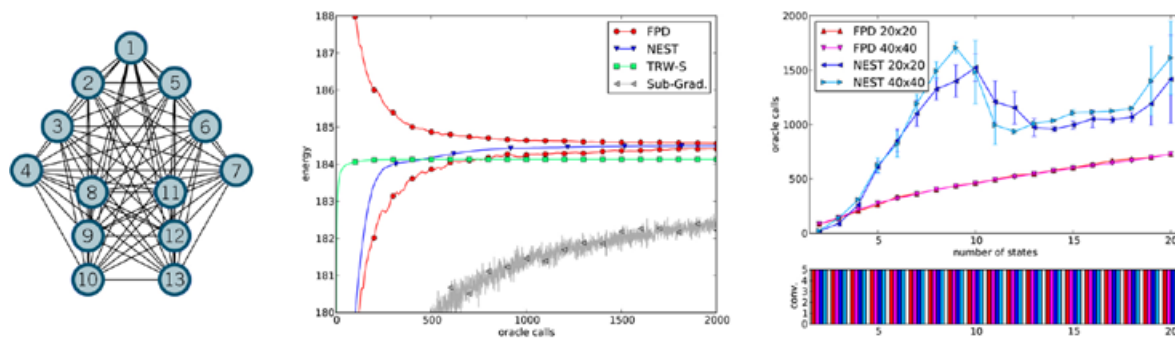


Fig. 1: Left: an example of a graphical model. Nodes correspond to random variables, edges describe conditional statistical dependence between variables. Center: Plot shows convergence of objective function value (the vertical axis) with respect to the time (measured in oracle calls) for different methods. The decreasing curve correspond to a primal objective, increasing curves - to dual ones. Red curves correspond to the investigated FPD method [3], other colors - to competing methods. The only visible curve for a primal objective belongs to FPD. Other primal objectives are incomparably worse - they even do not fit into the plot. However the fastest convergence w.r.t. the dual objective is demonstrated by our competing method NEST [2]. Right: Plot shows how the time (measured in oracle calls) needed to achieve a certain precision depends on the number of possible random variables' states (the horizontal axis). Red curves - the investigated FPD method, blue curves - our competing NEST method. The plot shows that as the number of labels increases, FPD performs better than others.

## Background and Goals

Markov random fields and graphical models associated to them play an important role for image processing. In the last years they became a modeling tool widely used in nearly all subfields from medical imaging to 3D scenes reconstruction. One bottleneck of this framework, which we treat in this project, is associated to the inference problem, i.e. estimating values of hidden variables of the field.

Since the problem is NP-hard in general one has to consider either its special cases or solvable re-

laxations. There is a family of methods based on so called "Graph Cuts". They are quite efficient, but can be applied only when the prior probability distribution (decoded in edges of the graph) has a certain form, i.e. they consider special cases of the problem.

Alternative class of methods, addressing convex relaxations of the problem does not have this restriction. However it turns out that even the simplest linear programming relaxation constitutes a convex problem with billions of variables and

out-of-the-shelf solvers either can not be used at all or are restricted to specific scenarios. Hence specialized solvers have to be developed. This fact was recognized by the community and a series of methods were proposed in the recent past years. These methods however operate either in primal or in a dual space of the corresponding linear programming problem. The dual objective is easier and thus can be easier optimized, however reconstructing a primal solution out of the dual one is not easy and could require significant computational efforts. Contrary, primal methods deal with more difficult optimization and thus are less efficient. They operate however with primal variables directly and getting an approximate primal solution in this case is quite straightforward. Our goal is to combine advantages of both approaches (primal and dual) in a primal-dual framework.

## Methods and Results

As the first step we considered (see [3] for details) the First-Order Primal-Dual (FPD) algorithm proposed in [1] and widely used in the related field of variational image processing. It has several advantages comparing to others: (i) its iterate converge to the optimum of the relaxed primal and dual problems, i.e. it recovers both solutions at once; (ii) it has a good and theoretically substantiated convergence rate; (iii) it can be easily modified to compute a duality gap, which leads to a clear stopping condition.

The method is very general and, what is very important, has a very high degree of possible parallelization. We compared its performance to a series of state-of-the-art dual solvers (see Fig. 1) and found that

- as expected, it significantly speeds-up convergence of the primal bound to the optimum comparing to purely dual methods;
- its convergence does not slow down rapidly as the number of variable states increases, as it is typical for dual methods;

However this algorithm has also several drawbacks:

- the method splits the initial problem into a collection of very small (and thus simple) subproblems. Specialized dual methods (like e.g. NEST proposed in our work [2]) treat larger subproblems and thus require less iterations to converge;
- it has to keep and operate directly all primal variables. This requires a lot of memory and purely dual methods does not have this drawback.

## Outlook and Future Work

The investigated primal-dual method

- is highly parallelizable;
- is guaranteed to converge to the optimum of the relaxed problem, moreover its convergence rate is optimal in a certain sense;
- demonstrates faster convergence of the primal objective, which indeed is of the interest for applications (not the dual one). Our future work will address its further specialization to the problem structure to obtain advantages of other existing methods while preserving its own positive properties.

Funding: HCI / IPA

## References

- [1] Chambolle, A. and Pock, T. "A first-order primal-dual algorithm for convex problems with applications to imaging". *Journal of Math. Imaging and Vision*, 2011.
- [2] Savchynskyy, B., Kappes, J., Schmidt, S., and Schnörr, C. "A study of Nesterov's scheme for Lagrangian decomposition and MAP labeling". In *CVPR*, 2011.
- [3] Schmidt, S., Savchynskyy, B., Kappes, J. H., and Schnörr, C. "Evaluation of a first-order primal-dual algorithm for MRF energy minimization". In *EMMCVPR*, volume 5681 of LNCS, pp 89–103. Springer, 2011.

## Pedestrian Path Prediction using Learned Motion Models

Future vehicle systems for active pedestrian safety will not only require a high recognition performance, but also an accurate analysis of the developing traffic situation. In this work a system for pedestrian path prediction at short time intervals ( $<1s$ ) is presented. Features extracted from dense optical flow are used to learn a low dimensional feature representation. These low dimensional features are integrated in a probabilistic filtering framework.

• Keller, C. and Schnörr, C.

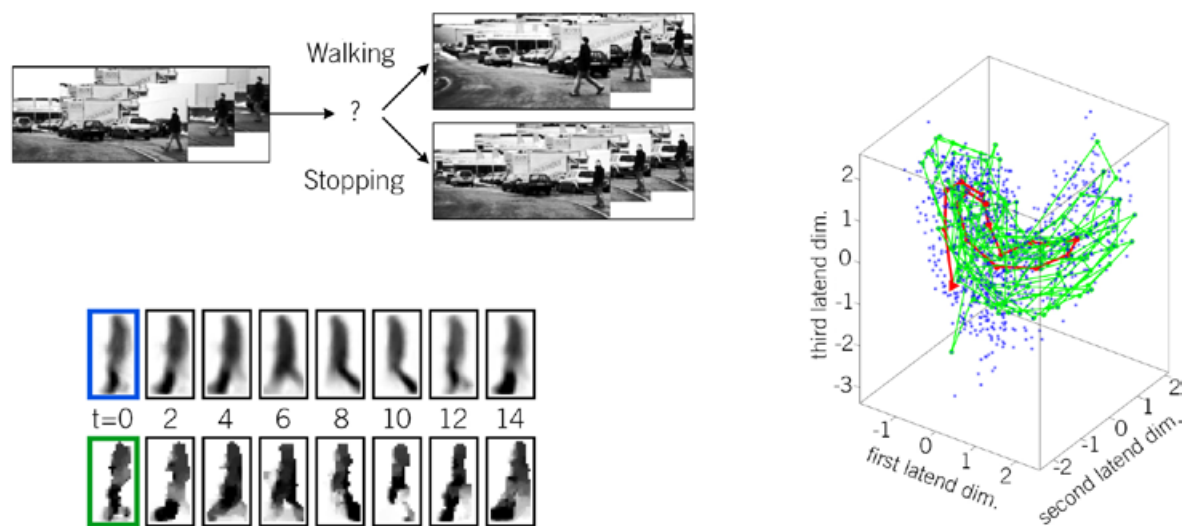


Fig. 1: (left/top) Will the pedestrian stop or walk.

(right) Low dimensional representation of dense optical flow features.

(left/bottom) Learning the dynamics from pedestrian trajectory data allows the prediction of motion patterns. Observed optical flow feature (green box) and corresponding reconstructed feature (blue box). Reconstruction of the latent space prediction of a feature for different prediction time-steps (top). Features that will be measured at the corresponding time-steps (bottom).

### Background and Goals

Strong gains have been made over the years in improving pedestrian recognition performance. However, the initiation of an emergency vehicle maneuver requires a precise estimation of the current and future position of the pedestrian with respect to the moving vehicle. One major challenge is the highly dynamic behavior of pedestrians, which can change their walking direction in an instance, or start/stop walking abruptly. As a consequence, prediction horizons for active pedestrian systems are typically short; even so, small

performance improvements can produce tangible benefits. Accident analysis shows that being able to initiate emergency braking 0.16s (4 frames @ 25Hz) earlier, at a Time-to-Collision of 0.66s, reduces the chance of incurring injury requiring hospital stay from 50% to 35%, given an initial vehicle speed of 50 km/h.

### Methods and Results

We present a system for accurate pedestrian path prediction from a moving vehicle, at short time intervals. Features are extracted from dense stereo

and dense optical flow data computed over the bounding box returned by a pedestrian detector. Lateral and longitudinal position of the pedestrian is obtained from disparity values on the pedestrian upper body. A low dimensional representation of optical flow features that captures motion patterns of moving pedestrians is learned from a set of training trajectories. Integrating the learned pedestrian motion model into a particle filter framework allows the prediction of future optical flow features. Speed changes in the pedestrian motion are derived from the predicted features. For larger prediction horizons (17 frames into the future) the proposed system outperforms state of the art Kalman Filter based systems with respect to localization errors.

Funding: Daimler AG

### References

- [1] Keller, C. G., Enzweiler, M., and Gavrila, D. M. "A new benchmark for stereo-based pedestrian detection". Intelligent Vehicles Symposium (IV), 2011 IEEE, pp 691–696, 2011.
- [2] Keller, C. G., Hermes, C., and Gavrila, D. M. "Will the pedestrian cross? probabilistic path prediction based on learned motion features". Proc. of the DAGM Symposium on Pattern Recognition, pp 386–395, 2011.

## Variational Methods for Image Segmentation with Shape Priors

Prior knowledge about the shape of objects constitutes an important cue for image segmentation. Constructing shape prior functionals entails a delicate trade-off between descriptive power and mathematical and computational feasibility. Simple approaches are often unsatisfying in properly describing the set of allowed shapes, while sophisticated techniques usually yield highly non-convex functionals that are difficult to handle from the optimization point-of-view. In this project we try to develop efficient approximations to powerful but computationally intractable shape-similarity measures and to combine them with recent progress concerning convex variational relaxations of the segmentation problem.

• Schmitzer, B. and Schnörr, C.



Fig. 1: A toy example. Left: a template shape represents the prior knowledge, middle: a given distorted input shape, right: output shape restored with our shape prior functional and a simple data fidelity term. Due to the metric-space representation the relative position and orientation of template and input does not play a role and the shape prior works completely isometry invariant.

### Background and Goals

Image labeling is one of the central problems in image processing and computer vision. One wants to assign a label to each point in the image domain based on local affinities and subject to regularity conditions for the transitions between regions of different assignments. Convex relaxation methods can today approximately solve such initially combinatorial problems with high accuracy.

However more complex criteria such as the shape of the labeled regions cannot be taken into account within this framework yet.

The question of how to mathematically describe and compare shapes has been raised in the context of the shape registration and classification tasks on 3D meshes. Representing shapes as metric spaces abstracts them from their embed-

ding into the surrounding space. The resulting metric spaces are then compared by the Gromov-Hausdorff and the related Gromov-Wasserstein distance.

While this yields promising results there are some obstacles for direct application to image segmentation: the underlying optimization problems are combinatorial and non-convex and thus expensive to solve. In addition noisy data requires that one must not only compute the distance between fixed shapes but one needs to optimize over the shape itself as well.

We seek to overcome these problems by means of convex relaxation, yielding feasible models, while trying to preserve as much of the initial descriptive power of the Gromov-Wasserstein distance as possible.

### Methods and Results

By two subsequent approximation steps the initial Gromov-Wasserstein distance is converted into an optimal transport problem with a problem specific cost function. Hence, at all steps standard linear solvers can be used. In contrast to conventional optimal transport problems with cost functions based on mere distances our approach can correctly establish correspondences between objects after Euclidean transformations. Optimizing over a joint functional with a data fidelity and a shape prior term can reveal the sought-after shape regardless of its position and orientation (see Fig. 1). Although some additional difficulties arise, this in principle extends to a geodesic framework.

### Outlook and Future Work

Currently the prior functional consists only of linear terms thus having only limited descriptive power. Future work will include investigating the potential of higher order terms.

Funding: DFG, grant GRK 1653

## Variational Recursive Joint Estimation of Scene Structure and Egomotion from Monocular Image Sequences

For driver-assistance systems it is essential to have a reliable representation of the surrounding scene. In this project we consider a monocular camera setup and develop an approach to jointly estimate the camera motion and a dense scene representation.

Our formulation balances the model expressiveness and computational efficiency.

• Becker, F., Lenzen, F. and Schnörr, C.

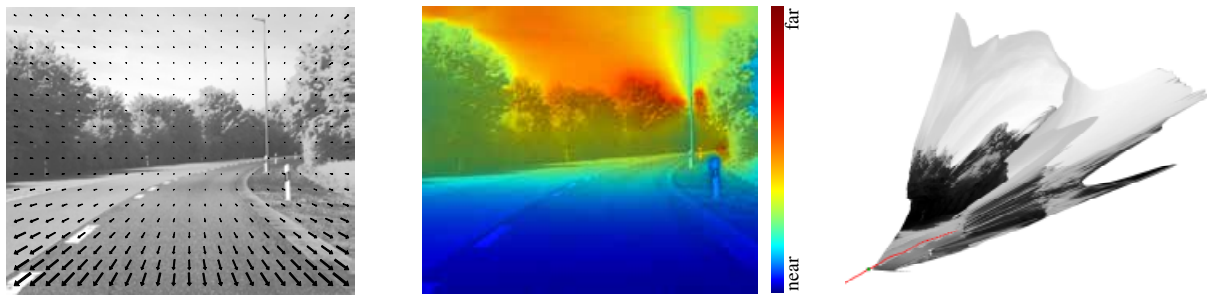


Fig. 1: Left: One frame of a monocular traffic image sequence with large displacements (arrows) up to 35 pixels induced by a fast moving camera. Our approach jointly estimates camera motion and (middle) a “dense depth map” (colour-encoded, superimposed on the frame). Right: Reconstruction of dense scene structure based on the depth maps from the camera’s viewpoint (green), and the corresponding camera track (red).

### Background and Goals

In this project we consider image sequences recorded by a single fast moving camera, e.g. mounted in a car. We exploit the apparent motion of the static scene induced by the camera movement – known as optical flow – to jointly estimate both the (unknown) camera trajectory as well as a scene representation.

In contrast to feature-based methods we estimate a dense depth map which provides distance information together with a reliability measure at any image position. Furthermore, we allow the camera to move freely (i.e. full translation and rotation) and not constrained to e.g. yaw and horizontal translation.

### Methods and Results

In view of an implementation in dedicated hardware, we chose a recursive formulation of the

highly involved chicken-and-egg problem of jointly estimating egomotion and the depth map. This ansatz reduces data storage to a minimum as it requires only the two most recently recorded image frames for computation. At the same time it allows to efficiently incorporate information from previous frames and thus increases robustness and temporal consistency.

We make use of established mathematical methods to solve the underlying optimisation problems arising from a variational formulation. Second-order Newton-like methods speed up convergence, especially for the high-dimensional depth map estimation. Accurate camera pose estimation is performed on the Euclidean manifold. For details we refer to [1].

The approach is evaluated by means of real traffic image sequences. The results compare favourably with two alternative settings that require more

input data: The depth map estimated by our approach is verified by comparing to stereo methods which are based on image pairs recorded by stereo setups with much better motion parallax than the monocular scenario. The computed egomotion is compared to the camera tracks provided by a bundle adjustment implementation which have access to all image frames simultaneously.

### Outlook and Future Work

Our current research concentrates at further refining the theoretical foundations of this approach. Future work involves verification of the accuracy and robustness as well as extension to motion-based segmentation of the scene.

Funding: HCI

### References

[1] Becker, F., Lenzen, F., Kappes, J. H., and Schnörr, C. “Variational Recursive Joint Estimation of Dense Scene Structure and Camera Motion from Monocular High Speed Traffic Sequences”. In 2011 IEEE International Conference on Computer Vision (ICCV), pp 1692–1699, 2011.

## CHAIR OF OPTOELECTRONICS PROJECT OVERVIEW

• Prof. Dr. Karl-Heinz Brenner

**96 | Accelerated calculation of z-scans in numerical light propagation**

Brenner, K.-H.

**98 | Design of a diffractive micro lens array for Shack-Hartmann wavefront sensing**

Stenau, T. and Brenner, K.-H.

**100 | Diffractive micro lens arrays with overlapping apertures – design, fabrication and application**

Liu, X., Stenau, T. and Brenner, K.-H.

**102 | Imaging properties of a multi-spectral fluorescence microscope**

Slogsnat, E., Fischer, P. and Brenner, K.-H.

**104 | Impact of different field calculation methods on local light absorption  
in periodic structured media**

Auer, M. and Brenner, K.-H.

**106 | Integration of micro-optical and electronic systems  
for the fabrication of Active Optical Cables**

Merchán, F. and Brenner, K.-H.

**108 | On the true inclination factor under realistic focusing conditions**

Brenner, K.-H.

**110 | Optimization of local absorption in layered media**

Brenner, K.-H.

**112 | Sensitivity-enhanced complex amplitude retrieval using multi-plane intensity detection  
and a micro lens array**

Liu, X. and Brenner, K.-H.

**114 | Talbot Focusing – A new effect of periodic structures and its utilization**

Buschlinger, R. and Brenner, K.-H.

**116 | Treatment of oblique illumination in numerical light propagation**

Brenner, K.-H.

## Accelerated calculation of z-scans in numerical light propagation

• Brenner, K.-H.

The numerical treatment of light propagation usually occurs between two planes perpendicular to the optical axis. In this case, an x-y-section (see fig.1, blue) is calculated and displayed.

For the analysis of focused beams, for wave guides, for Talbot carpets or in imaging situations for the investigation of depth of focus, also a x-z-section or a y-z-section (see fig.1, green) is of interest. Fig.2 shows such an example, where the focus for a thin element lens with a parabolic phase profile and a numerical aperture of 0.15 was analysed. The figure displays the amplitude instead of the intensity in order to enhance the low amplitude components.

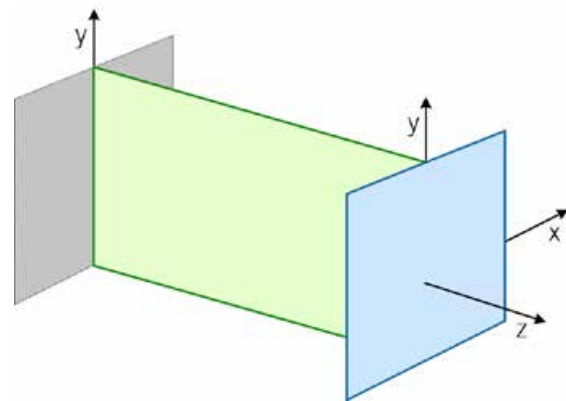


Fig. 1: Illustration of a x-y-section (blue) and a y-z-section (green)

The brute force method for obtaining such a z-scan is to select a start position  $z_0$  and a z-step  $dz$  and then to perform  $NZ$  single propagation operations, where in each propagation step, a horizontal or vertical line is extracted from the 2D-data. The combination of these lines to an image results in the desired z-scan.

The time for this brute force approach is clearly  $NZ$  times the time for a single propagation step. In case of angular spectrum propagation, a speedup by a factor of 2 can easily be obtained by starting with the object spectrum instead of the spatial object distribution. By precalculation of the propagator, which is constant for a fixed  $dz$ , only a multiplication and a back transformation needs to be carried out for each propagation step. The speedup is 2, since the number of Fourier transforms is half of that of the brute force approach.

For a speed-up by more than a factor of 2, a different approach is needed.

If the x-y section is of size  $N \times N$ , we achieved an additional speedup by a factor of approx.  $2N$  by the following method.

The basic idea for this acceleration is the application of the Fourier projection theorem. It basically states that the on-axis value is the sum over all contributions of the input distribution. The theorem can be generalized for two dimensions and for an arbitrary  $x_0$  or  $y_0$  position by the following integral:

$$u_z(x, y_0) = \iint \tilde{u}_z(v, \mu) e^{2\pi i(vx + \mu y_0)} dv d\mu = e^{2\pi i \mu y_0} \underbrace{\int \left( \int \tilde{u}_z(v, \mu) d\mu \right) e^{2\pi i v x} dv}_{\substack{\text{Projektion} \\ \text{1D-FFT}}} \quad (1)$$

The effort for one propagation step is therefore reduced from a two-dimensional Fourier transform to a one-dimensional projection and a one-dimensional Fourier transform.

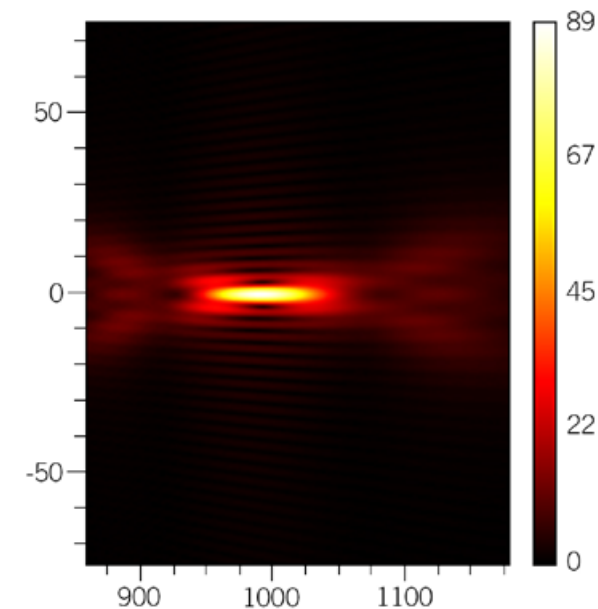


Fig. 2: x-z-Section of the focal amplitude for a thin lens with a parabolic phase profile and a numerical aperture of 0.15

Since the number of operations for a 2D-Fourier transform is  $2N^2 \ln N$  and number of operations for a 1D-Fourier transform is  $N \ln N$ , the additional speedup is

$$S = 2N \quad (2)$$

With this method, the time required for a 512x512 image can be reduced from a few minutes to a few seconds.

## Design of a diffractive micro lens array for Shack-Hartmann wavefront sensing

• Stenau, T. and Brenner, K.-H.

A common method to measure the aberrations of a wave front is the use of a Shack-Hartmann wavefront sensor. The two main components of this sensor are a refractive micro lens array with a given period and focal length, and a camera sensor which is placed in the focal plane of the micro lens array. An ideal wavefront produces a regular spot pattern on the camera. The spot pitch ( $P$ ) is determined by the pitch of the micro lens array. For a wavefront with small aberrations, the spots are shifted according to the local tilt of the incoming wave. From the spot shift, the gradient of the wavefront can be determined. The accuracy of the wavefront measurement depends on the accuracy of the measured spot shifts, which again depends on the sensor pixel size.

The spot shift is linear proportional to the focal length, thus the accuracy can be increased with longer focal lengths. Using refractive micro lenses, however, there is a limit with respect to the focal length ( $f$ ), since the diameter of the focal spot increases with decreasing numerical aperture ( $NA$ ). When the spot size exceeds the pitch, the accuracy limit is reached.

By using a diffractive micro lens array, we are able to avoid this problem. For these lenses,  $NA$ ,  $f$  and  $P$  can be chosen independently [1]. This is possible, since diffractive micro lenses can be designed with overlapping aperture. Therefore, a long focal length can be combined with small focal spots, allowing a detection of very small wavefront tilts.

We designed and produced a binary diffractive micro lens array consisting of  $22 \times 28$  replicas of a  $320 \mu\text{m} \times 320 \mu\text{m}$  elemental cell. The primitive cell has a resolution of  $128 \times 128$  pixels and is shown in figure 1. For the focal length we chose 10 cm at the HeNe laser wavelength of 633 nm and the design  $NA$  was chosen to 0.02.

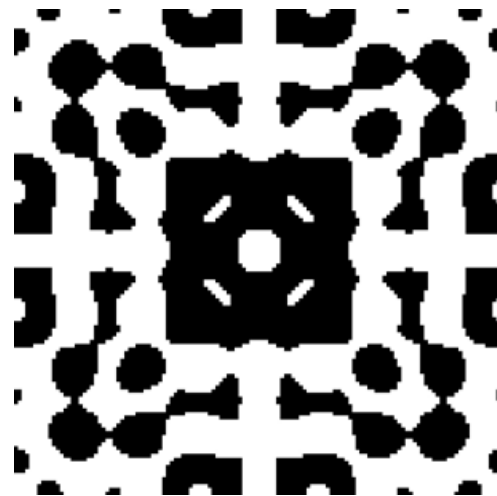


Fig. 1: Primitive cell of the diffractive micro lens array.

In a lithographic process we transferred this structure to a float glass substrate coated with photoresist. The height of the developed photoresist resulted in a phase shift of  $\pi$ . A microscope image of the produced diffractive micro lens array is shown in figure 2.

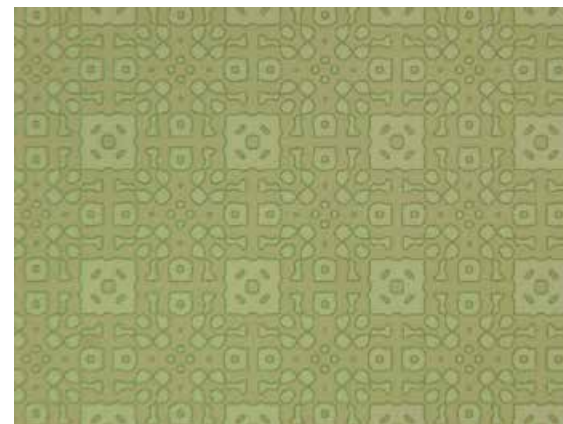


Fig. 2: Microscope image of a few primitive cells of the produced diffractive micro lens array.

In a numerical simulation, we illuminated the element with a plane wave. The cross section of the amplitude in the designed focal plane at  $z = 10$  cm is shown in figure 3.

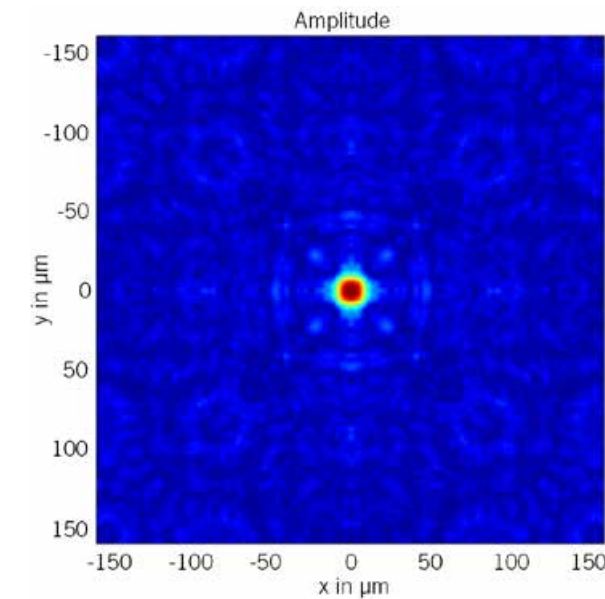


Fig. 3: Amplitude in the designed focal plane.

The spot size of a comparable refractive micro lens array with the same focal length and pitch would be  $400 \mu\text{m}$ , which is significantly larger than the pitch. Here, the width of the focal spot is approx.  $20 \mu\text{m}$ . For a CCD with  $2 \mu\text{m}$  pixel size, a spot shift of  $0.5 \mu\text{m}$  is safely detectable. Thus, the achievable angular resolution should be better than  $5 \cdot 10^{-6}$ . The performance of this new type of Shack-Hartmann sensor is presently investigated by a group at the Laser-Laboratorium Göttingen e.V.

### References

[1] Liu, X, Stenau, T., Brenner, K.-H., „Diffractive micro lens arrays with overlapping apertures”, 11th Euro-American Workshop on Information Optics (WIO 2012).

# Diffractive micro lens arrays with overlapping apertures – design, fabrication and application

• Liu, X., Stenau, T. and Brenner, K.-H.

Diffractive micro lens arrays offer a fundamental advantage over refractive ones: the effective numeric aperture ( $NA$ ) can be selected independent of the lens pitch and the focal length. The cell  $NA$  is defined by

$$NA_{cell} = \frac{P}{\sqrt{P^2 + 4f^2}} \quad (1)$$

where  $P$  is the pitch and  $f$  the focal length of the micro lens array. The effective  $NA$  is given by the diameter of the pupil (magenta in fig.1). If the effective  $NA$  is larger than the cell  $NA$ , an overlapping micro lens array is realized. By lens overlapping, a dense array with large working distance and high numerical aperture is possible.

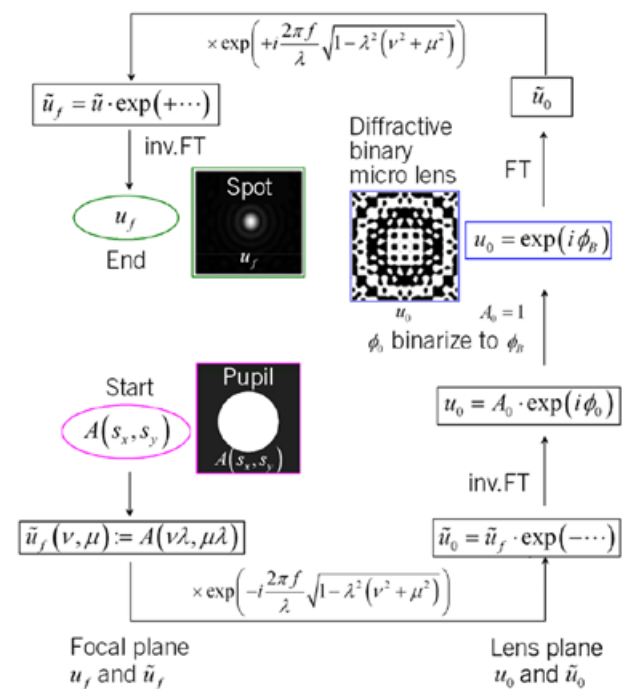


Fig. 1: Design procedure: pupil function (magenta); diffractive binary micro lens (blue); spot diagram (green).

The design procedure, shown in figure 1 is similar to the method in reference [1]. With this design procedure, the effective  $NA$ , the focal length and the pitch of each micro lens can be chosen independently. In figure 2 we compared a refractive micro lens array with a diffractive one, where both had a lens pitch of  $256 \mu\text{m}$  and a focal length of  $10 \text{ mm}$ . The  $NA$  of the refractive micro lens is  $0.0128$ , equal to the cell  $NA$ . The effective  $NA$  of the diffractive micro lens is  $0.036$ , about  $2.8$  times larger than the cell  $NA$ . Due to the overlapping aperture, the diffractive focal spot is clearly sharper than the refractive one.

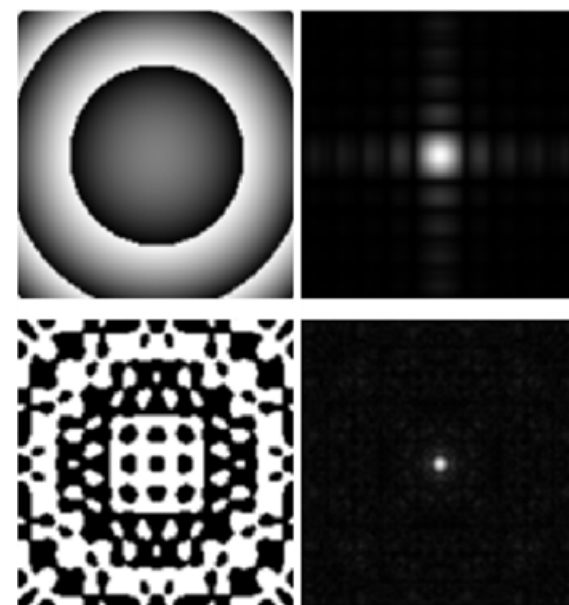


Fig. 2: Comparison of a refractive micro lens (top) and a diffractive one with overlapping aperture (bottom). In both cases,  $f=10 \text{ mm}$ ; phase (left) and focal amplitude (right).

For the fabrication of diffractive micro lens arrays, we applied our laser lithography. The photo resist was Shipley S1805. Here for simplicity, we used the resist layer as the phase structure and the measured phase shift deviated from  $\pi$  only by a few percent. In figure 3 we show a microscope image of the fabricated micro lens and the focal intensity by illumination with a laser diode. The line plots through one focal spot confirm a good agreement between calculated and measured spot intensities.

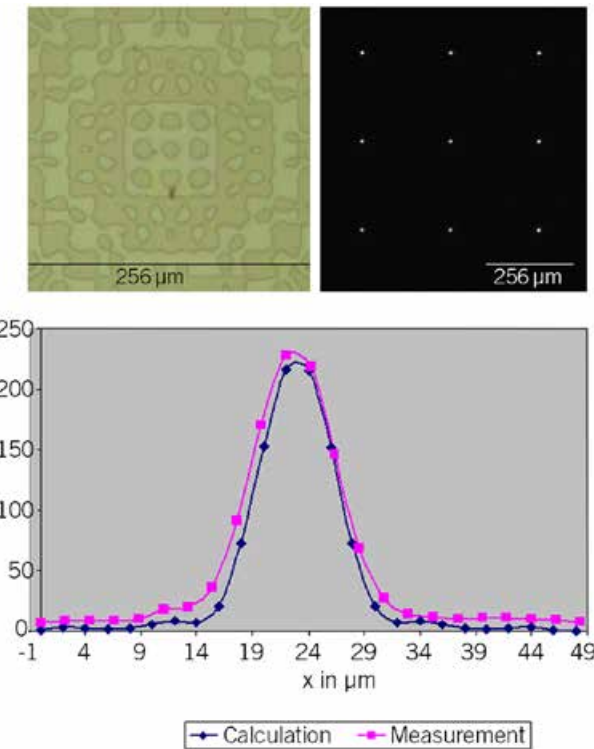


Fig. 3: Microscope picture of fabricated micro lens (top left), intensity spot diagram with  $3 \times 3$  focal spots shown (top right), line scans of calculated and measured spot intensity (bottom)

In one of our current projects, such an overlapping diffractive micro lens array was applied to multi-plane iterative phase retrieval. By applying a diffractive micro lens array to Hartmann-Shack wave front sensing, the spot density can be increased without changing the focal length, thus enabling a higher spatial resolution.

Further applications are multi-spot scanning microscopy or light concentration [1, 2].

## References

[1] Hulsken, D., Vossen, S. and Stallinga, S., "High-NA diffractive array illuminators and application in a multi-spot scanning microscope", J. Europ. Opt. Soc. Rap. Public. 12026 Vol. 7 (2012).  
[2] Brenner, K.-H. and Buschlinger, R., "Talbot Focusing – a new effect of periodic structures and its utilization", DGaO Annual meeting in Eindhoven, Netherlands (2012).

## Imaging properties of a multi-spectral fluorescence microscope

• Slogsnat, E., Fischer, P. and Brenner, K.-H.

The realized microscope setup is able to acquire images of four different fluorophores at the same point in time. The schematic setup is shown in Fig.1.

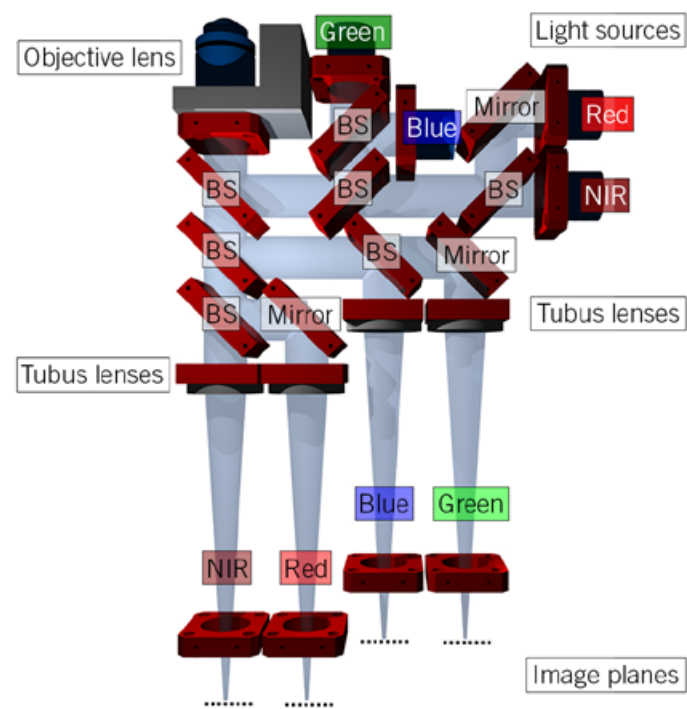


Fig.1: Schematic setup of the multi-spectral fluorescence microscope

The resolution of each channel is analyzed by imaging a Siemens star with 30 spokes and a radius of  $400\ \mu\text{m}$  (Fig. 2). In order to be able to measure the magnification, it is surrounded by a square-shaped frame with a length of the edges of  $500\ \mu\text{m}$ . Due to the mainly spherical deformations of the used beam splitters, all channels show astigmatism except the NIR channel, where the beam splitters are only used in transmission.

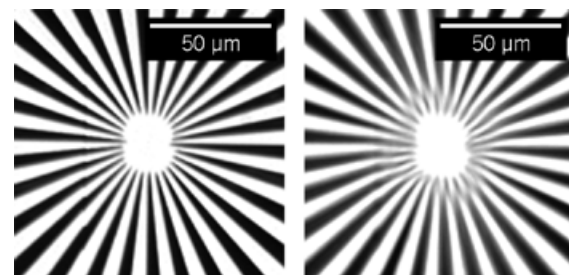


Fig.2: Camera images of Siemens stars (left: NIR channel; right: red channel)

The resolution of the NIR channel is below  $1\ \mu\text{m}$ , of the red channel  $2.7\ \mu\text{m}$ , of the blue channel  $2.2\ \mu\text{m}$  and of the green channel  $2.5\ \mu\text{m}$ .

The NIR channel matches the ideal magnification of 10, whereas the other channels show slight deviations and produce smaller images of the object. This is caused by the process of refocusing in order to compensate the astigmatism. The magnification in the red channel is 9.95, in the blue channel 9.82 and in the green channel 9.92.

High power LEDs are used as excitation light sources. Only in the red channel a halogen bulb – coupled into a fiber – is used, because there is no high power LED available which features the required spectrum. Fig.3 shows the fluorescence images of the NIR and the red channel.

The exposure time of the NIR channel is 6 s, of the red channel 9.8 s, of the blue channel 80 ms and of the green channel 4 s.

It is striking that the exposure times of all channels except the blue channel are very high. Only in the blue channel an exposure time which makes fast scanning of the probe possible is achieved. The reason for these high exposure times is the low optical power of the light sources and the different quantum yields of the fluorophores. The blue

channel features the light source with the highest optical power of 9.13 mW at the object plane, whereas the source in the red channel, where only an underexposed image at the maximum exposure time of the camera was obtained, has just an optical power of 0.85 mW.

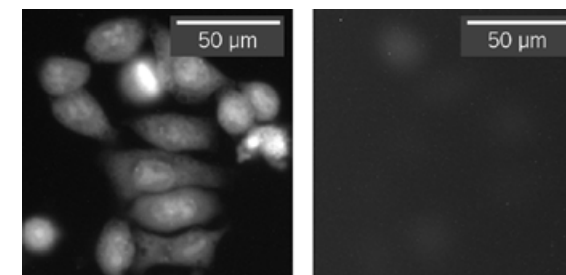


Fig.3: Fluorescence images (left: NIR channel; right: red channel)

### Conclusion

The blur of the images in the red, blue and green channels arises from the deformations of the beam splitters and can be eliminated by exchanging these elements through optical flat beam splitters. Then the obtained images will be as sharp as in the NIR channel.

Exposure times suitable for fast scanning microscopy can be achieved by using lasers instead of high power LEDs. Lasers which feature the required spectrum and optical power are available for each channel.

## Integration of micro-optical and electronic systems for the fabrication of Active Optical Cables

• Merchán, F. and Brenner, K.-H.

In recent years, the development of active optical cables has been incentivized by the requirements of the rapidly growing high performance computers and correspondingly the interconnections market, moreover, the optimization of the fabrication process and the development of smart and efficient solutions has become a research topic. The most important factors that must be considered already in the design phase are the feasibility with available technology, costs and the possibility of automation of the fabrication and adjustment processes. The fabrication of AOC's is driven by these factors; consequently, all processes involved have to be optimized in order to meet the requirements.

The replication of metal masters for the fabrication of optical couplers has been confirmed as a very accurate and cost effective method. In order to complete the optimized fabrication chain, the optical systems have to be integrated with the electronics, which is fabricated with well-known, available methods. For this purpose, a modular construction is implemented so that the optical- and the electronic sub-systems are constructed and after their functionality is proven, the systems are aligned using standard mechanics. The constructed system has 5 degrees of freedom: the cartesian coordinates and two tilt angles that are critical to achieve the desired coupling efficiency. The tilt angle around the transversal axis of the VCSEL array is the most critical one (see Fig.1). Measurements show that this angle is up to  $2.3^\circ$  in the worst case for a standard manual flip-chip process. This precision is inherent to the used laboratory machine and might be better in current automated industrial processes.

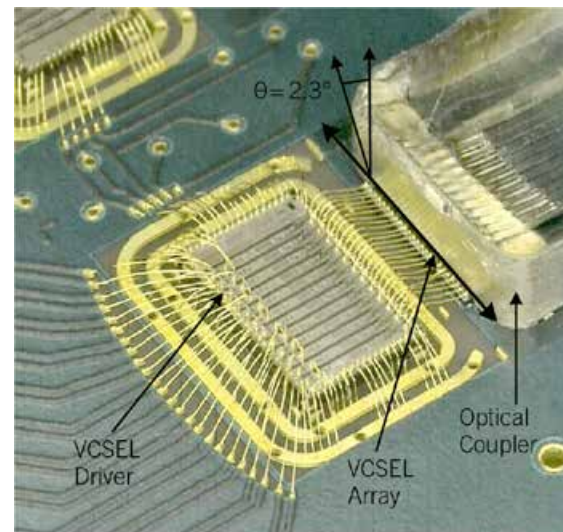


Fig. 1: Adjustment of the coupler on the PCB

With this angle adjusted, a coupling efficiency of about 50% can be assured. For systems that are some meters in length (up to 10 m), this coupling efficiency is acceptable. In order to reach higher coupling efficiencies, an active adjustment is required. The Fig.2, shows the coupling efficiencies that can be reached with passive alignment and the improvement if active alignment is made. When using active alignment the coupling efficiency is, in the worst case, about 90%; which represents a considerably higher efficiency than that reached using passive alignment.

Optical couplers, VCSEL-Driver, VCSEL-Array, Transimpedance-Amplifier and Photodiode-Array are integrated in a  $22 \times 25 \text{ mm}^2$  and 3mm height PCB (see Fig.3). With commercially available devices it is possible to achieve up to 12.5 Gbit/s per channel and in the complete AOC up to 300 Gbit/s duplex.

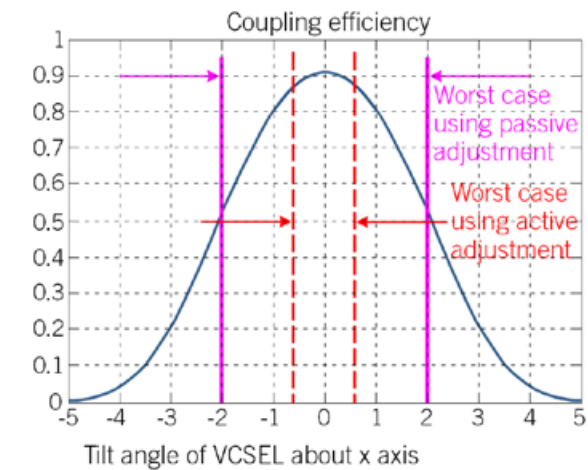


Fig. 2: Coupling efficiency on tilt angle dependency

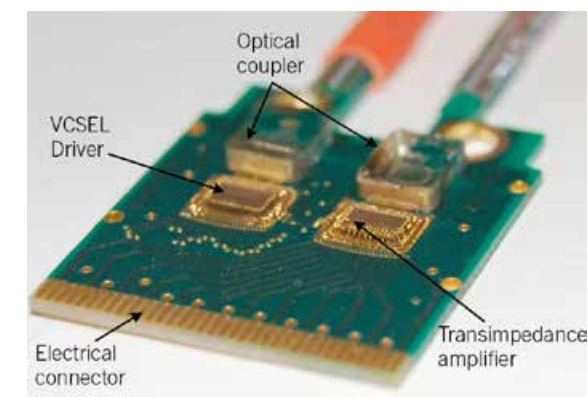


Fig. 3: Fabricated Active Optical Cable

### References

[1] Merchán, F., Brenner, K.-H. „Novel integrated micro-optics system for the fabrication of Active Optical Cables“, (Online-Zeitschrift der Deutschen Gesellschaft für angewandte Optik e. V.), ISSN: 1614-8436-urn:nbn:de:0287-2012-B036-5, 113. Jahrestagung, 29. Mai-02. Juni 2012, Eindhoven, (2012).

## Impact of different field calculation methods on local light absorption in periodic structured media

• Auer, M. and Brenner, K.-H.

Precise knowledge of the spatial location of light absorption in structured media is needed for the optimization of optoelectronic devices like detectors, solar cells or photolithographic systems. Recently we reported a definition for local absorption, which is derived from electromagnetic near fields [1]:

$$a(\mathbf{r}) = \frac{k_0^2}{k_{inc,z}} \frac{1}{A} \text{Im}(\epsilon(\mathbf{r})) \cdot |\mathbf{E}_1(\mathbf{r})|^2 \quad (1)$$

Unlike the global absorption  $A$ , where energy conservation is obtained by definition,

$$A = 1 - \text{Transmission} - \text{Reflection} \quad (2)$$

the local absorption  $a$  depends on the method of field calculation, which is not unique.

In the RCWA algorithm the inverse Li-rule [2] improves stability in the calculation of reflection and transmission coefficients in case of complementary discontinuities in permittivity and field. The standard field calculation approach uses the same inverse rule, expressed by the mode limited Matrix  $\mathbf{E}_a^{-1}$ :

$$E_x = \sum_m e_m(z) e^{ik_x m x}, \mathbf{e}(z) = -i \mathbf{E}_a^{-1}(\mathbf{W} \cdot \mathbf{Q} \cdot \mathbf{D}(z)) \quad (3)$$

Due to the discontinuity of the materials at boundary surfaces, a second method, introduced by Lalanne and Jurek (PLMJ) [3], derives the E-field from a continuous D-field and multiplies with the original non-mode limited permittivity  $\epsilon(x)$ :

$$E_x = \frac{1}{\epsilon} \sum_m d_m(z) e^{ik_x m x}, \mathbf{d}(z) = -i(\mathbf{W} \cdot \mathbf{Q} \cdot \mathbf{D}(z)) \quad (4)$$

In a third method (KHB) Brenner [1] likewise derives the E-field from a continuous D-field. But because the material distribution is mode-limited and thereby continuous, he returns to a purely mode-limited implementation, avoiding the inverse Li-rule:

$$E_x = \sum_m e_m(z) e^{ik_x m x}, \mathbf{e}(z) = -i \mathbf{E}^{-1}(\mathbf{W} \cdot \mathbf{Q} \cdot \mathbf{D}(z)) \quad (5)$$

In order to compare the various field calculation methods in two- and three-dimensional structured media, we introduced three criteria:

Our first criterion is based on convergence. We compare low mode count results to a converged, high mode count result. Secondly we check Maxwell's continuity conditions, which require tangential field components to be continuous. The third criterion tests conservation of energy, which in this case means an agreement of global absorption (eq. 2) and integrated local absorption (eq. 3) over the full grating:

$$A \stackrel{!}{=} \iiint a(\mathbf{r}) dV \quad (6)$$

In a test case, a 2D absorbing GaAs-grating is illuminated with a TM-polarized plane wave ( $\lambda = 1 \mu\text{m}$ ). The global absorption from RCWA is 1.39%.

In the two-dimensional case (fig.1) we can see that for a small mode count the PLMJ-method and the KHB-method both satisfy the third criterion much better than the standard method. While the PLMJ-method has more visual similarities with the converged field solution, the KHB-method brings in self-consistency by staying compatible with the mode limitation of the RCWA.

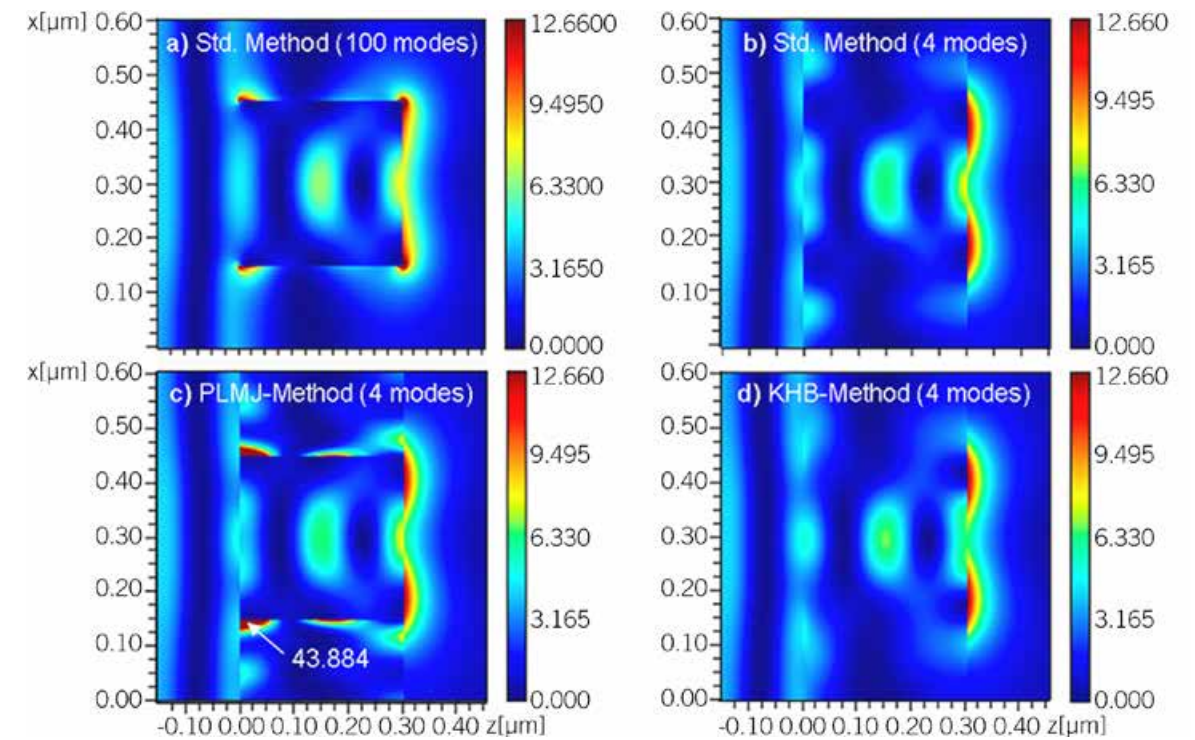


Fig. 1: Different field calculation methods and their effect on local absorption. Integrated absorption (and deviation):

- a) Std. method (100 modes): 1.447% (= +4.1% dev.)
- b) Std. method (4 modes): 1.475% (= +6.12% dev.)
- c) PLMJ-method (4 modes): 1.391% (= +0.14% dev.)
- d) KHB-method (4 modes): 1.398% (= +0.58% dev.)

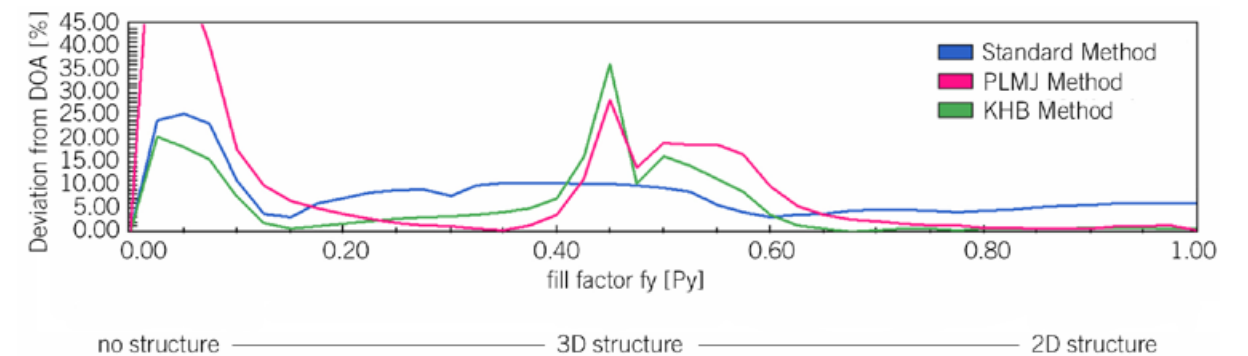


Fig. 2: Deviation between global absorption and integrated local absorption for various three-dimensional gratings

### References

- [1] Brenner, K.-H., „Aspects for calculating local absorption with the rigorous coupled-wave method“, Opt. Express, 10369-10376, 2010.
- [2] Brenner, K.-H., „Aspects for calculating local absorption with the rigorous coupled-wave method“, Opt. Express, 10369-10376, 2010.

In the three-dimensional case the results are less clear. Here the results strongly depend on system geometries (fig. 2). Nevertheless the three criteria are a useful instrument to validate simulation results with small mode counts.

- [3] Lalanne, P. and Jurek, M.P., „Computation of the near-field pattern with the coupled-wave method for transverse magnetic polarization“, Journal of Modern Optics, Vol. 45, No. 7, 1357-1374, 1998.

## On the true inclination factor under realistic focusing conditions

• Brenner, K.-H.

Light focusing is important in many applications of optics, like in particle trapping, laser welding or in optical storage. The standard treatment of a focusing lens was given by Richards and Wolf [1] as a vectorial extension of the scalar Debye approximation [2]. Although the work of Debye is mentioned in [1], a reference to this paper is missing there. The focal distribution in [1] is given as  $(\mathbf{s}_\perp = (s_x, s_y))$

$$\mathbf{e}(\mathbf{r}) = \frac{-ik}{2\pi} \iint_{\Omega} \frac{\mathbf{a}(\mathbf{s}_\perp)}{s_z} e^{ik(\Phi(s_\perp) + \mathbf{s} \cdot \mathbf{r})} d^2s_\perp \quad (1)$$

In Wolf's derivation, the conversion from a plane wave to a spherical converging wave was treated in an abstract way as a system, obeying the sine condition. The amplitude change follows from the law of energy conservation and results in the inclination factor

$$\mathbf{a}(\mathbf{s}_\perp) = f \cdot \sqrt{s_z} \cdot \mathbf{e}_1$$

where the polarization vector  $\mathbf{e}_1$  follows from a decomposition of the incident field into TE- and TM-components which are transferred across the interface.

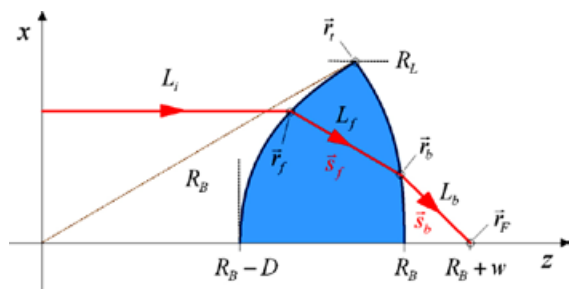


Fig. 1: Geometry of the perfect focussing lens

In this work, we have analyzed a realistic lens with perfect ray focusing properties (fig.1). Since the polarisation treatment is the same as in [1], we only compared the pupil amplitude.

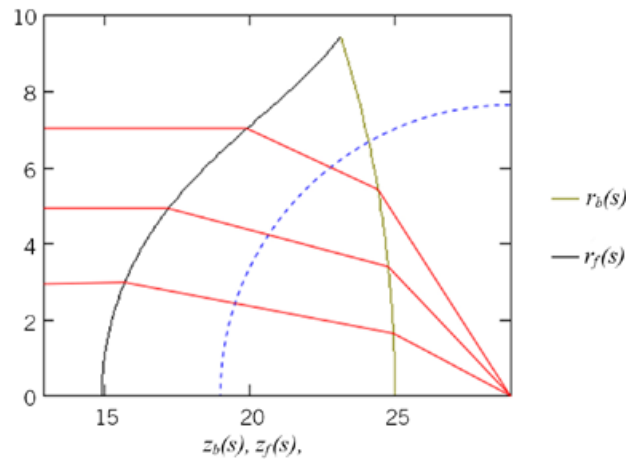


Fig. 2: Analytic shape of the front and back surface of a perfect focusing lens, together with three raypaths (red) and reference sphere for the paraxial  $f$  (blue).

We modeled the perfect focusing lens with aspheric front surface,  $n_{lens} = 1.52$  and spherical back surface  $R_B = 25\text{mm}$ , as shown in fig.1. This problem can be solved analytically by using  $s$  as the  $x$ -component of  $s_b$  as a parameter. Hence, both, the front surface  $r_f(s)$  and the back surface  $r_b(s)$  are available in an analytic form and can be plotted as shown in fig.2.

Using the law of energy conservation for the Poynting vectors

$$\mathbf{S}_{in}(s) d\mathbf{A}_{in} = \mathbf{S}_{out}(s) d\mathbf{A}_{out} \quad (3)$$

we can use the fact that the area element is planar at the input and spherical at the output. Thus the directions of  $\mathbf{S}$  and  $d\mathbf{A}$  agree in both cases. If we choose  $f$  as the paraxial focal length, we obtain

$$a(\mathbf{s}_\perp) = \frac{1}{f} \sqrt{\frac{s_z}{2s_\perp} \frac{\partial r_{f,\perp}^2(s_\perp)}{\partial s_\perp}} \quad (4)$$

which is to be compared with the inclination factor  $f \cdot \sqrt{s_z}$  from eq. 2. Figure 3 shows such a comparison with the Richards-Wolf result shown as blue, dotted curve and the inclination factor according to eq. 4 with  $NA = 0.85$ ,  $R_L = 9.44\text{mm}$  in red.

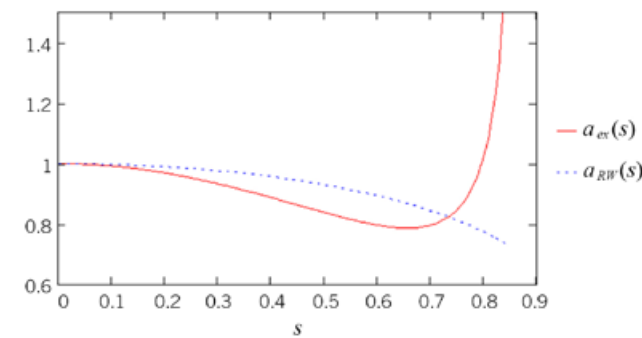


Fig. 3: True inclination factor (red) for a perfect focusing lens compared to the Richards-Wolf result (blue)

The pupil amplitude falls off more rapidly at small angles and increases strongly towards the lens edge, which results in sharper spots than predicted in [1]. These results are confirmed using the Fresnel formula.

### References

- [1] Richards, B., Wolf, E., "Electromagnetic diffraction in optical systems, II. Structure of the image field in an aplanatic system," Proc. R. Soc. London Ser. A 253, 358–379, (1959).
- [2] Debye, P., "Das Verhalten von Lichtwellen in der Nähe eines Brennpunktes oder einer Brennlinie" Ann. Phys. 335(14), 755–776, (1909).

## Optimization of local absorption in layered media

• Brenner, K.-H.

Local absorption plays an important role in all semiconductor detectors and solar cells. Since all the standard multilayer stack theories only provide global absorption, being defined as the difference of incoming power and the sum of reflected and transmitted power, information is lost, concerning the exact position along the stack, where absorption takes place. In semiconductors, the photon to electron conversion is most efficient, if the absorption takes place at or near the depletion layer, while absorption at other positions only contributes to heat generation. Being able to compute local absorption, allows an optimization of a structure with respect to conversion efficiency.

The theoretical basis for describing local absorption has been published in [1] for the standard RCWA-implementation. For a stack of layers with different thicknesses and permittivities, a different approach using Poynting vector differences was recently published in [2]. Our theory of local absorption can be adapted to a layer stack [3] in a straight forward manner and shows perfect numerical agreement with the results in [2].

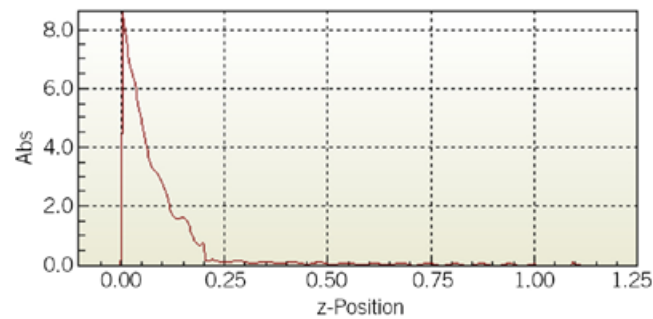


Fig. 1: Local absorption  $a(z)$  for a typical solar cell structure. Most of the light is absorbed at the interface between air and the amorphous silicon layer.

If the layers are assumed constant in the x-y plane and z is the direction along the stack, we define the integrated absorption by

$$A_{z_1, z_2} = \int_{z_1}^{z_2} a(z') dz' \quad (1)$$

It describes the ratio of incident power to the power absorbed in the interval between  $z_1$  and  $z_2$ . Using the equations derived in [1], we can write the

$$a(z) = \frac{\partial A(z)}{\partial z} = \frac{k_0^2}{k_{z,i}} \text{Im}(\epsilon) |\mathbf{E}_i(z)|^2 \quad (2)$$

Here,  $k_{z,i}$  is the z-component of the incident k-vector,  $\epsilon$  is the permittivity of the medium at position z and  $\mathbf{E}_i$  is the local electric field, resulting from an incident electromagnetic plane wave with an electric field amplitude of one. Note that  $a(z)$  has a dimension of 1/m and  $A_{z_1, z_2}$  is dimensionless since it describes a ratio.

For a layered stack of amorphous silicon, polysilicon, silicon oxide and steel, as is usual in solar cells, we can calculate the local absorption for different layer thicknesses. A typical profile is shown in fig.1. As one can see, most of the light is absorbed at the interface between air and the amorphous silicon layer, while very little light is absorbed near the a-Si - poly-Si interface.

By varying the thickness of the first two layers, a map (fig. 2) for the absorption in a given region can be computed, which may serve as the basis for optimizing absorption in the desired region.

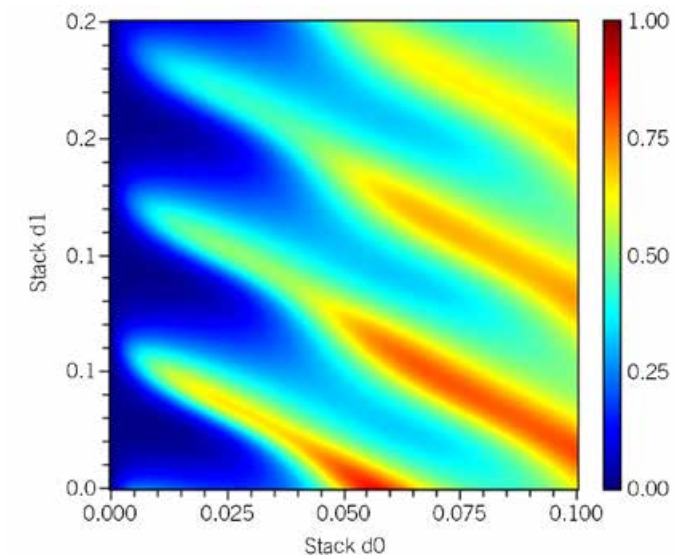


Fig. 2: Variation of the thicknesses of layer 1 and layer 2 shows pronounced absorption maxima in layer 0, which can be used for optimization

The optimization of a detector structure is of equal importance, since the increase in photo current goes along with a reduction in heat generation. The technique can also be extended to polychromatic light.

### References

- [1] Brenner, K.-H., "Aspects for calculating local absorption with the rigorous couple-waved method", *Opt. Express*, 18, 10369-10376, (2010).
- [2] Deparis, O., "Poynting vector in transfer-matrix formalism for the calculation of light absorption profile in stratified isotropic optical media", *Opt. Lett.* 36, 3960-3962 (2011).
- [3] Brenner, K.-H., "Optimization of local absorption in layered media", 8th EOS Topical Meeting on Diffractive Optics, Delft/NL, (2012).

## Sensitivity-enhanced complex amplitude retrieval using multi-plane intensity detection and a micro lens array

• Liu, X. and Brenner, K.-H.

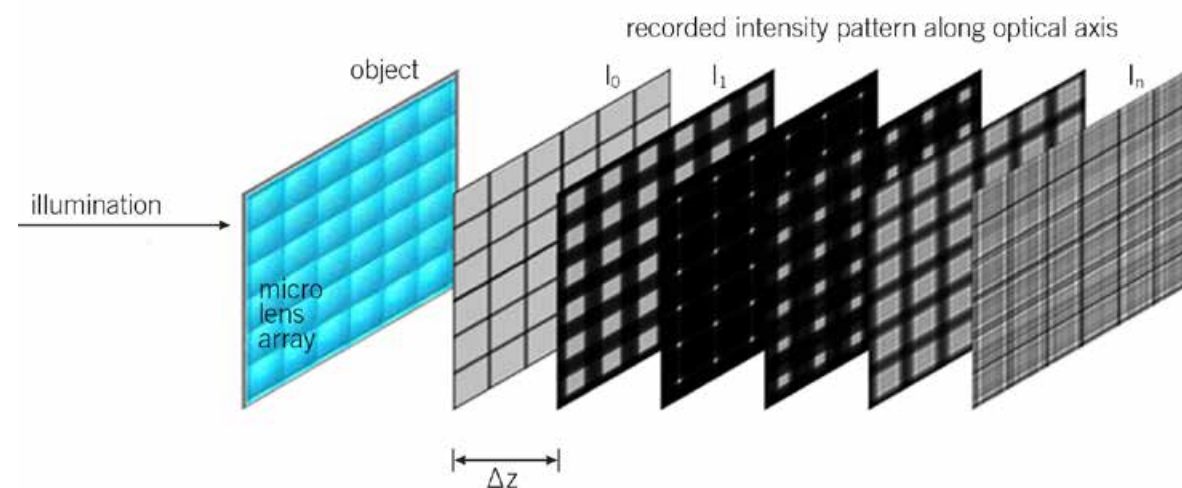


Fig.1: Scheme for multi-plane measurement of intensity around the focal plane

Phase retrieval methods like the classical Gerchberg-Saxton algorithm have an advantage compared to interferometric and holographic methods, in that they require no reference wave. Thus no laser is required and the set-up can be very simple and stable. Pedrini has extended this method to obtain the complex amplitude from a sequence of diffraction intensities [1, 2]. Unfortunately, the method is only reliable for non-smooth phase distributions. For smooth phase distributions, the intensity change along the propagation direction  $z$  is too small for a reliable reconstruction, thus phase retrieval is only possible with highly increased  $z$ -sampling. Here we propose an extension of his method by including a micro lens array, similar to a Hartmann-Shack-sensor (HS). The lens enhances the intensity variation of the recorded intensity patterns and it is numerically easy to eliminate from the recovered phase distribution. The improved performance of the algorithm is firstly demonstrated by numerical simulations.

For HS-sensing, only the focal plane intensity is used to recover the wave front and the spatial sampling of the wave front is determined by the micro lens pitch. Classical HS-sensing is reliable only for smooth phases and the resolution is limited by the pitch. By combining the HS-sensor with multi-plane phase retrieval, the limitations of both methods can be removed. Here, a sequence of intensity measurements performed symmetrically around the focal plane is recorded and used to recover the wave front (figure 1). With this method, a phase distribution with both, smooth and non-smooth contributions can be reliably reconstructed.

Figure 2 shows a simulation result for recovering an inclined plane wave (left). Without the introduction of the auxiliary micro lens array, the intensity patterns at every propagation distance would be identical, resulting in a global constant as the reconstructed phase, which is obviously incorrect. With a refractive  $8 \times 8$  lens array placed at  $z=0$ ,

the intensity patterns show a variation, i.e. focusing and spot shift, which makes the recovery of complex amplitude possible. However, within each micro lens window there is one unknown constant phase shift (middle), which was removed by additional unwrapping and stitching (right).

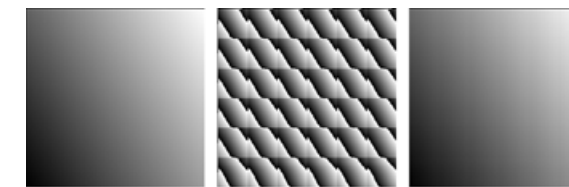


Fig.2: Simulation result for the recovery of an inclined plane wave from 20 intensities and 2 iterations. Left: initial phase distribution; middle: recovered wrapped phase distribution, greyscale corresponds to phase: white =  $\pi$ , black =  $-\pi$ ; right: recovered phase after unwrapping and stitching.

Figure 3 shows a simulation result for recovering the sum (left background) of a smooth (left top) and a non-smooth (left bottom) phase. Using the standard method, the smooth part of the phase will be lost. With this method, the reconstruction (right) is valid, confirming that the proposed method is reliable for both smooth and non-smooth phase distributions.

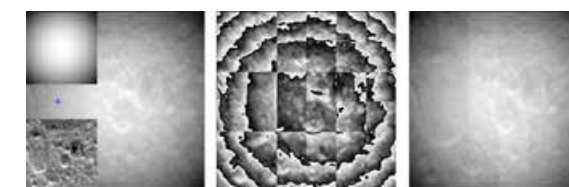


Fig.3: Simulation result to confirm that the proposed method is reliable for both smooth and non-smooth phase distributions (explanation: see text). The reconstruction was done with 20 intensity patterns und 2 iterations. Middle: recovered wrapped phase distribution; right: recovered phase after unwrapping and stitching.

### References

- [1] Pedrini, G., Osten, W. and Zhang, Y., "Wavefront reconstruction from a sequence of interferograms recorded at different planes", *Opt. Lett.*, Vol. 30, 833-835 (2005).
- [2] Almoró, P., Pedrini, G. and Osten, W., "Complete wavefront reconstruction using sequential intensity measurements of a volume speckle field", *Appl. Opt.*, Vol. 45, 8596-8605 (2006).

## Talbot Focusing – A new effect of periodic structures and its utilization

• Buschlinger, R. and Brenner, K.-H.

The Talbot effect is a well known phenomenon of self imaging, stating that either an amplitude or a phase distribution is replicated at the Talbot distance. Talbot imaging can also be observed at fractional Talbot distances [1] for special distributions. Talbot Focusing is a new effect, by which a highly concentrated focal spot appears at a particular distance from the periodic optical element. With this effect, the spot diameter is independent of the structure period and the focal length, enabling high NA-foci with large working distance or which are placed very dense.

By observing the intensity pattern behind a simple amplitude Ronchi grating (see fig.1), we see various effects. At the Talbot distance (here at 200 units), a perfect image of the input distribution is visible. At half the distance, a contrast inverted pattern is observed. What is most important, is that there are also certain distances, where pronounced on-axis focal spots appear.

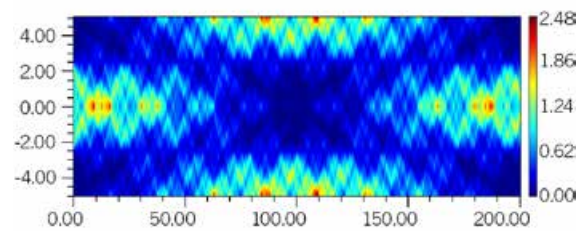


Fig.1: Light distribution  $I(x, z)$  behind a simple amplitude Ronchi grating. In addition to Talbot images, there are also focal spots on the optical axis.

These focal spots can be much smaller than focal spots generated with a micro lens of the same diameter. If we zoom into the first region between 0 and 50 units, we see, that these foci are not only very concentrated in the lateral direction but also in the longitudinal direction.

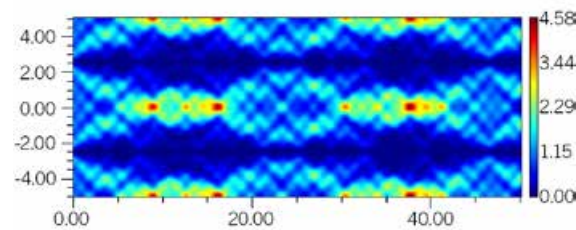


Fig. 2: Zoom into the intensity distribution of fig.1

A necessary condition for a focal spot is that the on-axis amplitude has a maximum. Taking into consideration, that the complex input transmittance is periodic, we can apply angular spectrum propagation for a periodic field and obtain

$$u_z(0,0) = \sum_{n,m} U_{m,n} e^{4\pi i \frac{\zeta}{\Lambda^2} \sqrt{1-\Lambda^2(m^2+n^2)}} \quad (1)$$

where  $\zeta = \frac{z}{z_T}$  is the z-position relative to the Talbot length and  $\Lambda = \frac{\lambda}{P}$  is the optical wavelength in

units of the element period.  $U_{m,n}$  are the Fourier coefficients of the input transmittance. From eq. 1 it is clear, that  $u_z(0,0)$  is maximized, when

$$U_{m,n} = e^{-4\pi i \frac{\zeta}{\Lambda^2} \sqrt{1-\Lambda^2(m^2+n^2)}} \quad (2)$$

A similar result has been obtained independently in [4]. With this result, quite unusual focusing arrays can be designed. In one extreme, an array with a numerical aperture of one was obtained for 1 mm focal distance and 32  $\mu\text{m}$  period. In another extreme, an array with a pitch of 300  $\mu\text{m}$  and a focal length of 10 cm was obtained.

These elements may find a large number of applications. The extremely long focal length elements e.g. can be used for the detection of wave-front tilts with an accuracy of  $10^{-6}$ . The high NA-elements can be used for scanning a microscopic sample with a high degree of parallelism.

### References

- [1] Lohmann, A. W., "An array illuminator based on the Talbot effect", *Optik*, 79, 41–45 (1988).
- [2] Buschlinger, R., Brenner, K.-H., "Light Focusing by binary phase gratings", 5th EOS Topical Meeting on Advanced Imaging Techniques (AIT), Engelberg/Ch (2010).
- [3] Brenner, K.-H., Buschlinger, R., "Parallel image scanning with binary phase gratings", *Journal of European Optical Society : Rapid Publications* 6, 11024 (JEOS:RP), (2011).
- [4] Stallinga, S., "High-NA diffractive array illuminators", EOS Topical meeting on Diffractive Optics, No. 4932, Delft (2012).

## Treatment of oblique illumination in numerical light propagation

• Brenner, K.-H.

In the thin-element-approximation (TEA), oblique illumination is usually treated by multiplying the input transmittance with the complex amplitude of a tilted plane wave, i.e.

$$u_0(x, y) = t(x, y) e^{i(k_x x + k_y y)} \quad (1)$$

For the object spectrum, this modulation results in a frequency shift, which increases the required real estate in the frequency domain – a problem, which has also been observed by Testorf [1].

The topic of this work is another, more serious problem with this method. In any numerical implementation, the true simulated object is a periodic replication of the central period. By multiplying the input transmittance with a tilted plane wave, the true operation is a multiplication with a sawtooth phase, since, unknowingly, we apply the same linear phase to each period. Fig.1 illustrates this:

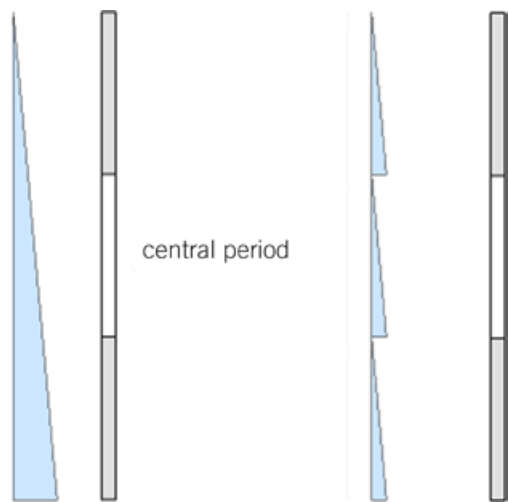


Fig.1: Oblique illumination can be considered as a linear phase element. In a periodic situation, a sawtooth phase (right) is effectively applied instead of an infinitely extended linear phase (left).

If  $P$  is the calculation period, then only for certain angles,

$$\sin \vartheta = m \frac{\lambda}{P} \quad (2)$$

the phase step height is an integral multiple of  $2\pi$ . For all other angles, the neighbouring periods experience a constant phase shift, which differs in all periods. The effect of this error phase is hardly visible in most numerical calculations. The error, however, becomes very prominent in Talbot imaging. This can be explained very simple without any mathematics. At the Talbot distance, the Fresnel propagation phase is zero (or a multiple of  $2\pi$ ), which leads to a perfect amplitude and phase image of the input distribution. Assume, the input is a rectangular slit, the Talbot image will also be an unshifted rectangular slit with linear phase modulation. For a correct simulation, it should, however, be a shifted slit. This simple example illustrates, that the error phase can lead to very severe errors. Another example is a diffractive focusing element with long focal length  $f$ . If we record a line scan at  $z=f$ ,  $y=0$  for different incident angles, we observe a light distribution shown in fig. 2.

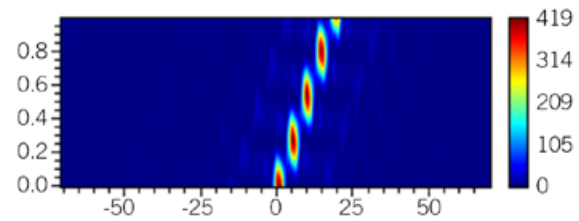


Fig.2: Variation of focal intensity  $I(x, 0, f)$  for incident angles from  $0^\circ$  to  $1^\circ$  using the standard method (eq. 1).

By rewriting the propagation equation, in such a way that the multiplication with the incident plane wave is replaced by a shift of the propagation phase,

$$\tilde{P}_z(\nu, \mu) = e^{ikz \sqrt{1 - (\lambda\nu + s_x)^2 - (\lambda\mu + s_y)^2}} \quad (3)$$

we obtain a very different simulation result (see fig. 3) for the same problem as in fig. 2.

In eq.3,  $s_x = \sin \vartheta \cos \varphi$ ,  $s_y = \sin \vartheta \sin \varphi$  are the lateral components of the unit direction vector of the incident plane wave.

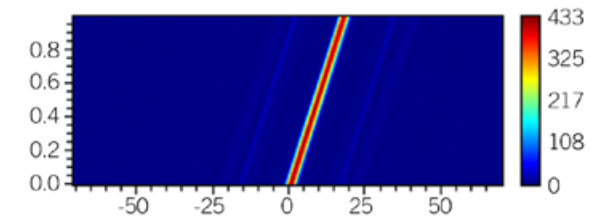


Fig. 3: Variation of focal intensity  $I(x, 0, f)$  for incident angles from  $0^\circ$  to  $1^\circ$  using the modified method (eq. 3).

Now we obtain exactly, what is expected. The focal spot position shifts linearly with the incident angle. Thus the treatment of oblique illumination by eq. 3 not only avoids an increase in space-bandwidth product, but it also corrects the error phase terms.

### References

- [1] Testorf, M. E., Fiddy, M. A., "Simulation of light propagation in planar-integrated free-space optics", Opt. Commun., 176 (2000) 365–372.

## RESEARCH GROUPS PROJECT OVERVIEW

### 120 | Research Group Advanced Computer Architecture

Fröning, H., Kapferer, S., Giese, A., Leber, C. and Silla, F.

### 122 | Research Group Application Specific Computing

Gerlach, T., Kretz, M., Kugel, A., Schroer, N. and Wurz, A.

### 124 | Research Group Dependable Robotics (DeBot)

Wagner, A., Zouaghi Mekacher, L. and Nordheimer, E.

### 126 | Research Group High Speed Short Range Interconnects

Wohlfeld, D., Lemke, F., Schenk, S., Fröning, H., Brenner, K.-H. and Brüning, U.

### 128 | Research Group New Detectors for Scientific- and Medical Applications

Peric, I.

### 130 | Research Group Next Generation Network Interfaces

Nüssle, M., Burkhardt, N., Geib, B., Kalisch, B., Giese, A. and Leber C.

### 132 | Research Group Unmanned Aerial Vehicles

Kandil, A. A., Koslowski, M., Alexopoulos, A., Zouaghi Mekacher, L. and Badreddin, E.

## Research Group Advanced Computer Architecture

• Fröning, H., Kapferer, S., Giese, A., Leber, C. and Silla, F.

### Overview

The research group focuses on new and innovative techniques in the area of parallel distributed computing. Despite the fact that technological advances and architectural improvements steadily increase the amount of computing power, the demands of many applications still cannot be satisfied. The research areas this year include dynamic memory aggregation for data-intensive problems, and optimizations and analyses in messaging-based communication. This research has been conducted in close collaboration with the Technical University of Valencia, represented in this research group by Prof. Dr. Federico Silla.

### Scalable Resource Compositions using Global Address Spaces

Our dynamic memory aggregation technique called MEMSCALE allows overcoming static partitioning of distributed resources in a way that any node of a system can access any memory location. Obviously performance disparities can be significant both in terms of latency and bandwidth, but for many cases this is not only the faster alternative, but also the less complex. Based on MEMSCALE, scalable resource compositions are now possible and the constraints imposed by the memory capacity wall can be overcome. In addition, the dynamic assignment of memory resources to processors allows reverting from provisioning memory resources for the worst case (in order to avoid swapping) to provisioning for the average case.

Last year we had numerous publications about MEMSCALE, and this year exhibitions took over the dissemination process. For instance, MEMSCALE was presented at the EXTOLL booth during the International Supercomputing Conference (ISC) in Hamburg, Germany.



Fig.1: Demonstrating MEMSCALE at an international venue using an 8-node cluster  
(© Holger Fröning)

### Optimizations and Analyses for Messaging-based Communication

Message passing is the standard technique for communication in High Performance Computing (HPC) environments, and its strong scalability enables huge system sizes for suitable workloads. Although being the standard solution for more than one decade, multiple aspects are still poorly characterized and offer opportunities for optimizations. First, the group has investigated new techniques for flow-control schemes in message-passing communication stacks. Goal is to maximize the utilization of receive buffers by dynamically re-assigning them to senders. The results of this work were published in [1] by Javi Prades, a student at Technical University of Valencia who is mainly supervised by Federico Silla. The impressive results show the potential of such an approach, which surprisingly comes at negligible costs in terms of network traffic and CPU cycles.

Another research effort includes an in-depth understanding of the communication patterns of various typical HPC workloads, in particular in terms of the message size distributing. Such analyses

describe how often certain message sizes have been used, which in turn allows for a better understanding of optimization opportunities.

### Future plans

With regard to MEMSCALE, future research will include an optimized integration into existing coherence domains. In addition, we plan to continue the work on messaging by further improving the flow-control scheme, by new data movement techniques for messaging libraries and by more detailed characterization efforts.

In cooperation with Technical University of Valencia, Spain.

### References

[1] Prades, J., Silla, F., Duato, J., Fröning, H., Nüssle, M.: "A New End-to-End Flow-Control Mechanism for High Performance Computing Clusters", IEEE International Conference on Cluster Computing, September 24 – 28, 2012, Beijing, China.

## Research Group Application Specific Computing

The objective of the research group is to design and build computer systems optimized for specific applications. This includes the development of hardware systems and software tools for specification and testing of systems plus application software. Primary application areas are high-performance data-acquisition and PC-hosted co-processors, both using custom reconfigurable hardware platforms based on FPGA technology.

The research group is involved in two international Physics experiments: ATLAS at CERN and XFEL at DESY.

• Gerlach, T., Kretz, M., Kugel, A., Schroer, N. and Wurz, A.

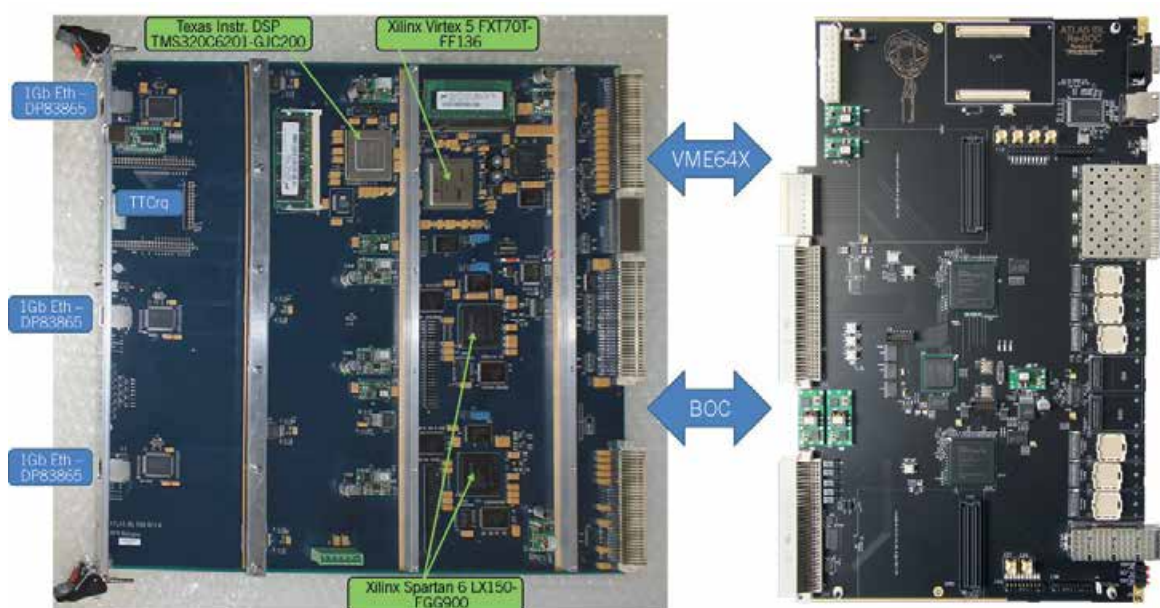


Fig. 1: ROD (left) – BOC (right) Card Pair

### ATLAS

The ATLAS detector at the LHC at CERN will be upgraded in 2014 with an additional B-layer inserted into its existing Pixel Detector. This layer requires new off-detector read-out electronics which is realized using dedicated VME-card-pairs, ROD and BOC (see Fig.1), similar to the existing system. The purpose of the BOC is to handle the different optical and electrical interfaces between the detector front end electronics, the ROD and the down-stream read-out.

It also controls the precise timing with respect to the master clock of the experiment and provides a link to the global detector control system of ATLAS.

The ASC group is responsible for the hardware development of the BOC card and contributes to the BOC firmware modules.

The ROD interacts with the detector data-acquisition system via VME and network. It controls configuration and steering of the FEE, checks and formats the acquired data for downstream transmission and prepares calibration and monitoring histograms. The ASC group contributes to the ROD firmware and software modules, in particular the ones related to histogramming and network operations.

The main achievements in 2012 were the successful completion of the ROD and BOC prototype tests [1][2], the performance evaluation of the FP-

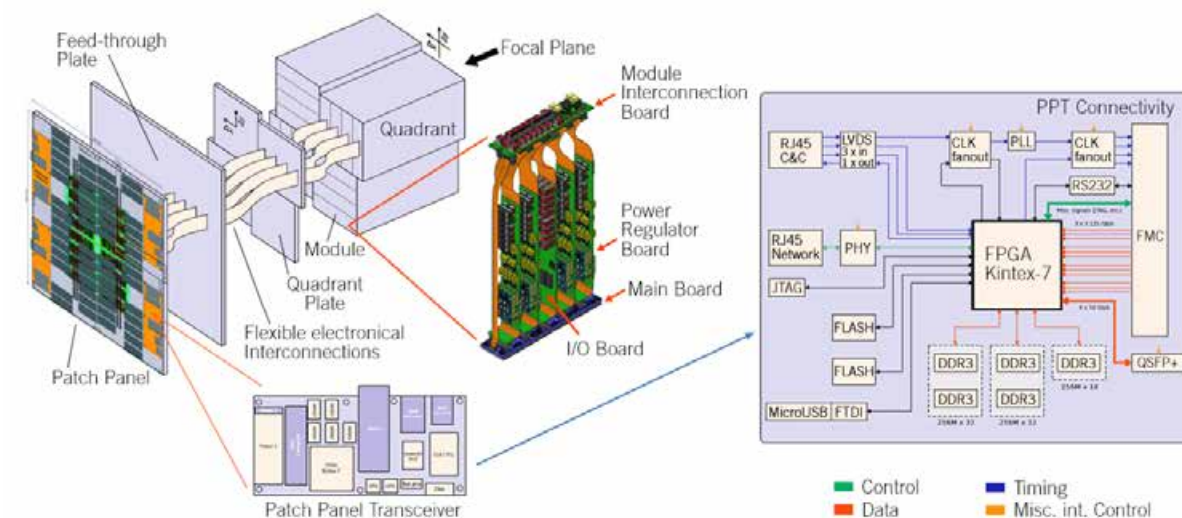


Fig. 2: XFEL DSSC Detector Sketch (left) and PPT Block Diagram (right)

GA-based network infrastructure [3] on the ROD and the initial design of the new ROD histogramming and calibration architecture [4].

ATLAS is supported by BMBF (05H12VH1) / In cooperation with CERN, INFN Bologna, NIKHEF Amsterdam, RHUL London, Göttingen University, Wuppertal University

### XFEL

The DSSC (DEPFET Sensor with integrated Signal Compression) is a 2D mega-pixel detector being developed for the European XFEL. XFEL will generate bursts of ultra-short X-ray flashes used by various scientific experiments. The analog data produced by the sensors of the DSSC detector are digitized immediately by dedicated sensor readout ASICs, and stored in digital memory blocks.

Data are transferred from the ASICs towards the main XFEL DAQ system by the DSSC DAQ subsystem during the inter-burst gaps. The main sensor voltages are switch off during the transmission to save power. The DAQ subsystem is composed of sensor-specific I/O modules (IOBs) and more complex controller boards (PPTs), located on the outer boundary of the detector. Fig. 2 displays a sketch of the detector assembly and a block diagram of the PPT control module.

In 2012 the IOB prototype [5] passed the final integration tests with the corresponding prototypes of ASIC, power supply and backend transceiver.

In 2012 the IOB prototype [5] passed the final integration tests with the corresponding prototypes of ASIC, power supply and backend transceiver. The schematics of the PPT module were completed and submitted to the layout company.

Supported by XFEL GmbH / In cooperation with MPIE Munich, DESY Hamburg, Politecnico di Milano, Bergamo University, Siegen University

### References

- [1] Balbi, G. et al: "Implementation and Tests of FPGA-embedded PowerPC in the control system of the ATLAS IBL ROD card", TWEPP, Sept 17–21, 2012, Oxford, UK.
- [2] Wensing, M. et al: "Testing and firmware development for the ATLAS IBL BOC prototype", TWEPP, Sept 17–21, 2012, Oxford, UK.
- [3] Kretz, M., Kugel, A.: "Linux on FPGA platforms: control software to connect custom peripherals", ACM SIGBED Review – 2nd Ewili Workshop, Volume 9 Issue 2, pp. 12–16, June 2012, New York, USA.
- [4] Kretz, M., Kugel, A., Männer, R.: "Studies Concerning the ATLAS IBL Calibration Architecture", Diploma Thesis, June 1, 2012, Heidelberg, Germany.
- [5] Gerlach, T., Kugel, A.: "An FPGA-based read-out module for the DAQ subsystem of the DSSC detector at the European XFEL", 18th IEEE-NPSS Real Time Conference (RT), June 11–15, 2012, Berkeley, USA.

## Research Group Dependable Robotics (DeBot)

• Wagner, A., Zouaghi Mekacher, L. and Nordheimer, E.

### Introduction

The goal of the research group dependable robotics is the development of a methodology for the modeling, the design and the realization of dependable systems in the area of industrial, medical and service robotics. Therefore, dynamic system modeling and modern controller design approaches for enhancing the dependability of computer-controlled systems are worked out based on new concepts for describing the fundamental dependability properties of such a system. The methods are applied to safety-critical application areas such as “Autonomous Mobile Robotics”, “Assistance Systems”, and “Medical and Rehabilitation Robots”. In the year 2012, the focus was on the “Surgical Robotics” area, where two new projects BOrESCOPE (Bionic Exoskeleton for Orthopedic Surgery) and ITD (Intelligent Tool Drive) could be acquired.

Medical systems such as medical and rehabilitation robots need to be highly safe and dependable since they directly influence health and live of patients. On the other hand, modern assistance technologies allow the design of highly sophisticated medical devices and the use of medical systems in a more flexible and interactive way. Thus, the dependability of human behavior in close interaction with a medical system has to be considered additionally to the basic system behavior and functions. A fundamental view on the overall system dependability can be achieved by modeling the technical system and the human operator on a behavioral description level and by its realization as functional descriptions.

### BOrESCOPE

The goal of the project BOrESCOPE is to develop a robotic exoskeleton for orthopedic interventions. It is attached to the surgeon's arm (Fig.1).

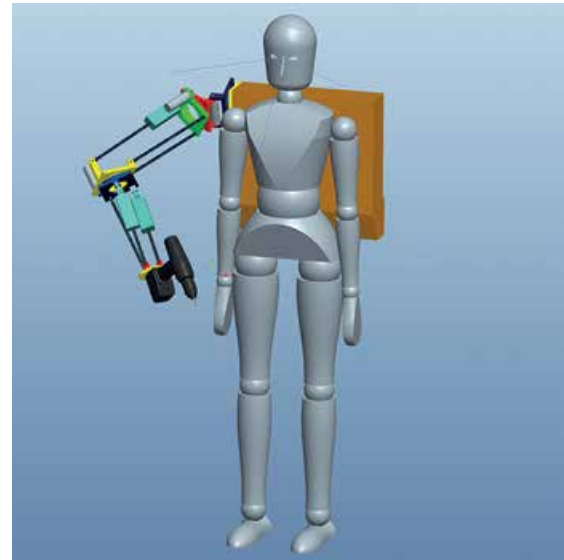


Fig.1: BOrESCOPE – conceptual design (<http://www.emk.tu-darmstadt.de/borescope/>)

The surgeon has to fulfill subtle tasks like milling cavities into the spine while maintaining high precision and avoiding the injury of live-critical physiological structures. From preoperative planning the target area and processing trajectories are known. During the operation this target area (bone) and the robotic arm are tracked by an optical measurement system. If the bone changes its position, the instrument, which is attached to the BOrESCOPE, follows the new position of the bone by a shared control of robot arm and the human operator. Thus, it is possible to stabilize the tool relatively to the bone as well as to compensate the surgeon's hand tremor. Moreover, the system is able to perform pre-programmed operation tasks and to partially compensate the weight of the surgical drill and the human arm enabling comfortable work without fatigue.

The main research topics are the miniaturization of the actuation technology and its MEMS-based inertial sensors as well as the dependable human-

robot interaction using opto-acoustic feedback channels of an intelligent display, which is mounted on the robotic system.

The project is funded by the BMBF under grant 16SV5773K.

The project partners are: Institute of Electromechanical Design, Technische Universität Darmstadt, and Automation Laboratory, ZITI, Heidelberg University.

### ITD

Aim of the project ITD is the development of a small hand-held 6-DOF (Degrees Of Freedom) robot for orthopedic surgery. The hand-held surgical robot combines the precision of robotic processing, the medical navigation and the surgeon's experience. The tremor of the surgeon's hand is compensated and the instrument tip will be automatically aligned against the patient. The envisioned application is the preparation of the human knee for implanting an artificial knee joint. Therefore, the system must perform predefined cuts in the bones of the leg (femur and tibia).



Fig. 2: ITD – functional prototype

The first functional prototype has been realized and tested in the lab in preliminary works (Fig. 2).

It consists of a hexaglide construction with linear motors, incremental and analogical sensors, an optical tracking system for the position measurement of the tool and the patient and a real-time control system.

In the current project phase, the hand-held device will be enhanced for pre-clinical experiments. Main aspects are the miniaturization and weight reduction of the machine, the improvement of the tracking system by fusing optical and inertial data. The role of DeBot is the design of a dependable and adequate control method in order to achieve high precision tool stabilization and user navigation, while safety-critical situation are avoided. Special requirements result from the surgical process in the operation theater in respect of hygiene, ergonomics, and safety.

The project is funded by the BMBF under grant (01EZ1205C) “KMU-innovativ Medizintechnik”.

The project partners are: MRC Systems GmbH (Coordinator), Laboratory for Biomechanics and experimental Orthopedics, OUZ, Heidelberg University, Automation Laboratory, ZITI, Heidelberg University, Binder Elektronik GmbH, Sinsheim, and EMB-Lab, Mannheim University of Applied Science.

### References

- [1] El-Shenawy, A., Wagner, A., Pott, P.P., Gundling, R., Schwarz, M., Badreddin, E.: Disturbance Attenuation of a Handheld Parallel Robot, IEEE International Conference on Robotics and Automation, Karlsruhe, 2013.
- [2] Pott PP, Wagner A, Köpfle A, Badreddin E, Männer R, Weiser P, Scharf H-P, Schwarz MLR: A handheld surgical manipulator: ITD – Design and first results. 18th international congress and exhibition of CARS, Chicago, USA, 23–26.6.2004.
- [3] Wagner Achim, Matthias Nübel, Essam Badreddin, Peter P. Pott, Markus L. Schwarz: Disturbance feed forward control of a handheld parallel robot, ICINCO 2007 – Fourth International Conference on Informatics in Control, Automation and Robotics, Proceedings – Robotics and Automation Vol. 1, Angers, France, May 9–12, 2007, p44–51.

## Research Group High Speed Short Range Interconnects

### Fabrication of optical high-speed short-range interconnects

The alignment requirements of Optical Engines on multi-chip-modules (MCM) are very strict. In order to achieve high coupling efficiencies between electro-optical components and fibers, a high precision replication stage for optical modules was build and characterized.

• Wohlfeld, D., Lemke, F., Schenk, S., Fröning, H., Brenner, K.-H. and Brüning, U.

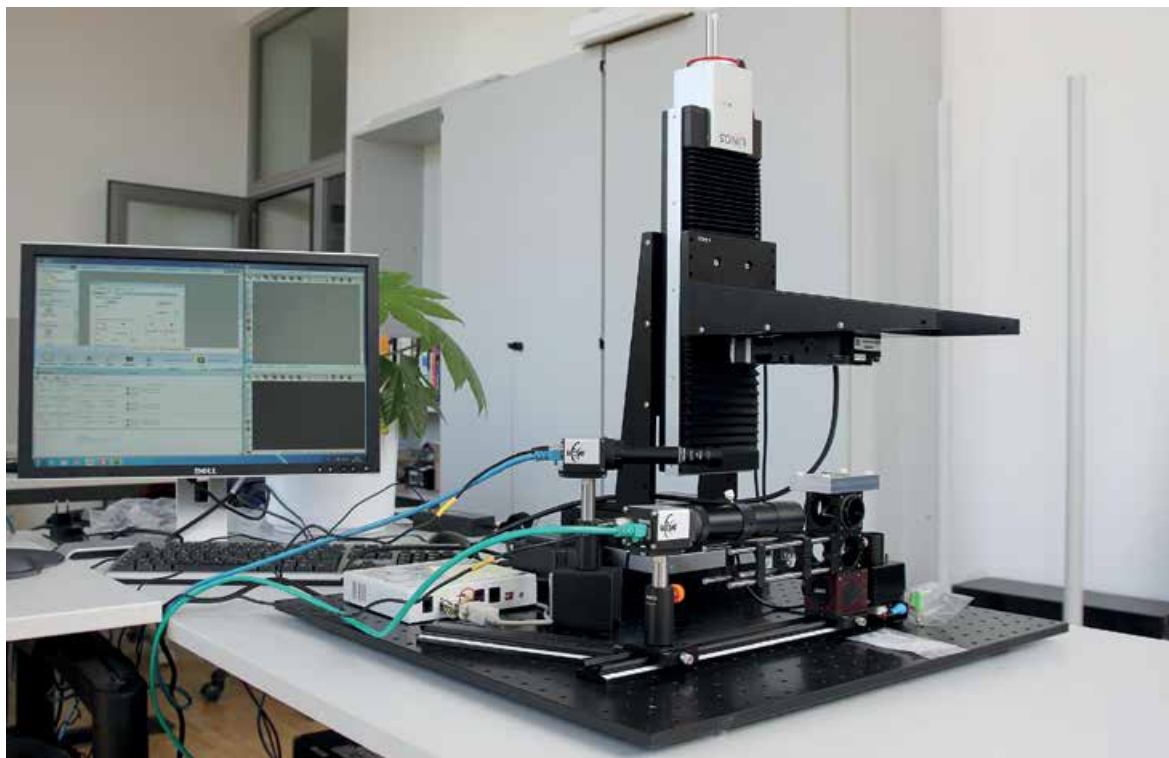


Fig.1: High precision stage for Direct Replication of Optical Engines

### Introduction

The replacement of electrical interconnects by optical solutions accelerates with the ongoing demand on bandwidth and lane speed [1]. At 10 Gbit/s and above, the length restriction of only several meters of passive electrical cables opened the market for a large variety of active optical cables (AOC). AOC are cables with an electrical interface but optical transmission. Based on the promising results of our HD-AOC prototypes, the research group focused on the high volume production in the next step.

### Fabrication of Optical Engines based on Direct Replication

The Direct Replication Process replicates an Optical Engine by molding a 3D structure including a 90° mirror directly on top of the electrical components. Due to the short distance between VCSEL/PD and fibers, no additional lenses are required. The requirements on the alignment accuracy between molding form and electrical components is in the range of  $< 10 \mu\text{m}$  and  $< 1^\circ$ . In order to prove the concept of high volume production, an automated high precision replication stage

was build. The replication stage consists of 3 linear position stages for X, Y and Z with a step size of  $0.5 \mu\text{m}$  and a reproducibility of  $15 \mu\text{m}$  over the complete working volume. An additional rotation stage allows for correction of angular misalignments between the PCB plane and the molding form. The optical system consists of 2 cameras. X and Y are controlled by 5MP camera combined with a telecentric lens and a resolution of  $4 \mu\text{m}$ , while the Z control is realized by the second 3MP camera. Figure 1 shows an early implementation of the replication stage and the control software.

### Results

Optical Engines based on Direct Replication can be realized using a high precision position stage. We achieved coupling efficiencies between 20% and 50%. Our misalignment in XY was in the range of  $10 \mu\text{m}$  and the angular variation of the mirror about  $1^\circ$ . In the next step, the software for the stage will be developed, including pattern recognition and semi-automation.

### References

[1] Wohlfeld, D., Brenner, K.-H.: "Aspects of short-range interconnect packaging", SPIE Photonics West Conference Optoelectronic Interconnects XII, 8267-26, Jan. 2012, San Francisco, USA.

## Research Group New Detectors for Scientific- and Medical Applications

### Development of Pixel Detectors for Particle Physics Applications

• Peric, I.

#### Overview

In 2012 our group participated in the following projects:

- 1) Development of HVCMOS detectors for CERN-experiments (ATLAS upgrade and CLIC)
- 2) Development of Mu3e pixel detector at PSI (Switzerland)
- 3) Design of SOI detectors
- 4) Readout chips of DEPFET vertex detector for Belle II experiment (KEK, Japan)

#### Development of HVCMOS detector for CERN-experiments

The HVCMOS detectors (also called “smart diode arrays” - SDAs) and the capacitively coupled pixel detectors, originally developed in our group, are now considered at CERN as an interesting option for several planned experiments. Currently, eight institutes are collaborating in the development of HVCMOS detectors for CERN: University of Bonn, LBNL Berkeley (USA), CPPM Marseille (France), CERN, University of Geneva (Switzerland), University of Göttingen, University of Glasgow (UK) and University of Heidelberg. We are investigating the possibility to replace the classical semiconductor particle sensors, based on passive elements, with the active CMOS detectors. The classical sensors are fabricated in the special sensor technologies, they are realized on high quality (high resistive) silicon substrates and contain no active circuits – no transistors. The HVCMOS sensors are fabricated in the commercial CMOS processes, their production cost is therefore relatively low. The use of transistors allows in-pixel signal processing, which has several advantages, e.g. a faster readout and a better time resolution. We have designed the first HVCMOS prototype detector for the CERN applications (HV2FEI4) end of 2011. The chip HV-2FEI4 has been successfully tested in 2012.

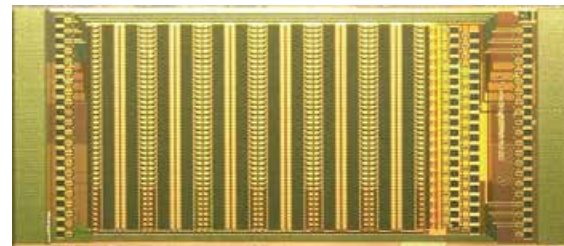


Fig. 1: Photograph of HV2FEI4 detector prototype

#### Publications

- 2) I. Peric for HVCMOS Collaboration; “Active Pixel Sensors in high-voltage CMOS technologies for ATLAS,” JINST 7, C08002 (2012).
- 3) I. Peric et al.; “Strip Technology and HVMAPS,” Proceedings of Science PoS 021 (Vertex 2012).

#### Talks

- 2) “Active pixel sensors for high energy physics in commercial technologies,” invited talk at the colloquium at University of Göttingen, Göttingen, 2012.
- 3) “Radiation Tolerance of HV-CMOS Sensors,” invited talk at the 9th International Conference on Radiation Effects on Semiconductor Materials Detectors and Devices - RESMDD 2012, Florence, Italy, 2012.
- 4) “Developments of HV-CMOS pixel sensors,” invited talk at TALENT 1st Annual meeting, CERN, 2012.
- 5) “Smart diode arrays - the high-voltage active pixel detectors for LHC applications,” invited talk at Vertex 2012, Jeju, Korea, 2012.
- 6) “High-Voltage Pixel Detectors in Commercial CMOS Technologies for ATLAS, CLIC and Mu3e Experiments,” Pixel 2012, Inawashiro, Japan, 2012.

#### Development of Mu3 detectors

The experiment Mu3e with the goal: search for the particle decay  $\mu^+ \rightarrow e^+ e^- e^+$ , has been approved by Paul Scherrer Institute (Switzerland) in February 2013. The project will be realized in collaboration between six institutes: University of Heidelberg (Institute for Physics and ZITI), PSI, ETH Zürich, University of Zürich and University of Geneva. The discovery of the decay would have important consequences for particle physics – it would confirm the expectations of some theories beyond the Standard Model. (According to the Standard Model the muons can not decay solely to electrons.) The muons will be generated from an intense particle beam with a rate of about two billions per second, they will hit an aluminum target, decay and a particle detector placed around the target will examine the decay products. The aim is to detect the unusual decay  $\mu^+ \rightarrow e^+ e^- e^+$  among the huge amount of normal decays.

The requirements for the Mu3e detector are: the ability to cope with a muon rate of  $2 \times 10^9/s$  and a particle hit rate  $50 \text{ MHz/cm}^2$ . Spatial resolution of  $100 \mu\text{m}$ , a small amount of material ( $10^{-3}$  of the radiation length) and a time resolution  $<1 \text{ ns}$  are also necessary. We will meet these requirements, among others, by the use of HVCMOS pixel detectors arranged in two layers. The planned detector area is  $1.9 \text{ m}^2$  and the pixel size is  $80 \mu\text{m} \times 80 \mu\text{m}$ . The sensor should be thinned to about  $50 \mu\text{m}$  and glued on a light carrier structure made only of kapton-foil. In 2012 we have design a prototype detector MuPixel3.

#### Thesis

- 1) Ann-Kathrin Perrevoort; “Characterisation of High Voltage Monolithic Active Pixel Sensors for the Mu3e Experiment,” Master Tesis, Heidelberg, 2012.  
<http://www.physi.uni-heidelberg.de/Publications/MasterPerrevoort.pdf>
- 2) Heiko Augustin; “Charakterisierung von HV-MAPS,” Bachelor Thesis, Heidelberg, 2012.  
<http://www.psi.ch/mu3e/DocumentsEN/BachelorAugustin.pdf>

#### Publications

- 1) A. Blondel, A. Bravar, M. Pohl, S. Bachmann, N. Berger, M. Kiehn, A. Schöning, D. Wiedner, B. Windelband, P. Eckert et al.; “Research Proposal for an Experiment to Search for the Decay  $\mu \rightarrow eee$ ,” 2013.
- 2) Niklaus Berger, et al.; “A Tracker for the Mu3e Experiment based on High-Voltage Monolithic Active Pixel Sensors,” in press, NIMA, 2013. In internet:<http://dx.doi.org/10.1016/j.nima.2013.05.035>

#### Conference talks

- 1) Dirk Wiedner; “A Novel Experiment Searching for the Lepton Flavor Violating Decay  $\mu \rightarrow eee$ ,” Vertex 2012, Jeju, Korea, 2012.
- 2) Ann-Kathrin Perrevoort; “Charakterisierung von HV-MAPS für das MU3E-Experiment,” DPG Frühjahrstagung, 2012.

#### Other projects

Our group is also involved on the development of the detectors in SOI technology. Our second SOI detector prototype has been successfully tested in 2012.

We are also involved in the development of the “Belle II pixel detector”. Our main task is the design and production of the readout chip (DCD) and the high voltage driver chip (SWITCHER). The construction of the Belle II pixel detector is funded by BMBF, our project part with 635T€. In 2012 we have designed and tested a new SWITCHER version.

Supported by: ZITI, BMBF, Faculty for Physics and Astronomy of University of Heidelberg, CPPM Marseille.

## Research Group Next Generation Network Interfaces

• Nüssle, M., Burkhardt, N., Geib, B., Kalisch, B., Giese, A. and Leber, C.

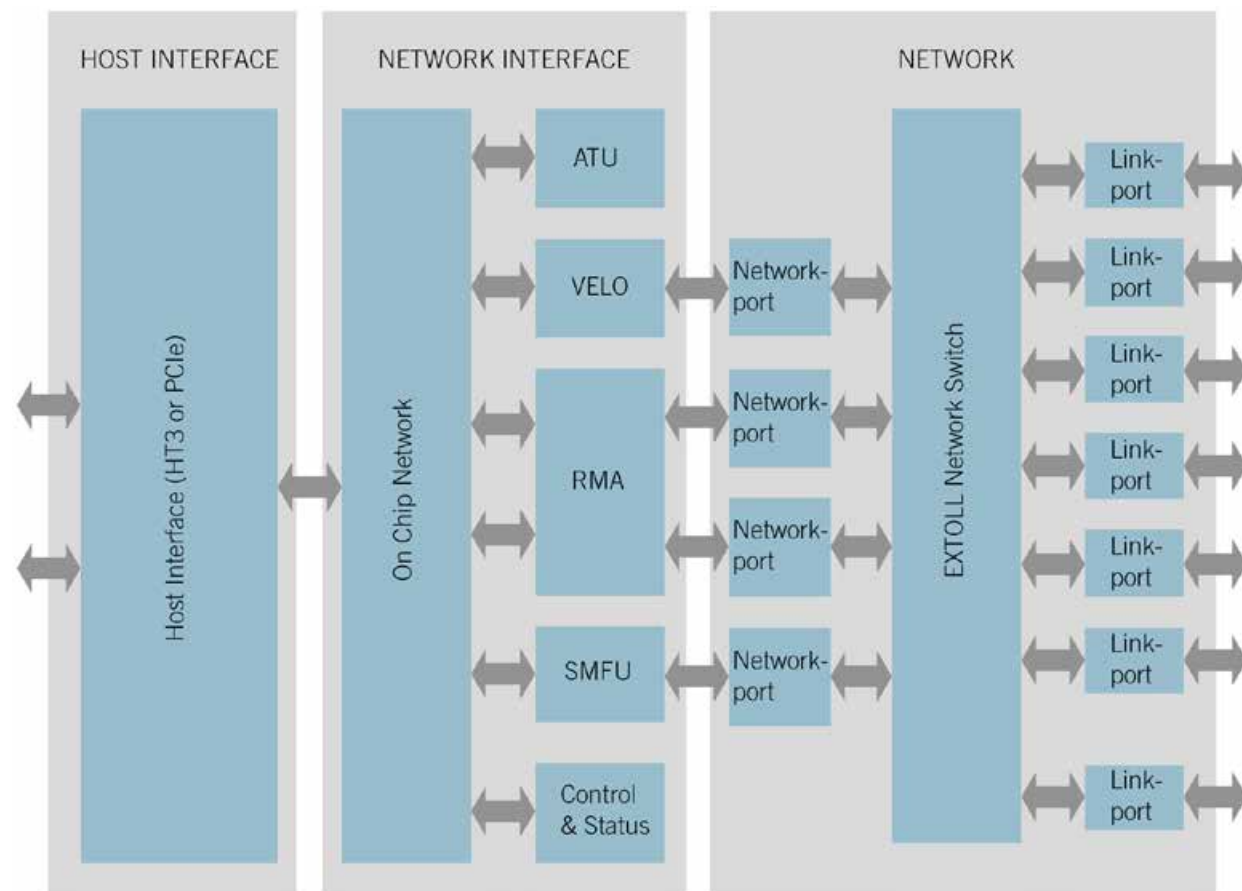


Fig. 1: Planned EXTOLL R2 ASIC block-diagram

The research group “Next Generation Network Interfaces” is committed to the research of interconnection networking in the area of High-Performance Computing. Interconnection networks play a major role on all levels of current systems that rely more and more on massive parallelization to realize performance increases.

Within the research group, networks for parallel cluster machines, which are wide spread in HPC, are analysed, architected and developed. Especially, work on the EXTOLL architecture is advanced.

Prior to 2012, the group was already deeply involved with the EXTOLL project. Work on both EXTOLL R1 and EXTOLL R2 has been conducted. In 2012, four major points were in the focus of the research group.

First of all, the verification of the R2 architecture was strengthened. This led to significant improvements in the methodology of verifying the correctness of very complex systems. It is also a major step for the architecture to ensure the necessary design quality to use EXTOLL in more and more complex real world scenarios.

Secondly, the improvements embodied in R2 in the previous time frame were consolidated and finished. This included further work on the NIC and switch architecture as well as the software side.

The third point involved work to prepare a high-performance ASIC implementation of the EXTOLL R2 architecture. Many of the necessary analysis and implementation details for an ASIC implementation could be performed. One of the very first results was the definition of a potential target ASIC technology and the related parameters of the EXTOLL R2 for this target. A 65nm standard CMOS process was chosen. On this process, the EXTOLL NIC and network architecture can provide approximately 10GB/s bandwidth per link or communication engine, with an internal clock rate of 750 MHz. Figure 1 shows the top-level block-diagram of the EXTOLL R2 as it was planned for an ASIC implementation.

The fourth point is an increasing amount of research performed within the European FP7 project DEEP. Here, software was co-developed to enable a very efficient bridging between Infiniband and EXTOLL networks, which offload nearly the complete communication to the network devices and do not use any memory bandwidth on the bridging machine. A prototype of this architecture was successfully built and tested.

Within DEEP, the so called “Booster” part of a large parallel machine is built from Intel Many-Integrated-Core (MIC) chips, notably the Knights Corner family of chips, directly interconnected by an EXTOLL network. Here, the EXTOLL network chips has to act as a root port device, which in turn will be used to boot the MIC into Linux over the network. Within the research group work was done to prototype and to implement the necessary hardware and software components. Figure 2 shows the experimental test platform that was used to design, analyse and debug the EXTOLL root port extensions.

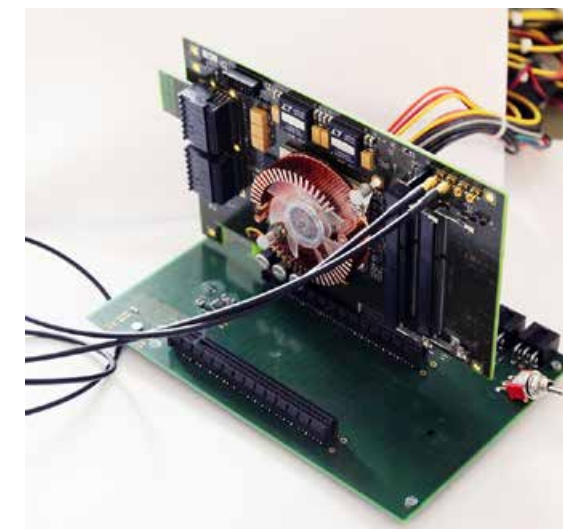


Fig. 2: Root-port test-bed with PCIe backplane and FPGA board

Again, the group continued its work in the area of High Frequency Trading (HFT).

At the International Supercomputing Conference in Hamburg (ISC'12) and the Supercomputing Conference in Salt Lake City (SC12), the current state of the EXTOLL project was shown at a booth presentation.

During 2012 the EU-project DEEP continued throughout the year, while the BMWI project closed in the first quarter.

In part supported by: BMWI (03EFT5BW24), EU Project DEEP (ICT-287530)

## Research Group Unmanned Aerial Vehicles

• Kandil, A. A., Koslowski, M., Alexopoulos, A., Zouaghi Mekacher, L. and Badreddin, E.



Fig. 1: Unmanned helicopter experiments on Ladenburg airfield

### Introduction

Unmanned Aerial Vehicles (UAVs) and especially autonomous helicopters have been popular research platforms since the last few years. Their vertical take-off and landing (VTOL) capability and the hovering flight qualify them for several tasks mainly aerial mapping, surveillance, inspection and search and rescue missions. For all applications it is required to hold the UAV at a desired position to perform the planned missions safely. The integration of control strategies to follow trajectories or to support the execution of desired missions is therefore indispensable. Moreover, before controller design takes place, a mathematical model of the UAV has to be found out and the parameters of the model are to be identified. In order to test new control structures, the developed model can be used to simulate the controllers before the implementation on the real helicopter platform.

### Modeling and identification for control

First part of our research was the control modeling and an identification approach for the Scout B1-100 autonomous unmanned helicopter (of the Heidelberg University) in hovering flight. In [1] the unmanned helicopter platform was presented by depicting the assembly of the experimental helicopter platform and its different hardware components. A nonlinear dynamic model was driven from the first principles and then linearized to obtain a linear state-space model presentation of thirteenth order. To identify the unknown parameters, the state-space model has been divided into subsystems as presented in [2]. The parameters of the different subsystems could be determined by applying a suitable identification method such as the prediction-error minimization (PEM) method. A sequential quadratic programming technique (SQP) was used to obtain feasible initial values of the parameters to be identified. Finally, the gained

model of the UAV has been validated using the correlation factor and the mean-square error (MSE), which represent mathematical functions. The model can be used for controller design in hovering flight.



Fig. 2: Heidelberg University Scout B1-100

### Integrated distributed monitoring for mission based systems

The second part of our research presents a new approach of an integrated distributed monitoring system for an autonomous unmanned helicopter, demonstrated on mission based navigation. The navigation mission consists of reaching areas of interest, on a path composed of specific waypoints (WP) as depicted in Fig. 2. The task of such a monitoring system is to determine whether the helicopter behaves as intended in order to detect faults in the mission execution early and to enable a re-planning of the mission or a failure recovery. This is an important issue for autonomous systems as they have to cope not only with ordinary subsystems failures, but also with unexpected situations which make the mission goals unreachable. The approach uses a special combination of Petri Nets and Monte Carlo Methods (particle filter) and integrates different layers of the system architecture such as control actions (path-planning, low-level control), environment perception (vision-based recognition of landmarks), state observation (estimation of speed, position, attitude) and decision making (mission planning and re-planning) in a unified model.



Fig. 3 a): The waypoints viewing from above

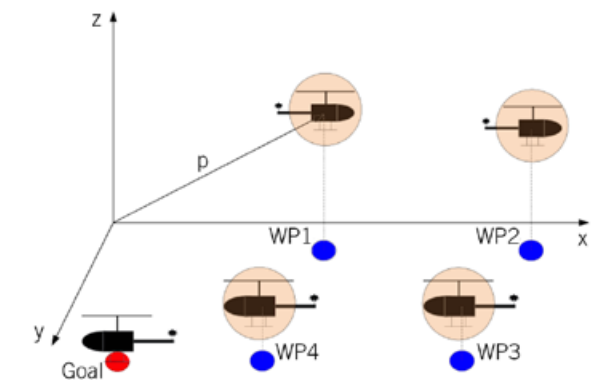


Fig. 3 b): Helicopter navigation under consideration of the location uncertainty

### References

- [1] Koslowski, M., Kandil, A. A. and Badreddin, E.: "Platform Description and System Modelling for Control of an Unmanned Helicopter", IEEE International Conference on Intelligent Systems, Sept. 6–8, 2012, Sofia, Bulgaria.
- [2] Koslowski, M., Kandil, A. A. and Badreddin, E.: "Modeling and Identification of a Small-Scale Unmanned Autonomous Helicopter", IEEE/RSJ International Conference on Intelligent Robots and Systems, Oct. 7–12, 2012, Vilamoura, Algarve (Portugal).
- [3] Zouaghi, L., Alexopoulos, A., Koslowski, M., Kandil, A. A. and Badreddin, E.: "An Integrated Distributed Monitoring for Mission-Based Systems", IEEE International Conference on Intelligent Systems, Sept. 6–8, 2012, Sofia, Bulgaria.

## Members and Staff

### Professors

Last Name	Name	Chair
Badreddin	Essameddin	Automation
Brenner	Karl-Heinz	Optoelectronics
Brüning	Ulrich	Computer Architecture
Fischer	Peter	Circuit Design
Fröning (Juniorprofessor)	Holger	Computer Engineering Group (since Oct 1, 2011)
Männer	Reinhard	Computer Science V
Schnörr	Christoph	Computer Vision, Graphics and Pattern Recognition

### Secretaries

Last Name	Name	Chair
Fischer	Ursula	Automation
Seeger	Andrea	Computer Architecture, Computer Engineering Group, Computer Science V
Volk	Sabine	Optoelectronics
Wilhelm	Evelyn	Computer Vision, Graphics and Pattern Recognition
Wunsch	Beate	Circuit Design

### Administration

Last Name	Name
Binder	Michaela
Geppert	Dina

### Ph.D. Candidates and Research Assistants

Last Name	Name	Chair
Alexopoulos	Alexander	Automation
Armbruster	Tim	Circuit Design
Auer	Max	Optoelectronics
Bähr	Jochen	Optoelectronics
Bakulina	Alena	Computer Science V
Beier	Florian	Computer Science V
Berger	Johannes	Computer Vision, Graphics and Pattern Recognition
Bartolein	Christian	Automation
Burkhardt	Niels	Computer Architecture
Denitiu	Andreea	Computer Vision, Graphics and Pattern Recognition
Erdinger	Florian	Circuit Design
Frey	Dirk	Computer Architecture
Gerlach	Thomas	Computer Science V
Giese	Alexander	Computer Architecture
Gipp	Markus	Computer Science V
Hlindzich	Dzmitry	Computer Science V
Hüsken	Nathan	Computer Science V
Kalisch	Benjamin	Computer Architecture
Kandil	Amr	Automation
Kapferer	Sven	Computer Architecture
Kappes	Jörg	Computer Vision, Graphics and Pattern Recognition
Kirchgessner	Manfred	Circuit Design
Koslowski	Markus	Automation
Krackhardt	Ulrich	Computer Architecture
Keller	Christoph	Computer Vision, Graphics and Pattern Recognition
Kreidl	Christian	Circuit Design
Krieger	Michael	Circuit Design
Kugel	Andreas	Computer Science V
Leber	Christian	Computer Architecture
Leibig	Christian	Computer Architecture

Last Name	Name	Chair
Lemke	Frank	Computer Architecture
Leys	Richard	Computer Architecture
Litz	Heiner	Computer Architecture
Liu	Xiyuan	Optoelectronics
Marcus Martinez	Guillermo	Computer Science V
Mekacher Zouaghi	Leila	Automation
Merchan Alba	Fernando	Optoelectronics
Miksch	Tobias	Automation
Mueller	Markus	Computer Architecture
Neufeld	Andreas	Computer Vision, Graphics and Pattern Recognition
Neuwirth	Sarah	Computer Architecture
Nordheimer	Eugen	Automation
Nüssele	Mondrian	Computer Architecture
Peric	Ivan	Circuit Design
Petra	Stefania	Computer Vision, Graphics and Pattern Recognition
Rady Abdel Ghany ElAsmar	Sherine	Automation
Rathke	Fabian	Computer Vision, Graphics and Pattern Recognition
Razmyslovich	Dzmitry	Computer Science V
Richter geb. Wellenreiter	Andrea	Automation
Ritzert	Michael	Circuit Design
Rüdiger	Jan	Automation
Rukletsov	Alexander	Computer Science V
Sacco	Ilaria	Circuit Design
Sadeghzadeh	Nargess	Automation
Schatral	Sven	Computer Architecture
Schenk	Sven	Computer Architecture
Slogsnat	Eike	Optoelectronics
Schmitzer	Bernhard	Computer Vision, Graphics and Pattern Recognition
Schreiber	Thomas	Computer Vision, Graphics and Pattern Recognition
Schuppe	Oliver	Computer Science V
Sismanidis	Evangelos	Computer Science V

Last Name	Name	Chair
Soldat	Jan	Circuit Design
Stenau	Tim	Optoelectronics
Stolzenberger	Frank	Automation
Stumpfs	Wolfgang	Optoelectronics
Swoboda	Paul	Computer Vision, Graphics and Pattern Recognition
Thil	Christophe	Circuit Design
Thürmer	Maximilian	Computer Architecture
Wagner	Achim	Automation
Watson	Myles	Computer Architecture
Werner	Barbara	Computer Vision, Graphics and Pattern Recognition
Wohlfeld	Denis	Computer Architecture
Wolf	Martin Joachim	Automation
Wurz	Andreas	Computer Science V
Zern	Antjorn	Computer Vision, Graphics and Pattern Recognition

## Third-party funded Projects

Research at ZITI is funded by various national and international programs and sponsors.

Funding by	Project Title	Project Funding Amount	Project Funding Period	Chair
AiF	Entwicklung eines kardiologischen klinischen PAC (Patient Archiving and Communication)	175.000 €	07.2010–04.2012	Computer Science V
BMBF	ATLAS: Betrieb, Wartung und Entwicklung von HLT/DAQ-Komponenten	338.722 €	07.2009–06.2012	Computer Science V
BMBF	Borescope	149.994 €	02.2012–08.2014	Automation
BMBF	CBM Data Acquisition at FAIR	258.500 €	07.2009–06.2012	Computer Architecture
BMBF	ITD	312.000 €	07.2012–06.2015	Automation
BMBF / PT DESY	BELLE II - Auslesechips für den Vertexdetektor Bei BELLE II	635.478 €	07.2012–06.2015	Circuit Design
BMBF / PT DESY	SUPER BELLE – Auslesechips und Bumping für den DEPFET Vertexdetektor bei SuperBelle	290.360 €	07.2009–06.2012	Circuit Design
BMBF / PT DESY	FAIR-CBM III - Front End Elektronik	255.600 €	07.2012–06.2015	Circuit Design
BMBF / PT GSI	FAIR-CBM II – Front End Elektronik	260.000 €	07.2009–06.2012	Circuit Design
BMW	EXIST Forschungstransfer: EXTOLL – Innovative skalierbare Hochleistungs-Rechnersysteme	383.856 €	09.2010–02.2012	Computer Architecture
DESY / ESRF	XNAP - Development of an APD 2D Pixel Array Detector	315.200 €	01.2009–12.2012	Circuit Design
DESY / MPE	XFEL-Projekt DESY/DAQ	310.150 €	04.2009–03.2013	Computer Science V
DFG	3D-Tomographie mit wenigen Projektoren in der experimentellen 3 D-Strömungsmessung	1 BAT IIa/E13 (100 % pos.) + 25.900 €	04.2010–03.2012	Computer Vision, Graphics and Pattern Recognition
DFG	Graduiertenkolleg 1653/1 Spatio/Temporal Graphical Models and Applications in Image Analysis	585.000 €	04.2010–09.2014	Computer Vision, Graphics and Pattern Recognition
DFG	Cyclobot	171.000 €	08.2009–06.2014	Automation

Funding by	Project Title	Project Funding Amount	Project Funding Period	Chair
DFG + Industrie	Heidelberg Collaboratory for Image Processing (HCI)	1.675.589 €	01.2008–10.2012	Computer Vision, Graphics and Pattern Recognition
EU	DEEP Dynamical Exascale Entry Platform	507.350 €	12.2011–11.2014	Computer Architecture
EU	SUBLIMA - SUB nanosecond Leverage In PET/MR Imaging	1.000.250 €	09.2010–08.2014	Circuit Design
IMC Trading B.V.	Accelerated Computing using FPGAs	264.803 €	10.2009 ongoing	Computer Architecture
Jäger, MSC, Kuroda	Test und Inbetriebnahme von HTX-Boards (Anwendung gesicherter Erkenntnisse - AgE)	51.105 €	03.2009 ongoing	Computer Architecture
NVIDIA		7.000 USD	one-off payment	Computer Engineering
Universidad Politecnica de Valencia		127.194 €		Computer Engineering
VW	GRACE II	60.000 €	04.2010–12.2012	Computer Science V
XFEL GmbH	XFEL – Development of a Large Format X-ray Imager with Mega-Frame Readout Capability based on the DEPFET Active Pixel Sensor	1.024.600 €	04.2009–09.2012	Circuit Design
Xilinx		50.000 USD	one-off payment	Computer Engineering

## Selected Project Partners and Collaborators

Company/Institution	Location	Chair
AAST (Arab Academy of Science and Technology)	Alexandria, Egypt	Automation
AGH University of Science and Technology	Cracow, Poland	Computer Architecture
American University of Beirut (AUB)	Beirut, Lebanon	Automation
ATLAS Collaboration CERN	Geneva, Switzerland	Computer Science V
Binder Elektronik GmbH	Sinsheim, Germany	Automation
BMBF	Germany	Circuit Design
BMBF	Germany	Computer Architecture
CBM Collaboration GSI	Darmstadt, Germany	Computer Science V
Delft University of Technology	Delft, The Netherlands	Circuit Design
DLR (Deutsches Zentrum für Luft- und Raumfahrt / German Aerospace Center)	Goettingen, Germany	Computer Vision, Graphics and Pattern Recognition
École polytechnique fédérale de Lausanne (EPFL)	Lausanne, Switzerland	Circuit Design
ESRF	Grenoble, France	Circuit Design
EU-XFEL GmbH	Europe	Circuit Design
Fraunhofer ITWM	Kaiserslautern, Germany	Computer Architecture
Georgia Institute of Technology	Atlanta, GA, US	Computer Engineering
Ghent University	Ghent, Belgium	Circuit Design
Goethe University Frankfurt/Main	Frankfurt/Main, Germany	Circuit Design
GSI	Darmstadt, Germany	Computer Architecture
Heinrich-Hertz-Institut, Fraunhofer Institut	Berlin, Germany	Optoelectronics
Hochschule Mannheim	Mannheim, Germany	Automation
IBM	Böblingen, Germany Zurich, Switzerland	Optoelectronics
Indian Institute of Technology Kharagpur iitkgp	Kharagpur, India	Computer Architecture
Jagiellonian University	Cracow, Poland	Circuit Design
Johann Wolfgang Goethe-Universität	Frankfurt, Germany	Computer Architecture

Company/Institution	Location	Chair
King's College	London, United Kingdom	Circuit Design
Klinikum Mannheim	Mannheim, Germany	Computer Science V
Kyoto University	Kyoto, Japan	Automation
La Vision GmbH	Goettingen, Germany	Computer Vision, Graphics and Pattern Recognition
MPI Semiconductor Laboratory	Munich, Germany	Circuit Design
MRC Systems GmbH	Heidelberg, Germany	Automation
National Astronomical Observatories, Chinese Academy of Sciences	Peking, China	Computer Science V
NVidia Corporation	Santa Clara, CA, US	Computer Engineering
Otto Bock Mobility Solutions GmbH	Königsee, Germany	Automation
Philips Research	Eindhoven, The Netherlands	Circuit Design
Polytechnico di Milano	Milano, Italy	Circuit Design
RWTH Aachen University	Aachen, Germany	Circuit Design
RWTH Aachen University	Aachen, Germany	Computer Architecture
Siemens AG	Nürnberg / Karlsruhe, Germany	Automation
SMOS	Walldorf, Germany	Optoelectronics
Technical University of Chemnitz	Chemnitz, Germany	Computer Architecture
Technical University of Dresden	Dresden, Germany	Computer Architecture
Technical University of Valencia	Valencia, Spain	Computer Architecture
Technical University of Valencia	Valencia, Spain	Computer Engineering
Technolution B.V.	Gouda, The Netherlands	Circuit Design
TU Darmstadt	Darmstadt, Germany	Automation
Universitäts-Klinikum, OUZ	Mannheim, Germany	Automation
Universitat de Barcelona	Barcelona, Spain	Circuit Design
Universitat Politècnica de València	Valencia, Spain	Circuit Design
University Hospital Aachen	Aachen, Germany	Circuit Design
University of Bergamo	Bergamo, Italy	Circuit Design
University of Bonn	Bonn, Germany	Circuit Design

Company/Institution	Location	Chair
University of Castilla-La Mancha	Castilla-La Mancha, Spain	Computer Architecture
University of Muenster	Muenster, Germany	Circuit Design
University of Siegen	Siegen, Germany	Circuit Design
Various European Universities in conjunction with EU-Project IntelliCIS	Europe	Automation
VRmagic GmbH	Mannheim, Germany	Computer Science V
XFEL Collaboration DESY	Hamburg, Germany	Computer Science V
Xilinx, Inc.	San José, CA, US	Computer Engineering

### Conferences

Title	Location	Chair	Date
1st Workshop on Unconventional Cluster Architectures and Applications (UCAA), co-located with ICPP	Pittsburgh, PA, US	Computer Engineering	September 10, 2012
CBM FEE/DAQ/FLES Workshop	Mannheim, Germany	Circuit Design	January 25–27, 2012
SUBLIMA Consortium Meeting	Mannheim, Germany	Circuit Design	September 19–20, 2012

## Publications

### Chair of Automation

- Alexopoulos, A., Zouaghi, L. and Badreddin, E.:  
“Associative memory for modified Petrinet based monitoring of mobile robot navigatio”,  
1st International Conference on Innovative Engineering Systems (ICIES),  
December 7–9, 2012, Alexandria, Egypt.
- Koslowski, M., Kandil, A. and Badreddin, E.:  
“Modeling and Identification of a Small-Scale Unmanned Autonomous Helicopter”,  
IEEE/RSJ International Conference ‘Intelligent Robots and Systems’, Vila Moura,  
October 7–12, 2012 Algarve, Portugal.
- Koslowski, M., Kandil, A. and Badreddin, E.:  
“Platform Description and System Modelling for Control of an Unmanned Helicopter”,  
IEEE International Conference ‘Intelligent Systems’,  
September 6–8, 2012, Sofia, Bulgaria.
- Rady, S.:  
“Information-theoretic environment modeling for mobile robot localization”,  
Dissertation, Universität Mannheim, Germany.
- Rady, S. and Badreddin, E.:  
“Hybrid map-building and localization for unstructured and moderately dynamic environment”,  
IEEE International Conference ‘Intelligent Systems’,  
September 6–8, 2012, Sofia, Bulgaria.
- Wagner, A., Nordheimer, E. and Badreddin, E.:  
„Hierarchical Constraint-Based Singularity Avoidance”,  
16th International Conference on System Theory, Control and Computing (ICSTCC),  
October 12–14, 2012, Sinaia, Romania.
- Wolf, M.J., Ninov, V., Babel, H., Hütter, K., Staudt, R., Storhas, W. and Badreddin, E.:  
„A Laboratory Experiment for Teaching Bioprocess Control – Part 1: Hardware Setting”,  
9th IFAC Symposium on Advances in Control Education,  
June 19–21, 2012, Nizhny Novgorod, Russia.
- Zouaghi, L., Alexopoulos, A., Koslowski, M., Kandil, A. and Badreddin, E.:  
“An Integrated Distributed Monitoring for Mission-Based Systems”,  
IEEE International Conference ‘Intelligent Systems’,  
September 6–8, 2012, Sofia, Bulgaria.
- Zouaghi, L., Wagner, A. and Badreddin, E.:  
„Benutzerinteraktion beim Online-Monitoring der Navigation eines autonomen Rollstuhls“,  
Proceedings of AUTOMED – Automatisierungstechnische Verfahren für die Medizin,  
March 29–30, 2012, Aachen, Germany.

### Chair of Circuit Design

- Aguilar, J.:  
“Infrastructure for Detector Research and Development towards the International Collider”,  
et al. (EUDET Collaboration), arXiv:1201.4657v1
- ATLAS Collaboration:  
“Measurement of the b-hadron production cross section using decays to  $D^* + \mu - X$  final states in pp collisions at 7 TeV with the ATLAS detector”,  
Nuclear Physics B, Volume 864, Issue 3, Pages 341–381,  
November 21, 2012.
- Lisauskas, T., Matula, P., Claas, C., Reusing, S., Wiemann, S., Erfle, H., Lehmann, L., Fischer, P., Eils, R., Rohr, K., Storrie, B. and Starkuviene, V.:  
“Live-Cell Assays to Identify Regulators of ER-to-Golgi Trafficking Traffic”,  
Volume 13, Issue 3, pages 416–432, 2012.
- Porro, M., Andricek, L., Aschauer, S., Bayer, M., Becker, J., Bombelli, L., Castoldi A., De Vita, G., Diehl, I., Erdinger, F., Facchinetti, S., Fiorini, C., Fischer, P., Gerlach, T., Graafsma, H., Guazzoni, C., Hansen, K., Kalavakuru, P., Klär, H., Kugel, A., Lechner, P., Lemke, M., Lutz, G., Manghisoni, M., Mezza, D., Müntefering, D., Pietsch, U., Quartieri, E., Randall, M., Re, V., Reckleben, C., Sandow, C., Soldat, J., Strüder, L.W.J., Szymanski, J. Weidenspointner, G. and Wunderer, C.B.:  
“Development of the DEPFET Sensor with Signal Compression: a Large Format X-ray Imager with Mega-Frame Readout Capability for the European XFEL”, IEEE Transactions on Nuclear Science”,  
Volume 59, Issue 6, Pages: 3339–3351, Part 2, 2012.

### Chair of Computer Architecture

- Geib, B.:  
“Hardware Support for Efficient Packet Processing”,  
Dissertation on the MADOC Document Server,  
March 21, 2012.
- Leber, C.:  
“Efficient hardware for low latency applications”,  
Dissertation on the MADOC Document Server,  
August 20, 2012.
- Lemke, F.:  
“Unified Synchronized Data Acquisition Networks”,  
Dissertation on the MADOC Document Server,  
November 30, 2012.

- Lemke, F. and Brüning, U.:  
“Design Concepts for a Hierarchical Synchronized Data Acquisition Network for CBM IEEE”,  
18th Real-Time Conference 2012 (RT12),  
June 11–15, 2012, Berkeley, CA, USA.
- Mohr, B., Zimmermann, N., Thiel, B.T., Mueller, J.H., Wang, Y., Zang, Y., Lemke, F., Leys, R., Schenk, S., Brüning, U., Negra, R. and Heinen, S.:  
“An RFDAC Based Reconfigurable Multistandard Transmitter in 65nm CMOS”,  
June 17–19, 2012, Montreal, Canada.
- Prades, J., Silla, F., Duato, J., Fröning, H. and Nüssle, M.:  
“A New End-to-End Flow-Control Mechanism for High Performance Computing Clusters”,  
IEEE International Conference on Cluster Computing,  
September 24–28, 2012, Beijing, China.

### Chair of Computer Engineering

- Prades, J., Silla, F., Duato, J., Fröning, H., Nüssle, M.:  
“A New End-to-End Flow-Control Mechanism for High Performance Computing Clusters”,  
IEEE International Conference on Cluster Computing,  
Sept. 24–28, 2012, Beijing, China.

### Chair of Computer Vision, Graphics and Pattern Recognition

- Andres, B., Beier, T. and Kappes, J.H.:  
“OpenGM: A C++ Library for Discrete Graphical Models”,  
ArXiv e-prints, 2012.
- Andres, B., Kappes, J.H., Beier, T., Köthe, U. and Hamprecht, F.A.:  
“The Lazy Flipper: Efficient Depth-limited Exhaustive Search in Discrete Graphical Models”,  
ECCV 2012, 2012.
- Becker, F., Wieneke, B., Petra, S., Schröder, A. and Schnörr, C.:  
“Variational Adaptive Correlation Method for Flow Estimation”,  
IEEE Transactions on Image Processing, 21(6):3053–3065,  
June, 2012.
- Kappes, J.H., Savchynskyy, B. and Schnörr, C.:  
“A Bundle Approach To Efficient MAP-Inference by Lagrangian Relaxation”,  
CVPR, 2012.

- Lellmann, J., Lenzen, F. and Schnörr, C.:  
“Optimality Bounds for a Variational Relaxation of the Image Partitioning Problem”,  
Journal of Mathematical Imaging and Vision, 47(3):239–257, 2012.
- Lenzen, F., Becker, F., Lellmann, J., Petra, S. and Schnörr, S.:  
“Variational Image Denoising with Adaptive Constraint Sets”,  
Proceedings of the 3rd International Conference on Scale Space and Variational Methods in Computer  
Vision 2011, pages 206–217, Springer, 2012.
- Nair, R., Lenzen, F., Meister, S., Schäfer, H., Garbe, C.S. and Kondermann, D.:  
“High accuracy TOF and stereo sensor fusion at interactive rates”,  
Computer Vision--ECCV 2012, Workshops and Demonstrations, pages 1–11,  
Springer Berlin Heidelberg, 2012.
- Petra, S., Schnörr, C. and Schröder, A.:  
“Critical Parameter Values and Reconstruction Properties of Discrete Tomography:  
Application to Experimental Fluid Dynamics”,  
arXiv:1209.4316 [math.NA], September 19, 2012.
- Savchynskyy, B., Schmidt, S., Kappes, J.H. and Schnörr, C.:  
“Efficient MRF Energy Minimization via Adaptive Diminishing Smoothing”,  
UAI 2012, 2012.
- Schmitzer, B. and Schnörr, C.:  
“Weakly Convex Coupling Continuous Cuts and Shape Priors”,  
Scale Space and Variational Methods (SSVM 2011), pages 423–434, 2012.

#### Chair of Optoelectronics

- Auer, M. and Brenner, K.-H.:  
“Calculation of Local Absorption in three-dimensional Structures using RCWA”,  
8th EOS Topical Meeting on Diffractive Optics,  
February 27–March 1, 2012, Delft, NL.
- Brenner, K.-H.:  
“Optimization of local absorption in layered media”,  
8th EOS Topical Meeting on Diffractive Optics,  
February 27–March 1, 2012, Delft, NL.
- Brenner, K.-H. and Buschlinger, R.:  
“Talbot Focusing – a new effect of periodic structures and its utilization”  
(Online-Zeitschrift der Deutschen Gesellschaft für angewandte Optik e. V.), 113. Jahrestagung,  
May 29–June 2, 2012, Eindhoven, NL.

- INVITED: Brenner, K.-H. and Liu, X.:  
“High resolution wavefront sensing with non-interferometric techniques”,  
11th Euro-American Workshop on Information Optics (WIO 2012), IEEE,  
August 20–24, 2012, Quebec, Canada.
- INVITED: Wohlfeld, D. and Brenner, K.H.:  
“Aspects of short-range interconnect packaging”,  
SPIE Photonics West Conference / Optoelectronic Interconnects XII, 8267-26,  
January 24–26, 2012, San Francisco, USA.
- Liu, X., Stenau, T. and Brenner, K.-H.:  
“Diffractive micro lens arrays with overlapping apertures”,  
11th Euro-American Workshop on Information Optics (WIO 2012), IEEE,  
August 20–24, 2012, Quebec, Canada.
- Merchà, F. and Brenner, K.-H.:  
“Novel integrated micro-optics system for the fabrication of Active Optical Cables”  
(Online-Zeitschrift der Deutschen Gesellschaft für angewandte Optik e. V.), 113. Jahrestagung,  
May 29–June 2, 2012, Eindhoven, NL .
- Slogsnat, E., Lehmann, L., Fischer, P. and Brenner, K.-H.:  
“Concept and Implementation of a Compact Multi-Channel Fluorescence-Microscope Unit”  
(Online-Zeitschrift der Deutschen Gesellschaft für angewandte Optik e. V.), 113. Jahrestagung,  
May 29–June 2, 2012, Eindhoven, NL.